EFFECT OF CORROSION ON FLEXURAL BEHAVIOUR OF REINFORCED CONCRETE BEAMS

Thesis

Submitted in partial fulfilment of the requirements for the degree of

DOCTOR OF PHILOSOPHY

by

POORNACHANDRA PANDIT

DEPARTMENT OF CIVIL ENGINEERING

NATIONAL INSTITUTE OF TECHNOLOGY KARNATAKA

SURATHKAL, MANGALORE-575025

SEPTEMBER, 2014

D E C L A R A T I O N

I hereby *declare* that the Research Thesis entitled "**Effect of Corrosion on Flexural Behaviour of Reinforced Concrete Beams**" which is being submitted to the **National Institute of Technology Karnataka, Surathkal** in partial fulfilment of the requirements for the award of the Degree of **Doctor of Philosophy** in **Civil Engineering**, is a *bonafide report of the research work carried out by me*. The material contained in this Research Thesis has not been submitted to any University or Institution for the award of any degree.

POORNACHANDRA PANDIT

Register No.**100471CV10F02,**

Department of Civil Engineering

Place: NITK-Surathkal

Date: 23-09-2014

C E R T I F I C A T E

This is to *certify* that the Research Thesis entitled "**Effect of Corrosion on Flexural Behaviour of Reinforced Concrete Beams"** submitted by **POORNACHANDRA PANDIT** (Register Number: **100471CV10F02**) as the record of the research work carried out by him, is *accepted as the Research Thesis submission* in partial fulfilment of the requirements for the award of degree of **Doctor of Philosophy**.

Research Guide

Dr. Katta Venkataramana
Professor
Dept. of Civil Engineering
NITK, Surathkal - 575025

Dr. K.N.Lokesh
Chairman - DRPC
Department of Civil Engineering
National Institute of Technology
Karnataka, Surathkal – 575025,
Karnataka, INDIA

Dedicated to

MY BELOVED PARENTS

AND

TEACHERS

ACKNOWLEDGEMENTS

ABSTRACT

In coastal environment reinforcement corrosion is an obvious cause of deterioration of concrete structures, affecting strength and durability. The present study is an attempt to quantify the effect of reinforcement corrosion on the flexural strength of reinforced concrete beams. Experimental studies as well as numerical simulations have been performed. The basic need for this study is Load-deflection behaviour and crack pattern of beams how it is affected when it is corroded with Accelerated corrosion technique.

Since corrosion takes place over a considerable length of time, to achieve corrosion quickly, accelerated corrosion technique was adopted. Corrosion was measured using Applied Corrosion Monitoring (ACM) instrument. Corroded beams were tested in laboratory to evaluate their flexural behaviour. Totally 42 beams out of which, 21 made of Ordinary Portland Cement (OPC) and 21 of Portland Pozzolana Cement (PPC) were tested. The beams were tested as vertical cantilever beams; two hydraulic jacks were used one for bottom fixity and one for applying the load at the top. Strain gauges were used for measuring strains: two strain gauges on the reinforcement and the third on the surface of the concrete beam. Strains were measured by data acquisition system as well as manually. The beams were loaded till failure. The load-deflection and crack-propagation patterns were recorded for various corrosion levels.

For Control beam specimen it was observed that the control beams attained the higher load carrying capacity of about 23% more compared to theoretical ultimate load. The beams were corroded to 2.5%, 5%, 7.5% and 10% corrosion rate. As the rate of corrosion increases form 2.5% to 10%, stiffness and load carrying capacity decrease rapidly while deflection, crack width and curvature increase in beam specimens. It was observed that PPC beams behaved stiffer than OPC beams.PPC beams are 15% more corrosion resistant than OPC beams as chloride migration in PPC beams is less compared to OPC beams.

In the numerical study, finite element method was used. Comparative studies were done for different levels of corrosion. Results show that as rate of corrosion increases, the deflection also increases but load carrying capacities of the beams reduce, for both OPC and PPC beams. It is observed that the stiffness of the beams is reduced nonlinearly when rate of corrosion is increased. The numerical modelling results are in conformity with experimental

values and it is concluded that numerical modelling can be applied satisfactorily to measure load-deflection behaviour and to predict crack patterns.

TABLE OF CONTENTS

LIST OF FIGURES

LIST OF TABLES

LIST OF NOTATIONS

Symbol	Description
B	Breadth of the beam
D	Depth of the beam
d	Effective depth of the beam
L	Length of the beam
E_s	Modulus of elasticity of steel
E_c	Modulus of elasticity of concrete
A_{st}	Area of tension steel
A_{sc}	Area of compression steel
f_{ck}	Compressive strength of concrete
f_y	Yield strength of steel
F	Faraday's constant
w_i	Initial weight of steel reinforcement
W	Equivalent weight of iron
T	Time in days
ρ	Corrosion rate
i_{corr}	Corrosion current density

ν	Poisson's ratio
f	Stress
ε	Strain
ε_0	Ultimate strain
C	Mass of cement
S_c	Specific gravity of cement
S_{fa}	Specific gravity of fine aggregate
S_{ca}	Specific gravity of coarse aggregate
V	Gross volume of fresh concrete
b	Width of flange
I_{xx}	Moment of inertia about X axis
I_{yy}	Moment of inertia about Y axis
t_f	Thickness of flange
t_w	Thickness of web
r_{min}	Minimum radius of gyration
λ_{min}	Minimum slenderness ratio
M_u	Ultimate moment
C_{uc}	Compressive force in Concrete

C_{us}	Compressive force in Steel
X_u	Depth of neutral axis
d'	Effective cover
l	Effective length of beam
m	Modular ratio
I_{cr}	Moment of inertia of the cracked section
I_{eff}	Effective moment of inertia
M_r	Cracking moment
Z	Lever arm
b_w	Breadth of web
P	Load
Φ	Initial diameter of bar
Φ_1	Reduced diameter of bar
p	Corrosion percentage

CHAPTER 1

INTRODUCTION

1.1 GENERAL

Corrosion is the breakdown or degradation of a material due to reaction with the environment. In the most commonly used words, this means an oxidant, such as oxygen, reacts with the electrochemical oxidation of the metal. Formation of an oxide of iron due to oxidation of the iron atoms in solid solution is a well-known example of electrochemical corrosion, commonly known as rusting. Corrosion phenomenon is not only happening in reinforcement, it is also taking place other than metals like ceramic. Generally because of corrosion in any material disintegration of material will takes place that reduces bonding of material causes decrease in strength. The term disintegration or degradation of material is more common in any type of corrosion.

Corrosion is the main factor which reduces the cross-sectional area of steel and reduces load bearing capacity of structures thereby induces brittle failure without prior warning. Therefore, the effect of corrosion has to be studied for better performance of structure. When the steel corrosion occurs, rust occupies a greater volume than steel. This development causes tensile stress in the concrete which can in the long run cause cracking, delamination and spalling. Development of corrosion causes some coupling effect: the protective layer of concrete cracking due to expansion of corrosion products; steel cross-section reduction and steel-concrete bond degradation (Malumbela et al. 2010). As a result of these effects, the load bearing capacity and service life of reinforced concrete structures are significantly reduced (Alonso et al. 1998). Research has become increasingly important, especially in corrosive environments such as coastal areas, in which the structure is exposed to an environment with high humidity and salt content. The moment carrying capacity of

reinforced concrete beams mainly depends on the strength of steel. Therefore, the loss of reinforcement may be critical and needs special attention.

1.2 MECHANISM OF CORROSION

Corrosion is caused by the destructive attack of chloride ions penetrating by diffusion or by other penetration mechanisms from the outside, by incorporation into the concrete mixture, by carbonation of the concrete cover, or their combination (Cabrera 1996). Carbonation of concrete or penetration of acid gases is the other specific cause of reinforcement corrosion. In addition to these, there are several other factors associated with specific quality, such as a water/cement ratio of the cement content in the concrete, composition of the impurities in concrete, the presence of surface cracks and other connections to the external environment such as moisture, oxygen, humidity, temperature, bacterial attack, etc., which influence the corrosion (Castro et al. 1997). Uncontaminated concrete cover is the main barrier to prevent direct contact with the external environment of the steel surface. It provides protection against corrosion of steel in strong alkaline chemical environment.

In the past few years, steel production and steel manufacturing in the field of technical progress to effectively develop a variety of corrosion-resistant steel used in the construction industry. This type of steel is called Thermo Mechanical Treated steel (TMT), which imparts better corrosion resistance against severe environment conditions.

Corrosion of steel embedded in concrete is an electrochemical method. The corrosive steel surface serves as a composite electrode which is electrically coupled by a combination of anode and cathode by the body of the steel itself, by associating the anodic and cathodic reactions. Concrete pore water functions as an aqueous medium, particularly a complex electrolyte. Therefore, a cell is formed by corrosion as shown in Fig. 1.1. The anode reaction is the oxidation, resulting in the dissolution or metal loss, while the cathode reaction is the reduction process, which results in reduction of dissolved oxygen forming hydroxyl ions.
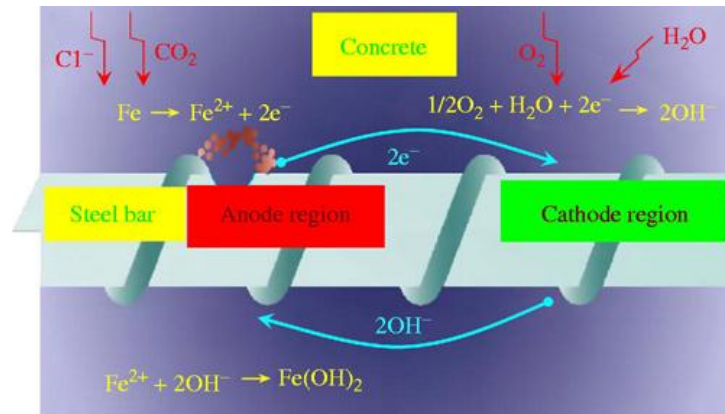
Fig. 1.1 Corrosion of reinforcement in concrete (Qiao et al. 2011).

The two main causes of reinforcement corrosion are (i) localized passive layer of steel with the removal of chloride ions, (ii) the general breakdown of passivity by neutralization with concrete, especially by reaction with atmospheric carbon dioxide. Due to industrial pollution, corrosion of the rebar is becoming the primary cause of failure. The magnitude of this problem has reached alarming proportions in different parts of the world. The following are the factors leading to corrosion failure.

1. Loss of alkalinity due to carbonation of concrete

2. Loss of alkalinity due to chlorides

3. Cracks due to mechanical loading

The early deterioration of concrete structures is inevitable when the concrete has to withstand extreme environmental conditions such as in coastal regions. Chloride is the main agent which has the ability to destroy Reinforced Concrete (RC) under alkaline conditions naturally by passivation. The degree of diffusion is strongly related to the quality of the concrete structure, the pores and cracks available on the surface area of the concrete and passivation time largely depends on the permeability of concrete. It is not feasible to produce almost no cracks in the concrete. Chloride ingress is significantly enhanced by cracks because the ions can penetrate the concrete cover from the walls of the crack as well as from the outer surface of the concrete by diffusion. Therefore along with steel, chlorides reach very quickly across the gap, can also quickly reach the adjacent areas of the steel in uncracked concrete. Delay in

3

corrosion activity has been reported in cases where thicker concrete cover to the reinforcing steel is used. Corrosion mechanism primarily depends on the availability of chloride ion and oxygen content around rebar surface which diffuse through the concrete cover which affects the reinforcement by reducing its cross sectional area (Liang et al. 1999).

1.3 EFFECTS OF CORROSION ON RC BEAMS

Concrete generally has a high alkalinity (pH values> 13.5), provides high protection to steel. In high alkalinity steel remain passivated. Moreover, a well consolidated and properly cured concrete with a low w/c ratio has a low permeability which minimizes entrance of corrosion inducing agents, such as chloride, carbon dioxide, moisture, etc. to the steel surface. Further, the high resistivity of concrete restricts the rate of corrosion by reducing the flow of electrical current from the anodic to the cathodic sites. In general, an accurately designed, constructed and maintained structure, there should be a slight problem of steel corrosion in its design life. Unfortunately, this condition of durability is not achieved in practise due to which corrosion of reinforcement in concrete has become a cause of deterioration in many RC structures in the recent years.

- Protective layer of concrete cracking and reduce slippage caused by corrosion, the bond strength between steel and concrete, reduces the stiffness of RC beams. As a result, the increase in RC beams deflection.
- Increased corrosion products may eventually lead to the formation of longitudinal cracks leading to loss of bond and concrete spalling.
- The volume of rust formation as a result of corrosion is 2-4 times more than that of steel. The loss of the concrete cover may have a considerable reduction in the load carrying capacity of the structure and in addition, the steel may be more accessible to the aggressive agents leading to further corrosion at an accelerated rate. Considering the safety issue, if the steel provided in the

concrete was more than design limits, corrosion rate would be more in such beams.

- Pitting corrosion of steel is more dangerous than the uniform corrosion, as it gradually decreases the cross-sectional area of rebar to a point where steel can no longer resist the applied load leads to catastrophic failure of the structure.

In the proposed research work, an attempt has been made to find out the effect of corrosion reinforcement on the flexural strength of reinforced concrete beams.

Steel corrosion of concrete structures deteriorates in chloride environment; affect the durability and service life of RC structures (Cabrera 1996, Glass 2003, Poupard et al. 2006 and Zhang and Ba 2011). Furthermore, since the tensile stresses generated in the corrosion process, existing fine cracks and microcracks in the surrounding concrete tends to enlarge and forms a network of interconnected cracks.

1.4 ACCELERATED CORROSION TECHNIQUE

The impressed current technique, also called as galvanostatic method, consists of applying a constant current from a DC source to the steel embedded in concrete to induce significant corrosion in a short period of time. After applying the current for a given duration, the degree of induced corrosion can be determined theoretically using Faraday's law, or the percentage of actual amount of steel lost in corrosion can be calculated with the help of a gravimetric test conducted on the bars after subjecting them to accelerated corrosion. Using the actual amount of steel lost in corrosion, an equivalent corrosion current density can be determined. In the present study the corrosion rate is measured using Applied Corrosion Monitoring (ACM) instrument which is a non-destructive testing method.

1.5 CRACK DEVELOPMENT IN CONCRETE

Cracking of concrete is one of the main problems in RC beams. Cracks in concrete will occur when the tensile strength of the concrete is exceeded. Concrete has a low tensile strength and low failure strain in tension, cracking normally unavoidable in RC members. In RC beam when corrosion occurs the volume of the bar increases which exerts pressure on the concrete that will lead to the formation of crack. These longitudinal cracks may affect the load carrying capacity of RC beams and shorten its life. If there is increase in corrosion rate there will be increase in beam crack width. Cracks in the concrete cover has a direct impact on the process, such cracks assist in the spread of the carbon dioxide or chlorine ions within the concrete. This is the main reason to entry of oxygen in such a way there by accelerating the process of corrosion and increasing the corrosion rate. It is also moderately due to the fact that the safety factors used in the structural design for strength used is often larger than those of serviceability, therefore, corrosion affected RC structures are more prone to cracking (Li et al. 2005).

Experimental study on corrosion induced in concrete, the corrosion process is generally accelerated through a variety of means to speed up the concrete cracking in a relatively short period of time (Ahmed 2009). In addition to concrete properties, rebar corrosion rate and cover to diameter ratio are the key factors (Alonso et al.1998).

Crack width is a parameter of the most practical significance for the design and assessment of RC structures. Therefore, the determination of corrosion induced crack width is essential for the prediction of the serviceability of corrosion affected RC structures and do decision making regarding the repairs of the structure.

1.6 NUMERICAL MODELLING IN CONCRETE

The Finite Element Model (FEM) offers a powerful and general analytical tool for studying structural behaviour of reinforced concrete structures. Cracking, tension

6

stiffening, non-linear material properties, interface behaviours, and other effects previously ignored or treated in a very approximate by other numerical methods can be modelled rationally using FEM. The reliability of the method is largely dependent on the accuracy with which the model simulates the actual behaviour and geometrical characteristics of the prototype structure. Where simple analytical methods are not feasible for the solution of complex civil engineering problems, the FEM offers an effective, versatile and reliable approach to handle such cases.

From this point of view, in order to establish a numerical analysis method to appropriately evaluate the behaviour of RC beams, Finite Element (FE) analysis was carried out using the commercial FE package ANSYS 13. The tasks were to build a model which can represent the beam crack pattern and predict ultimate loads reasonably. Furthermore, experimental results obtained from tests were used to confirm an applicability of the proposed FE analysis method.

1.7 OBJECTIVES OF THE STUDY

1. To develop an empirical relation to determine the number of days required to obtain a specific corrosion percentage in RC beams.
2. To determine experimentally the effects of reinforcement corrosion on the strength and deflection of OPC and PPC beam specimens.
3. To investigate the effects of corrosion on crack development pattern and moment-curvature relations.
4. To validate a numerical model with experimental results for modelling corrosion effects.

1.8 ORGANIZATION OF THESIS

The thesis consists of 6 chapters. A brief overview is given below:

Chapter 1 gives the introduction on corrosion and corrosion mechanism in concrete. Significance of Accelerated Corrosion, Crack pattern and Numerical modelling is explained. Objectives of the work are presented.

Chapter 2 presents a detailed discussion on previous studies related to corrosion of RC beam, crack pattern and numerical modelling.

Chapter 3 describes the experimental details of the beams, accelerated corrosion technique and testing methods for beam specimens.

Chapter 4 describes the numerical modelling of beam specimens.

Chapter 5 discusses the results obtained from experiments and numerical method for different levels of corrosion. Numerical and experimental results have been compared.

Chapter 6 constitutes major conclusions drawn from present research. Scope for future study is also discussed briefly.

CHAPTER 2

LITERATURE REVIEW

2.1 GENERAL

Reinforced concrete structures in the coastal environment are exposed to aggressive sea water, leading to premature deterioration of concrete. The remaining lives of these structures are reduced due to deterioration of concrete or reinforcing steel. As reinforced concrete members lose its concrete cover, its permeability increases, corrosion initiates in the embedded steel. The corrosion of the steel and degradation of the concrete affects the flexural and shear strength of the structural member, thus reducing its residual life.

This chapter covers comprehensive review of literature on flexural strength of corroded beams, crack pattern after accelerated corrosion and numerical modelling of corroded beams.

2.2 FLEXURAL STRENGTH OF CORRODED BEAMS

Cabrera (1996) investigated effects of corrosion rate on cracking and bond strength loss using laboratory data. Examined the influence of fly ash on the rate of reinforcement corrosion.

Study concluded that when the corrosion level reached 9%, the beam deflection increased 1.5 times the deflection of the non-corroded beam. Fly ash concrete exhibited better resistance to corrosion damage than normal Portland cement concrete. The reduced level of corrosion in fly ash concrete is attributed to the higher resistivity of this concrete.

Rodriguez et al. (1997) investigated by using calcium chloride (3%) mixture of water and applied to corroded beams (150 $\times$ 200 $\times$ 2300mm) in experimental studies, a

constant current density of about $100\mu A/cm^2$ carried to reinforcement corrosion. Beams with different details were tested, taking consideration of the tension reinforcement, compression reinforcement and shear reinforcement.

According to the results, it was concluded that the corrosion of reinforcement affects the concrete beams performance, increasing both deflection and crack widths at service loads and reducing the strength at the ultimate load. Reinforcement corrosion modifies the type of failure in RC beams. Observations showed that the beams which were not corroded maintained the quality those were failed by bending while the beams which were corroded or deteriorated with reduction in cross sectional area and bond strength were failed by shear.

Ray et al. (1997) investigated the properties of the three types of corrosion reinforcement bar of TMT (PC-TMT, Cu-Cr TMT and Cu-TMT) and compared with those of conventional CTD bars. Conventional salt spray and accelerated corrosion methods were used for the electrochemical potentiodynamic measurements.

Results showed that low levels of TMT alloy (copper-bearing and copper / chromium bearing) were found to be 1.13 to 1.52 times stronger than the CTD rebars in corrosion. The CTD reinforcement is not good due to their higher carbon and manganese content. Among the TMT rebars Cu-Cr-TMT has better corrosion resistance, since the role of copper, chromium and nickel in inhibiting corrosion.

Castro et al. (1997) examined three kinds of concrete samples with different w/c ratios of 0.70, 0.50 and 0.46. A parallel series of concrete cylinders were cast, without reinforcement, to study chloride ion penetration. The curing time was 7 days in all cases and then exposed to tropical marine atmosphere for about 5 years. One objective of this program was the applicability of different techniques for measuring suspended electrochemical corrosion to assess long-term concrete durability performance to the direct influence of a tropical marine atmosphere. The method of linear polarization resistance (LPR) technique and electrochemical impedance spectroscopy (EIS) were selected for this study.

Test results showed that during the period of equal exposure, i_{corr} values were generally higher for the reinforced concrete with high w/c ratio compared to low w/c ratio of the concrete, because the permeability of concrete is more in higher w/c ratio.

Kostogloudis et al. (1998) performed experiments to investigate the corrosion resistance of steel-reinforced mortar specimens made from alinite cement along with ordinary Portland cement (OPC) specimens as reference. Specimens were prepared and exposed in three different environments: the exposure continuously suspended in tap water, interrupted exposure in tap water and the interrupted exposure in 3.5% NaCl solution. Weight loss of steel and half cell potential were measured v/s exposure time, up to age of 12 months.

Studies have shown that the duration of exposure in tap water, cement alinite provides adequate protection against corrosion of the steel reinforcement up to 12 months of exposure. In interrupted exposure in tap water, the cracking of chlorides and oxygen leads to higher weight loss values for samples compared to measured alinite OPC. The explanatory interrupted exposure in 3.5% NaCl solution a high rate of corrosion of the steel reinforcement was observed in both alinite and Portland cement mortar. Corrosion was larger in case of alinite cement due to their higher content of chloride.

Yoon et al. (2001) conducted experimental study on beam specimens of size (100 x 150 x 1170mm). Four-point bending (0-75% of the ultimate load) test setup was used for different load levels. Solution of sodium chloride (NaCl) in water was used to accelerate the corrosion process. The study concluded that the failure modes of reinforced concrete beams change from shear failure of the concrete to bond splitting as the rate of corrosion increased. The results show that for a rational service life prediction of reinforced concrete structures, the influence of the service load on the structure performance should be considered in combination with environmental conditions and material proportions.

Wei-liang and Yu-xi (2001) carried out a study to observe the causes of steel corrosion on the flexural strength of reinforced concrete beam. Two series of beams

(150 × 150 × 1140 mm) were prepared. Series-I specimens have a anchor length of 360mm. Beam specimens used in the series-II resembles the series-I used, but with a small anchor length of 100mm. Reproduce the corrosion process, a DC current was applied to the specimen embedded in the concrete, it was immersed in 5% NaCl solution for several days, using integrated system incorporating small current power provided with a in-built ammeter to monitor the current.

From the above discussion, they concluded that the increase in the corrosion of the reinforcement, the mode of beam failure changed from ductile to brittle and distribution of cracks of corroded RC beams was concentrated instead of scattered. Bending strength and rigidity of RC beams decreased with increase of reinforcement corrosion.

Almusallam (2001) experimentally investigated the effect of corrosion rate of reinforcing steel and the mechanical properties of the bars. Reinforcing steel, 6 and 12mm in diameter bars were corroded in concrete specimens, were removed and tested in tension.

It is observed that even with high degree of corrosion, there is no significant change in the tensile strength of the bars using the actual cross section calculated. The steel structures of 12.6% or more corrosion of reinforcements show brittle behaviour. Also, the elongation of bars with 12% or more corrosion is generally less than that specified by ASTM A 615, i.e. 9%.

Andrade et al. (2002) provided information on the rate of corrosion in concrete structures in actual size measured on site. Where the values in the experimental laboratory samples was relatively large. Most of the laboratory experiments on the relative humidity and temperature were controlled in room, even if the weather outside was usually full as seasonal cycles of temperature and day-night. These cycles or natural weathering, influence the relative humidity in concrete and the corrosion rate of the steel.

Four main meteorological processes are known to affect the rate of events due to changes in the hydrothermal condition of concrete against corrosion: (a) the cycles of day and night, (b) seasonal cycles, (c) temperatures extreme and (d) periods of rain. Under the conditions described, is the rain (moisture content of the concrete), which controls the rate of corrosion. Concrete protection against rain, temperature is the aspect of control of moisture content. Resistivity is complete, if no such factors as the oxygen in the liquid from the pores or the amount of oxide in the reinforcing bar, which affects the inverse values of i_{corr} and consequently found the i_{corr} can measure directly, if the calculation of the transmission time needed to corrosion.

Ballim and Reid (2003) carried out an experimental evaluation of the current test methods used to assess the effects of reinforcement corrosion on the serviceability deflections of reinforced concrete beams. Two series of RC beams subjected to corrosion of reinforcements while being tested to maintain a constant load. The test conditions were similar for both sets of tests, except that the constant load, 23% and 34% of the design capacity for the series 1 and series 2 beams. The constant load on load balancer compression spring which is placed on top of the beam to consider the effects of simultaneous load and corrosion on cracking of the beam at very low corrosion test to examine the effects of the load in real time and the corrosion cracking of the beam is applied again. The bottom surface of the beam and the supports in a sealed container (3% NaCl solution) is used as an electrolyte and galvanized steel rod, which acts as the cathode for accelerating the corrosion process.

The results of this investigation show that, in order to better understand the effects of corrosion on structural performance, it is necessary to conduct tests under simultaneous load and corrosion conditions. For the same extent of corrosion, the deflection ratio increased as the magnitude of the sustained load also increased. At a 6.2% extent of corrosion, increasing the sustained load from $0.23P_u$ to $0.34P_u$ resulted in an increase in the deflection ratio from 1 to 1.42.

Li (2003) made observations on the life cycle modelling of corrosion affected concrete structures. This paper made an attempt to present the idea of evaluating the performance of a lifetime of structures located in a marine environment. Study found

that the time required for reinforcement corrosion in marine environment concrete structures is negligible for the test of life and therefore the attempt must be devoted to the effects of reinforcement corrosion on the deterioration of structural investigations.

Soleymani and Ismail (2004) compared the activity of corrosion in reinforced concrete samples using many methods for corrosion measurement. Four methods were regularly selected (TP, LPR, HCP and the chloride content in the concrete) to measure the activity of the corrosion of reinforcing steel embedded in concrete. Concrete cylindrical specimens of 150 x 300mm, a diameter of 13mm rebar embedded in the centre were used for the study. Corrosion of reinforcing steel caused by chloride under controlled laboratory conditions. The samples were subjected to four modified solution of chloride concentrations (0%, 1%, 3% and 5%). The base of each cylinder was kept a waterproof coating, in order to ensure that access of ingress chloride was coming from adjacent circumferential only. To accelerate the corrosion of reinforcing steel, after 28 days of standard curing all samples were exposed to cycles of alternate wetting and drying.

Results of four corrosion testing methods used to study the predicted level of corrosion similar to the samples examined for 24% of corrosion. In cases where the samples include different levels of activity were estimated corrosion, the method of the chloride content is usually lower than the level of corrosion activity while LPR and Taffel methods predict the maximum corrosion activity level. The Half-cell potential method generally estimate the level of corrosion activity fell between estimates given by other methods. While the LPR testing results were 10% to 30% higher than Taffel plot testing results both methods suggested identical corrosion activity levels for more than 96% of the specimens studied.

Poupard et al. (2006) studied corrosion damage analysis of reinforced concrete beam after 40 years natural exposure in marine environment. In addition to visual observation and electrochemical measurements, the total depth of carbonation and chloride content were determined. Physical and chemical measurements confirmed almost chlorine ions are responsible for reinforcement corrosion. The half-cell

potential gradient measurement technique is very effective to locate the corrosion area within a concrete structure. It was observed that the rate of corrosion depends on the level of the tensile stress in the beam and also the possibility of bleeding and settling effect of fresh concrete.

Andres et al. (2007) investigated the effect of corrosion on the flexural strength for small concrete beams ($100 \times 150 \times 1500$ mm). This study shows the results of a test program carried out, the relationship between the deterioration of the corrosion-supported concrete beam and small changes based on an accelerated corrosion methodology. Concrete beams with chlorides were used in the study. Additional acceleration of the corrosion was performed by applying a current stable 80 μA/cm^2 nominal anode of about 50 to 180 days. Therefore, the beams were tested in flexure under three-point bending. The average corrosion penetration X_{AVER}, the maximum crack width of the concrete CW_{MAX} and maximum reinforcement pit depth PIT_{MAX}, were estimated for each corroded beam using gravimetric metal loss procedure.

The results showed that the residual load capacity ratio (Ratio of capacity for corroded elements to the capacity for the non-corroded specimens), reduces by 30% to 40%, respectively. Besides this, if the corrosion is highly localized (with deep pits) the remaining load capacity ratio reduced by 60% of its design value.

In the study by Vidal et al. (2007) 36 reinforced concrete beams ($280 \times 150 \times 3000$ mm) were cast, and then were placed in service load under chloride environmental considerations impact bending cracks. At different stages beam experimental study conducted to measure the the development of flexural and corrosion cracking, to measure chloride content and to analyze the evolution of the mechanical behaviour. In aggressive environments by spraying salt spray (sodium chloride 35g/l of salt water equivalent to concentration of sea water) was created. After six years of storage, the beam has been exposed to wetting-drying cycles to accelerate the corrosion process.
The results show that the structural performance in service load is, the flexural strength was mainly influenced by corrosion of reinforcing steel due to reduction of the cross-section of steel and steel-concrete bond.

Val (2007) conducted a study to determine the cause of corrosion on the reinforcing steel with respect to bending and shear strength. Study also investigate the reliability of reinforced concrete beams. The results showed that the corrosion of the stirrups, especially pitting corrosion, had a great influence on the reliability of reinforced concrete beams.

The study examined the cause of pitting and general corrosion about the reliability of reinforced concrete beams. Two possible failure modes were considered in bending and shear. The results show that the analysis of the performance of the concrete beams in corrosive environments should include the effect of corrosion of stirrups on the shear strength of a beam, if not then considerably overestimates the reliability of the beam.

A comprehensive numerical simulation system was proposed by Maruya et al. (2007) to solve the problem of corrosion of steel in concrete by the decomposition of reinforced concrete structures in chloride contaminated environment. The distribution of the amount of corrosion and the rate of corrosion along the reinforcing bars were estimated from models of macro cell, the circuit includes micro cell. The models were quantified in terms of the effects of exposure experiments under two environments, a cyclic drying and wetting in a laboratory and another in a splash zone located offshore.

The results showed that the comparison of the half-cell potential as a function of time, the location of corrosion and the amount of corrosion that indicates the qualitative coincidence between the results of the numerical simulation and experiment.

Manoharan et al. (2008) conducted experiments to study effect of water-reducing admixtures and waterproofing experiments using commercially available additives in reinforced concrete structures dissemination of results of corrosion. Size of 150mm concrete cube was used to investigate. M25 grade concrete, four different percentages (0.5%, 0.75%, 1.0% and 1.25%) was cast using two different admixtures. A 100mm

long TMT bars embedded in the concrete of cover 25mm. After 28 days of conventional curing the cubes were ponded in 3% sodium chloride (NaCl) solution on one side of the cube to keep the penetration of chloride unidirectional. To accelerate corrosion, other wetting and drying were carried out periodically. The studies conducted on the specimens were Electrochemical Technique (AC Impedance), Gravimetric Technique.

The results revealed that the corrosion rate of concrete admixeture decreases with time with respect to the concrete without admixture. The performance of waterproofing admixture was effective at higher rates compared with respect to the lower percentages of admixture. Also the efficiency of the water-reducing admixture in corrosion resistance was high in relation to the water proofing admixture. TMT bars were found to perform well in concrete with admixture compared to concrete without admixture.

Apostolopoulos and Papadakis (2008) studied the additional effects of corrosion on the tensile behaviour of reinforcing steel bars which were used in the structures during the period of 1960–1990 in Greece. Samples were corroded by laboratory salt spray test for various exposure times. The tensile properties of the corroded materials were compared against the requirements set in the standards for involving steels in reinforced concrete structures. Retrieved from accelerated corrosion tests on bare steel bars were compared with the results from steel bars embedded in the aged concrete.

Salt spray exposure of more than 20 days, the tensile strength was reduced by 14%. The experimental test results of accelerated corrosion of bare steel bars embedded in good qualitative agreement with the results of the steel bars in the old concrete. It was also observed in both cases that bars subjected to corrosion resistance may have a loss of medium strength but significant loss in ductility.

Ortega and Aveldano (2008) carried out experimental study on reinforced concrete beams subjected to mechanical stresses and simultaneously affected by a corrosion process of their reinforcements. The corrosion process was galvanostatically

accelerated by applying a certain current density to a limited area of the reinforcements, which were under constant wetting with a solution of sodium chloride. The influence of the different degrees of tension in the process of reinforcement corrosion was analyzed through electrochemical monitoring, the cracking advancement in the concrete cover and the loss of base material in the bars.

Observations showed that the loaded beams exhibited cracks that advanced more quickly than in unloaded beams. A clear increase of the cracking with the increased rebar stress was verified. In this case, where concrete is in tension, its variation followed a linear behaviour. When the load on the beams increased, the variation of the maximum cracking widths presented a clear increase in time. The first cracks appeared earlier in the loaded beams than in the unloaded ones. This fact, as well as the increase in cracking areas and maximum cracking widths, reaffirmed that stresses in the reinforcements speed up the effects of the corrosion. The increase in rebar stress appeared to have influence in the delay of pseudo-passivation, as long as the flexural cracking load was not reached. When that limit was crossed, more passive potentials were obtained. A direct relationship between the affected area and the acting stress in the bars was not found for loads below the flexural cracking load; however, once said load was surpassed, the corrosion extension was much larger, in the most heavily loaded beams.

The experimental study was provided by Revathy et al. (2009) on RC columns (150mm diameter and 900mm in height.) with reinforcement Corrosion, assessing the residual strength and ductility of the column performance. In this study, the samples were subjected to 0, 10 and 25% of the corrosion rate. All samples were then tested for their performance in uniaxial compression test. The technique of accelerated corrosion was conducted by applying a current source having an output of 32 Volts and 11 Amps. High voltage was used to accelerate corrosion and reduce the test time. The columns were immersed in 3.5% NaCl solution for one day to ensure complete saturation.

Studies have shown that the ultimate strength was decreased by 3% to 12% for 10% to 25% of the column is reduced to corrosion. The deflections of the columns reduced with increasing the reinforcement corrosion, which leads to a decrease in the ductility of the columns. Reduction of ductility found to be 1.5% to 9% respectively for Columns subjected to 10% to 25% of corrosion rate. Corroded columns performed less lateral strain to their corresponding stress levels. This would be due to the decrease in cross-sectional area of the steel reinforcement.

Ahmad (2009) provided technical information for the induction of accelerated corrosion of steel in concrete. In the paper, an effort has been made to explain the impressed current technique is often used to accelerate steel corrosion in small as well as large size concrete specimens. Studies suggest that the proposed alternative method could be used to accelerate the steel corrosion.

Melchers and Li (2009) investigated the corrosion of reinforcing steel exposed in marine environment. In some cases in practice corrosion has been observed to commence already within a few years of exposure even with considerable concrete cover to the reinforcement and apparently high quality concretes. However, there are a number of other cases in practice, for which corrosion initiation took much longer, even if the quality of the concrete cover relatively small and modest concrete. Many of these structures showed acceptable long-term performance of the structure, despite the high level enhancement in chloride concentration limits.

Observations have shown that blast furnace cement concrete have corrosion durability properties. The data also strongly recommended to prepare the concrete with limestone or dolomite aggregates or other non-reactive form of a high level of calcium carbonate are favourable reinforcement corrosion properties. Both corrosion initiation and significant damage were delayed. For reinforced concrete structures exposed to the marine environment in the information provided here show that the corrosion initiation time was not strongly dependent on the concentration of chloride reported.

Malumbela et al. (2010) studied the tensile deformed steel reinforced concrete beams (153 × 254 × 3000 mm) by considering different levels of sustained load and two different corrosion processes (wetting process for 4 days and drying cycle for 4 days and corrosion process of four days wetting cycle and two days drying) as the main variable factor. Tensile strength of the reinforcing steel beam has been artificially corroded in a local area in its middle portion corresponding to a length of 700mm. Partial length corrosion of steel tension rods was created around the area to corrode through the construction of a pool with 5 mm thick polyvinyl chloride.

The results showed that the highest level of the corrosion takes place, which had longer drying cycles and the sustained load has little effect on the corrosion rate. The ultimate moment capacity decreases linearly with the extent of corrosion and maximum weight loss for each 1% of the steel, there was a corresponding 0.7% reduction of the ultimate capacity of beams.

Ismail et al. (2010) discussed about the long-term weather resistance movements caused by the deterioration of reinforced concrete structures. Compressive strength of reinforced concrete structures and prototype steel corrosion has developed six years of destructive and non-destructive testing, including periodic coring, compressive strength, resilience, ultrasonic pulse velocity, half-cell, carbonation, and tensile strength tests were monitored. Prototype structural elements show that in the case of an abandoned situation built in an open space. Structure which consisted of slab specimens of 1500mm length and 1000mm width and 150mm thick and the columns were of size 150 × 150mm with a height of 600mm. All reinforcing bars were mild steel and 10mm in diameter.

According to the preliminary investigation of the compressive strength development, especially in the first 28 days was normal, but turned out to be slow until 32.1MPa peaks reached in the whole year. Beyond this limit, the gradual reduction in the next two years was observed and recorded a loss of much higher strength by about 27.6% at 6 years.

Zhang and Ba (2011) conducted experiments on accelerated testing of concrete in a chloride environment with migration equipment for chloride ions. The concentration of chloride in the anode compartment has been improved a linear relationship with time and the test for a certain stage. Study concluded that the life of 10mm in concrete cover in chloride environment is between 11.89 and 12.45 years.

2.3 CRACK PATTERN OF CORRODED RC BEAMS

Alonso et al. (1998) introduced a new concept for the quantification of the ratio of reinforcement corrosion and cracking of the cover. The variables studied were the cover/diameter ratio, proportions of cement, water/cement ratio, cast position of reinforcement and corrosion rate. The corrosion is caused by applying stable currents to accelerate the reinforcement to act as anode. Study showed that the loss of the reinforcement radius losses of 15-50μm was required to produce a crack width of 0.05 to 0.1 mm.

Vu and Stewart (2002) investigated the possibility to study the cracking and spalling of the concrete cover structure exposed to the aggressive environment. In time corrosion cracking/spalling was done experimentally, RC slabs were tested from accelerated corrosion test to measure the quality of concrete (w/c ratio or strength), concrete cover, the relationship between crack propagation and time. The possibility of cracking and spalling of the protective layer of concrete was considered to be deteriorated by the use of life cycle model of structural reliability.

The results showed that the proportion of reliability model can be used to predict the concrete surface may spall for any reference period.

Vidal et al. (2003) made observations to introduce a set of relationships linking the distribution of reinforcement corrosion and the crack width that results from corrosion. Study concluded that crack initiation depends on the cover/diameter ratio and bar diameter.

Li et al. (2005) presented methods for determining the corrosion induced cracking process of reinforced structures in an analytical manner and a theoretical model was derived. The model was directly related to critical factors namely the corrosion rate, the concrete geometry and property. Study concluded that the model could predict corrosion induced crack width with reasonable accuracy.

Li et al. (2007) introduced a new method for predicting the theoretical time to cause a deterioration of the concrete due to corrosion of reinforcing steel. The method was based on fracture mechanics and its deterioration as the criterion for crack width of concrete. The corrosion rate was the most important factor which affects the time to concrete deterioration. The proposed technology compared with the test results and empirical model a good agreement obtained. Study showed that the method presented in the paper can predict the time to corrosion-induced deterioration of concrete with adequate accuracy.

Boutz et al. (2008) proposed a model for reproduction of digital penetration of chloride ions in concrete structures in different weather conditions that predict the result of maintenance work in the life of the structural concrete. The transport mechanisms of chloride ions (free), both diffusion and convection through the pore water. This requires a superior model for moisture transport both saturated and unsaturated area. In the case where the surface of the concrete structure in contact with liquid water, the speed is controlled by the front of the saturated zone due to the balance between absorption and scattering.

Val et al. (2009) provided information about the corrosion caused by crack formation and propagation studying them experimentally and numerically. FE model was first described briefly and confirmed with the available experimental data. The results showed that the amount of the corrosion products penetrating from the concrete before crack initiation was more. The cracks are filled slowly with time, and the thick concrete cover required more time to completely fill a crack. These preliminary results indicate that more experimental research is needed.

Malumbela et al. (2010) introduced a new concept for the experimental study of reinforced concrete corrosion related to rate of widening of cracks in RC beams (153 × 254 × 3000 mm) that were subjected to corrosion rate at different levels of sustained load. The results obtained indicate that the expansion of each corrosion cracking depends on the overall rate of corrosion crack pattern. 1% of the mass loss of steel was found to introduce corrosion crack width of about 0.04 mm.

Balafas and Burgoyne (2010) discussed the environmental conditions, wherein the concrete cracking occurs due to the production of rust pressure cause on the surface of the stainless steel. To find out this time, the volume of concrete compatibility was assumed, which approved the compaction of all materials under pressure, including compaction of rust itself. The concept was also used in fracture mechanics for signal cover failure.

Study found that the cracking cover period was a function of rust production system. The corrosion rates were higher in late autumn and in the early spring. On the other hand the highest resistance of the system to corrosion production was during summer, since the humidity levels reach low values. Therefore, structures with humidity levels close to 90% and high temperatures gave the shortest times to cover failure. Moreover, the structures exposed to humid summer would experience producing high rust and fast cover spalling.

2.4 FEM MODELLING OF RC CORRODED BEAMS

Damian et al. (2001) investigated the general behaviour of finite element models represented by load deflection values in the mid-span, which showed good agreement with test data. However, finite element models have shown a little stiffer than the test data for the linear and nonlinear regions. Bond-slip (between the concrete and steel reinforcement) and the impact of micro-cracks occur in the actual beam was excluded in the finite element model and promote a higher stiffness for finite element model. The first cracking load was more in ANSYS compared to experimental data. This was probably because the relative homogeneity of the finite element model based

compared to real heterogeneity of beams which contains micro-cracks. The final loads of experimental results were 5% more than FEM results. This may be due to the inclined portion of the reinforcement, ignoring the effect of the concrete toughening mechanisms and the assumed materials property values used, rather than the measured value. The crack pattern for the final loads from the FE model corresponds well with the failure modes observed in experimental beams.

Table 2.1 Comparison between experimental and Numerical results (Damian et al. 2001)

	Experimental	Numerical
Load at First Crack (kN)	78.3	104.5
Load at Failure (kN)	476	454

Wolanski (2004) investigated and analyzed RC beams using the finite element analysis. From the finite element method load deflection plot was found to be good match with the experimental results.

Table 2.2 Comparisons between experimental and Numerical results (Wolanski 2004)

	Experimental	ANSYS
Load at First Crack (lb)	4500	5216
Load at Failure (lb)	16310	16382

Parande et al. (2008) made observations on the structural performance of corroded and non corroded RC beams with a finite element model in three dimensions. Non linear finite element analysis with ANSYS was performed. Solid65 and Link8 elements correspond to concrete and steel reinforcing bars. Based on each of the actual characteristics of the component, the material properties for the both non-linear elements have been defined.

In this study with M20 concrete beam specimens were cast and tested for bending strength. ANSYS predictions and field data to assess the terms of the deflection, stress, strain and cracks in concrete were made. Satisfactory results were observed.

Saether and Sand (2009) provided information on the application of FE analysis to simulate the mechanical behavior of reinforced concrete with corrosion of steel bars using the FE program DIANA. Since the corrosion effects were taken into account, the loss of steel bar section and reducing the connection between the deteriorated concrete and corroded reinforcement have considered in this work.

The results show that the simulation validation study was limited to medium-sized beams and based only on test results published earlier. From the FE simulation the failure load of the beam was considered to be in good agreement with the experimental value.

Ibrahim and Salman (2009) adopted numerical solutions using ANSYS to evaluate the ultimate shear strength of reinforced concrete beams, with FRP laminates in simple, cheaper and rapid way compared with experimental full scale test. The general behaviour of the finite element models shows good agreement with observations and data from large-scale experimental beam tests. The addition of the FRP reinforcement to the control beams shift the behaviour of the control beams from shear failure near the ends of the beam to bending failure at the centre of the beam. The results obtained demonstrate that carbon fibre polymer was efficient more than glass fibre polymer in strengthening the reinforced concrete beams for shear. The finite element model can be used for further research to design rules extended to strengthen reinforced concrete structures with FRP laminates.

Table 2.3 Comparisons between experimental and Numerical results (Ibrahim and Salman 2009)

Beam	Ultimate load (kN)	
	Experimental	Numerical
Control Beam	69	66
Beam Strengthened using CFRP	125	119
Beam Strengthened using GFRP	116	107

Chanaswat et al. (2009) developed three-dimensional FE model to simulate the behaviour of full-scale reinforced concrete beams strengthened with fibre reinforced polymer sheets. The FE models showed qualitative trends in the observations with full scale beam test. Stress-strain curves showed a local and general behaviour of selected locations FEA showed good agreement with experimental data. Load - deflection curve across the finite element model has a similar trend for those from the experimental beam, but the FE models were slightly stiffer than the experimental results in both linear and nonlinear regions. Models crack at the ultimate load of the FE models correspond well with the experimental beam failure modes. FEA end loads are lower than the experimental end loads from 6% to 18%.

Phuvoravan (2010) made observations on the effect of rate of corrosion of steel in bending behaviour of reinforced concrete beam for nonlinear finite element analysis. Concrete was modelled as three dimensional volume elements, while all steel reinforcements were represented by the truss elements with non-linear characteristics for both materials.

The finite element analysis used to be reliable in bending of RC beams with different levels of reinforcement corrosion. It has also been found that the corrosion of the reinforcements in the central portion of RC beam, the percentage reduction in the moment capacity was approximately same as that of total percentage of the corrosion, corrosion of reinforcements along entire length of the RC beam, the percentage reduction in moment capacity was significantly higher than the rate of corrosion.

Vasudevan et al. (2011) studied the concrete structure characteristics; mesh density, use of steel cushions to support and loading point, the effect of transverse reinforcement on bending behaviour, convergence criteria and the impact of percentage of reinforcement in RC beams with ANSYS. In the vicinity of the first cracking stage and the steel yielding stage lower convergence limits have been used for the accurate prediction of behaviour. The total load is divided by the number of suitable load step (load increment) were analyzed to obtain a smooth load-deformation curve. To predict the flexural behaviour of the total deflection steel cushions may not required. However, the detailed study of stress concentration in the

loading position and the support, the steel cushions was incorporated. The initial cracking behaviour does not change with percentage of reinforcement. Tension and shear reinforcements were precisely incorporated in discrete modelling techniques, in order to obtain a more precise behaviour.

Saifullah et al. (2011) presented non-destructive testing of simply supported beams in the laboratory and load-deflection data were recorded. The FE analysis of ANSYS, SAS 2005 performed by using the same material properties. Ultimately, both computer modelling and experimental data results compared. From the comparison, it was found that computer modelling can be an excellent alternative to destructive testing laboratory with acceptable variation of the results. In addition, conducted a survey analysis for a beam with ANSYS, SAS 2005, with a different proportion of the reinforcements (under, balanced, over). Observed mainly in the performance of reinforced concrete beams at different points of interest and then tabulated and compared. Based on observations, it was shown that the first Cracking takes place in 0.43L to 0.45L from the support. Maximum deflection at failure was also observed for the beam that had balanced reinforcement.

Table 2.4 Comparisons between experimental and Numerical results (Saifullah et al. 2011)

	Load (lb)		Deflection (in.)	
	Experimental	Numerical	Experimental	Numerical
At First Crack	2633	2702	0.065	0.032
At Failure	5250	6690	0.2402	0.374839

Pan and Wang (2011) analyzed the reinforcement corrosion and chemical attacks lead to premature debounding of steel mortar, concrete cracks and sudden failure of structures, if it was not well attended. In practice the conventional heterogeneous concrete treated as a homogeneous medium, is often seen in the development of the penetration of chemicals and cracking of the concrete need to be determined. This hypothesis caused prediction and assessment of the structure life significantly inaccurate.

This study presents three key steps in the life of reinforced concrete structures designed to assess the finite element model: Chemical entrance, steel corrosion and concrete cracking. Mass conservation principle was applied in a variety of chemical species model into the first step in the application becomes saturated heterogeneous concrete matrix. By using Faraday's law, steel corrosion and produces radial expansion and then formulated into instantaneous displacement boundary conditions for subsequent analysis of concrete cracking. Crack patterns expansion force under the action of concrete corrosion products, characterized by the use of cohesive-fracture approach. Finite element model was validated with laboratory experiments and good agreement was observed.

Xiaoming and Hongqiang (2012) carried out on the load carrying capacity of corroded reinforced concrete beams using ANSYS finite element investigation. In these FE models, element of Solid 65 was used for concrete, element of Link 8 was used for bars and element of Combin 39 was used to simulate the bond and bond slip between bars and concrete. In addition to reduction of cross-sectional area of the bar and lowering the bar yield stress was also considered for load carrying capacity of corroded reinforced concrete beams with different corrosion rates. The study concluded that due to increase in corrosion rate will reduce the stiffness of corroded beams, with an increase of corrosion in RC beams failure changes from ductile to brittle.

Coronelli et al. (2013) provided information on cover cracking, spalling and degradation occur in the many corroded reinforced concrete structures. Prior studies of corrosion leads to make the main concern along the reinforcement cracking, but often overlooked stirrup corrosion. Corrosion phenomena, including corroded stirrups studied experimentally. A high level of corrosion reached for the main bar up to 20% and 34% of the stirrups. Crack initiation, propagation, and cover delamination occurred were examined. Accelerated corrosion technique was used in specimens; when a current was applied, keep the current density as low as practically possible for the duration of laboratory tests.

The results on the crack pattern and width were analyzed, showing the differences between samples with or without the stirrups. Finally, the effect of corrosion and the extent of the corrosion products in a finite element model, the result was mainly crack pattern and width were compared with test results. Numerical finite element model was used to simulate the test. The results correspond to the experimental observations, with close reproduction of crack pattern and provide a good interpretation of the results.

2.5 SUMMARY

Considerable research has been devoted to study the corrosion of reinforcement in reinforced concrete dealing with various issues related to corrosion process, its initiation and damaging effects. After the review of available literature and noting the areas where further work is needed, the following conclusion can be drawn;

- Ultimate load carrying capacity, deflection and stiffness of the RCC elements are reduced with increase in the degree of corrosion.
- Reduction in cross section of reinforcement, yield strength and cracks along the reinforcement are the main contributing factors for strength degradation of RCC element.
- As the degree of corrosion increases, the beam failure mode changes from ductile mode to brittle mode.
- To accelerate the corrosion process, generally current is impressed in the specimens immersed in electrolyte made with 3.5-5% NaCl mixed in water.
- Salt spray method or alternate drying and wetting may also be used for induced corrosion.
- Small level of sustained load has little effect on rate of corrosion.
- The results of an accelerated corrosion tests on bare steel bars are in good qualitative agreement with results from steel bars embedded in aged concrete.
- Various models have also been proposed for computing the service life of the RC member with corroded rebar, considering various aspects of corrosion. It

has been observed that in all the experiments conducted for validating the models, corrosion has been induced through impressed current technique.

- Collapse of beams occurred through either diagonal tension failure of the concrete in the shear span or flexural failure through crushing of concrete.
- Corrosion of stirrups, especially pitting corrosion, has a significant influence on the reliability of reinforced concrete beams.
- The failure mode of the reinforced concrete beams appeared to shift from a shear failure of concrete to bond splitting as the degree of corrosion increased.
- Several studies have been conducted to find out the flexural strength of beam specimens, both experimentally as well as using various FEA softwares, Such as ANSYS.
- Finite element analysis could be used to realistically predict the flexural behaviour of reinforced concrete beams having various reinforcement corrosion levels.

CHAPTER 3

EXPERIMENTAL DETAILS

3.1 TEST PROGRAM

Sixteen reinforced concrete beams with Ordinary Portland Cement (OPC) and sixteen reinforced concrete beams with Portland Pozzolana Cement (PPC) of dimension 300mm x 400mm in cross section and 2150mm length were cast. The behaviour of reinforced concrete beams, under 2.5%, 5.0%, 7.5% and 10% corrosion were studied. Five beams were cast as control specimen (non-corroded beams) for each type of cement.

The details of experimental programme, materials used and method of testing are explained in following sections.

3.2 MATERIALS

The materials used for the experimental investigation were as follows.

- ➢ Cement
- ➢ Fine aggregates
- ➢ Coarse aggregates
- ➢ Water
- ➢ Reinforcing steel

All the materials used for the experimental work were tested as per the codal provisions.

3.2.1 Cement

OPC (43 Grade) and PPC conforming to IS 8112: 1989 and IS 1489 (Part-I):1991 respectively were used in the present investigation. They were tested as per IS

4031:1988 recommendations for the cement. The results are confirming with the requirements of IS code. The results are tabulated in Table 3.1 and Table 3.2.

Table 3.1 Test results on OPC

Sl.No.	Test Parameters	Results	As per IS 8112:1989 (Specifications of 43 Grade OPC Cement)
1	Setting time		
	Initial	70min	Not less than 30min
	Final	250min	Not more than 600min
2	Specific gravity	3.14	
3	Compressive strength		
	7 days	36.41MPa	Not less than 33MPa
	28 days	45.84MPa	Not less than 43MPa

Table 3.2 Test results on PPC

Sl No	Test Parameters	Results	As per IS 1489 (Part-I):1991 (Specifications of Portland Pozzolana cement)
1	Setting time		
	Initial	65min	Not less than 3min
	Final	250min	Not more than 600min
2	Specific gravity	2.92	
3	Compressive strength		
	7 Days	25.51MPa	Not less than 22MPa
	28 Days	39.84MPa	Not less than 33MPa

3.2.2 Fine Aggregate

Aggregates are the most important constituent in concrete. An aggregate provides shape to the concrete, reduces shrinkage and affect economy. Fine aggregates

normally consist of natural sand or crushed stone with sizes smaller than 4.75mm but larger than 0.075mm. Physical tests on fine aggregates confirming to IS standards were conducted. The results are tabulated in Table 3.3 and Table 3.4.

Table 3.3 Test results on fine aggregates used for OPC concrete mix

Characteristics of fine aggregate (natural river sand)		
1	Specific gravity	2.60
2	Water absorption	2.61%
3	Moisture content	2.0%
4	Grading	Zone-II

Table 3.4 Test results on fine aggregates used for PPC concrete mix

Characteristics of fine aggregate (natural river sand)		
1	Specific gravity	2.60
2	Water absorption	2.0%
3	Moisture content	2.0%
4	Grading	Zone-II

3.2.3 Coarse Aggregate

Coarse aggregates were in sizes greater than 4.75mm, but in general range between 9.5mm to 37.5mm in size. The size of the aggregate used was 20mm downsize and 12.5mm down size angular type coarse aggregate. Physical tests on coarse aggregates were conducted. Test results and sieve analysis are tabulated in Table 3.5 and Table 3.6.

Table 3.5 Test results on coarse aggregate of 20mm down size used for OPC mix

	Characteristics of coarse aggregate of 20mm down size	
1	Specific gravity	2.66
2	Shape	Angular
3	Water absorption	0.5%
4	Moisture content	Nil

Table 3.6 Test results on coarse aggregate of 20mm down size used for PPC mix

	Characteristics of coarse aggregate of 20mm down size	
1	Specific gravity	2.66
2	Shape	Angular
3	Water absorption	0.5%
4	Moisture content	Nil

3.2.4 Water

Water is an important ingredient of concrete, which is responsible for hydration of the cement, resulting in concrete strength gain. Fresh water is used for pouring concrete beams.

3.2.5 Reinforcing steel

Thermo Mechanically Treated (TMT) Fe-415 steel bars were used as reinforcing steel. Tensile strength of reinforcing steel bars was tested using Universal Testing Machine (UTM). The stress-strain curves for the 12mm, 16mm and 20mm steel bars were obtained by plotting the tension test data. Typical stress-strain curve for 20mm bar is shown in Fig. 3.1 and the values of yield strength and ultimate strength of all the bars are presented in Table 3.7.

Table 3.7 Yield and ultimate strength of TMT Fe-415 bars

Diameter of Bar (mm)	Yield Strength (MPa)	Ultimate Strength (MPa)	Percentage of elongation(%)
12	470	540	23
16	470	550	23
20	480	540	21
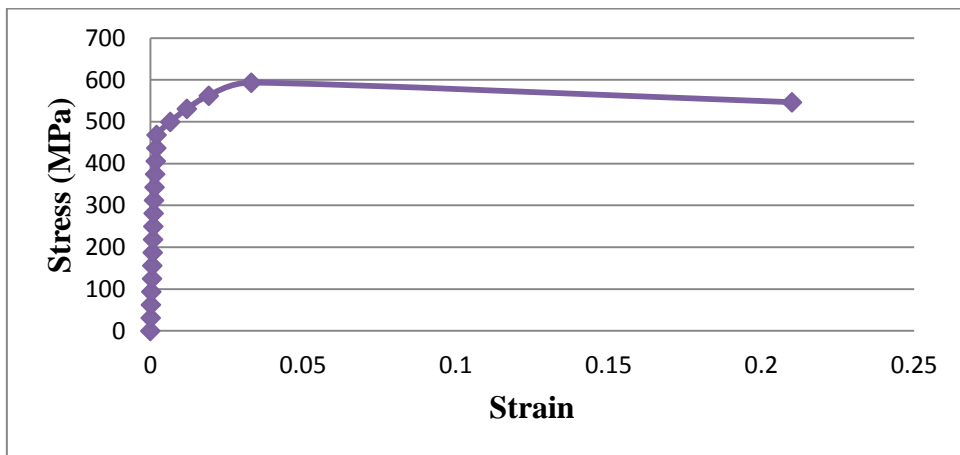
Fig. 3.1 Stress-strain curve for 20mm dia TMT Fe-415 reinforcing steel bar

3.3 CONCRETE MIX DESIGN

Ready Mixed Concrete (RMC) was used in the casting of the specimens as work would require large amount of concrete. Based on the properties of the concreting materials, many trials of mix designs were carried out in the laboratory by varying the cement content, water cement ratio and amount of admixture to get the slump in the range of 80-120mm and strength in the range of 20MPa (Shetty 2010).The details of mix design constituents and trial mixes for OPC carried out to determine the optimum mix proportion are tabulated in Table 3.8 and Table 3.9. Also the details of mix design constituents for PPC are tabulated in Table 3.10.

The concrete mix for M_{20} Grade was prepared as per IS 10262:1982 (2009) which is given in Appendix I and Appendix II.

Table 3.8 Mix design constituents of OPC concrete

Ingredients	Quantity
Cement	320.00kg/m^3
Fine aggregate	704.72kg/m^3
Coarse aggregate	1176.35kg/m^3
Water	164.80kg/m^3
Admixture	0.7 % weight of Cement
Mix Proportion C : F.A : C.A : W	1 : 2.20 : 3.67 : 0.50

Table 3.9 Trial mixes of OPC concrete

Designation	Cement Brand	Cement Content (kg/m^3)	Mix Proportion C:F.A:C.A	W/C ratio	Admixture (% of cement content)	Slump (mm)	Average 28 days strength (MPa)
A1	ACC	320	1: 2.26: 3.75	0.45	0.4	75	32.0
A2*	ACC	320	1: 2.24: 3.67	0.50	0.7	90	28.9
A3	ACC	340	1: 2.09: 3.49	0.45	0.6	100	32.7
A4	ACC	340	1: 2.04: 3.40	0.50	0.6	95	30.36
J1	JK	320	1: 2.29: 3.70	0.45	0.4	70	31.4
J2*	JK	320	1: 2.27: 3.65	0.5	0.7	80	29.3
J3	JK	340	1: 2.13: 3.44	0.45	0.6	90	30.07
J4	JK	340	1: 2.1: 3.36	0.5	0.6	80	29.6

* Mixes recommended for beams preparation

Table 3.10 Mix design constituents of PPC concrete

Ingredients	Quantity
Cement	330kg/m^3
Fine aggregate	817.01kg/m^3
Coarse aggregate	976.03kg/m^3
Water	169.95kg/m^3
Admixture	0.7 % weight of Cement
Mix Proportion Ratio C : F.A : C.A : W	1 : 2.45 : 2.95 : 0.50

3.4 PREPARATION OF SPECIMEN

Reinforced concrete cantilever beams of cross section 300mm x 400mm and 2150 mm in length were cast, with a clear span of 1750mm and bearing length of 400mm. Beams with an effective cover of 30mm were designed as per IS 456:2000. Beams were provided with two 20mm diameter and one 16mm diameter at top and same reinforcement was provided at bottom. Shear reinforcement of 12mm diameter bars with a spacing of 150mm c/c for a length of 1350mm from the free end and 12mm diameter bars with a spacing of 75mm c/c for remaining 800mm length of beam was provided. The shear reinforcement was provided to ensure that flexure failure would dominate over shear failure, as shown in the Fig. 3.2. Beams were prepared with concrete made of OPC and PPC. Two series of beams were cast: Series I beams of OPC concrete and Series II beams of PPC concrete. Before placing the concrete in the beam moulds, the ends of electrical wires were soldered to both ends of the main tension reinforcement bar. These wires were held in place such that it exited from the top face of the beam. At the free end, one yellow colour, multi-strand copper wire of 4mm^2 cross sectional area was connected to each reinforcement bar, which was used to pass the electric current. Similarly at a distance of 300 mm from the fixed end, one red colour, multi-strand copper wire of 2mm^2 cross sectional area was connected to

each reinforcement bar as shown in Fig. 3.3 which was used for continuous monitoring of the corrosion rate.
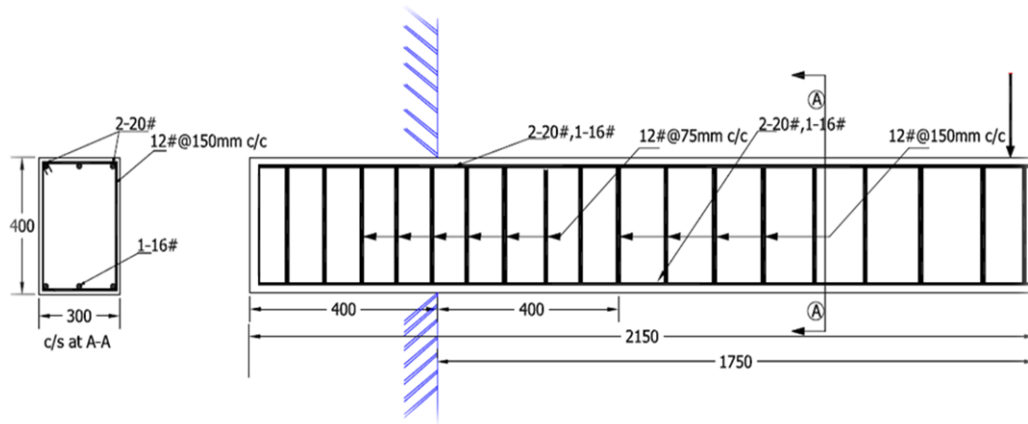
Fig. 3.2.Reinforcement details of beam specimen

Fig. 3.3 View of reinforcement details of beam specimens

3.4.1 Casting and curing of the test specimens

Casting of 42 beam specimens were carried out in 3 batches. Six concrete cubes were also cast from each batch of concrete mix to determine the corresponding compressive strength. In first two batches of concreting, 21 OPC beam specimens were cast using the Ready Mix Concrete. The PPC specimens were cast with in-situ concrete. The moulds were filled with concrete in three layers. After placement of each layer, the

concrete was vibrated with needle vibrator to ensure proper compaction as shown in Fig. 3.4.

(a)　　　　　　　　　　(b)

(c)　　　　　　　　　　(d)
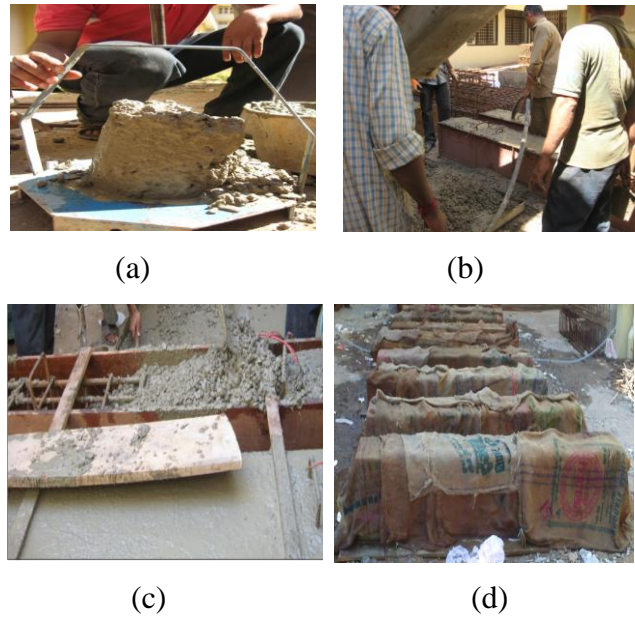
Fig. 3.4(a),(b),(c) and (d) Casting and curing of beam specimen

3.5 COMPRESSIVE STRENGTH OF CONCRETE

The average values of 28-day compressive strength of concrete, f_{ck} for each batch are shown in Table 3.11. It is observed that f_{ck} values varied from batch to batch, despite the use of same mix proportions, same materials and similar casting procedure.

Table 3.11 Average compressive strength of concrete after 28 days

Batch number	28 days average compressive strength of concrete (MPa)	
	OPC	PPC
First Batch	26.66	24.23
Second Batch	25.78	23.77
Third Batch	26.87	24.65

3.6 ACCELERATED CORROSION

Under natural conditions, the development of steel corrosion is very slow. Thus, laboratory studies need to accelerate the corrosion process, in order to achieve a short test period. This can be accomplished by applying a constant potential or an electric current of constant magnitude to the embedded steel. In accelerated tests, chloride penetration is enhanced by ion migration; corrosion rate is increased by an electric field on steel surface (Care and Raharinaivo 2007).

It is not easy to achieve a significant degree of reinforcement corrosion in a limited duration can be used to perform research studies include,

- Assessments due to corrosion of reinforced concrete structures load carrying capacity loss.
- Estimate the effectiveness of the prevention of corrosion of reinforcing steel used in electrochemical technology.

For this purpose, different techniques are available for the induction of accelerated corrosion of steel reinforced concrete (Ahmed 2003).

Accelerated corrosion tests may be incorporated by impressing the current between the steel in the concrete and a working electrode to study the processes of corrosion which are leading to cracking in concrete. In this practice, the samples which were made of concrete, reinforced with steel, will be immersed in a solution containing or not containing chlorides. The critical time relative to the occurrence of corrosion can be used in different ways by reducing the half-cell potential of steel or potential drop between embedded steel and a counter-electrode. These parameters represent the critical moments very similar and are related to the development of corrosion products and micro cracking. However, accelerated corrosion lead to the formation of cracks and corrosion of the bar, it differs considerably from the actual corrosion structure, in terms of speed and performance.

The corrosion in existing structures in natural corrosion process was very slow and therefore; although the bars will corrode and develop; Cracks may not always form in the surrounding concrete because of concrete creep and shrinkage. Another difference lies in the fact that in galvanostatic corrosion, the reinforcement was forced to corrode by impressing direct current and this result in all the reinforcing bars becoming anodic to external cathode stainless steel plate. This generally implies almost uniform corrosion rate (Zhang and Ba 2011). This might not be the case in a natural corrosion, the variation of the degree of rebar corrosion, depending on several factors, such that its distance from the concrete surface, moisture and salt content in the surrounding medium. However, it has by some researchers that the cracks formed by accelerated corrosion are quite similar to those formed during exposure tests detected. This justifies the choice of the accelerated corrosion induction method to cause a significant amount of corrosion in a short span of time in laboratory tests (Ortega and Aveldano 2008).

3.6.1 Accelerated corrosion technique

In the present study electrochemical corrosion technique was used to accelerate the corrosion of steel bars embedded in concrete. Direct current was impressed on the bar embedded in the specimens using an integrated system incorporating a small direct current power supply with an in-built ammeter, with an output of 64V and 10A, to monitor the current. After specimens were immersed in 5% NaCl solution for a day to ensure full saturation condition, the direction of current was arranged so that the steel bars in the specimens serve as the anode and a stainless steel plate is placed in the tank which acted as cathode. This arrangement was to ensure uniform corrosion current over the entire length of the bar in series with a constant current distribution. A schematic representation of the test set-up is shown in Fig. 3.5(a). To obtain the required levels of reinforcement corrosion, the electrifying time and current intensity need to be controlled (Andrade and Alonso 1996). Special care was taken to prevent full submergence beams in the solution, and a 10mm gap was maintained above the NaCl solution level as shown in Fig. 3.5(b). If the beams get fully submerged, the power would flow through the solution and no corrosion would occur within the beam.
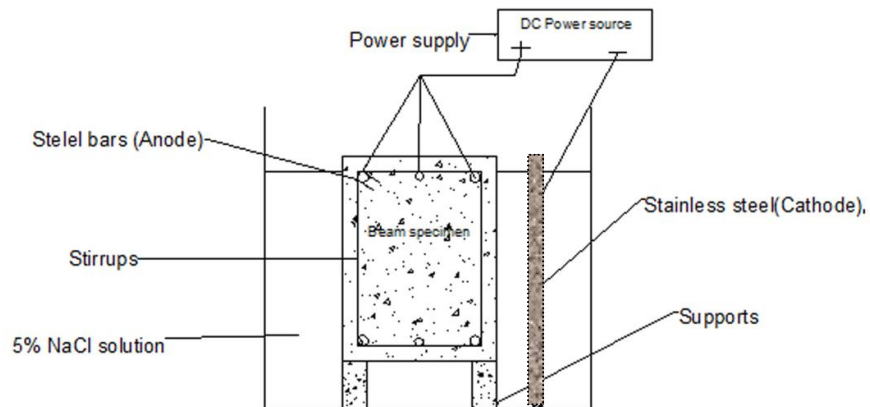
Fig. 3.5(a) Schematic representation of accelerated corrosion of beam

Fig. 3.5(b) Accelerated corrosion of beam specimens

3.7 TIME REQUIRED FOR DIFFERENT PERCENTAGES OF CORROSION

From Faraday's Law, we have

$$i_{corr} = \frac{\rho w_i F}{100 \Pi D L W T} \qquad (3.1)$$

w_i = initial weight of steel reinforcement in the specimen (in grams) = 52346g

F= 96487amp-sec

W = Equivalent weight of iron = 27.925g

πDL= Total surface area of steel for one beam =17688.5cm^2

T = Time in days

The corrosion rate (ρ) in percentage is given as :

$$\rho = \frac{(wi - wf)}{wi} \times 100$$

The corrosion current density (A/cm^2) is given as:

$$i_{corr} = \frac{\rho \times 52346 \times 96487}{100 \times T \times 17688.5 \times 27.925 \times 24 \times 3600}$$

$$= \frac{\rho}{T} \times 1.1835 \times 10^{-3} \quad (A/cm^2) \tag{3.2}$$

The current (I) to be applied in Amperes,

$$I = i_{corr} \times \pi DL$$

$$= \frac{\rho}{T} \times 1.1835 \times 10^{-3} \times 17688.5$$

$$I = \frac{\rho}{T} \times 20.934$$

Considering constant current of 10A supplied to specimens from battery sources, the time required (days) for specific corrosion rate is obtained as,

$$T = 2.0934\rho \tag{3.3}$$

By using above equation, number of days required for different levels of corrosion for OPC and PPC beams were calculated.

Corrosion rate, obtained using ACM instrument, can be expressed in percentages from Eq.(3.2) as:

$$\rho = (final\ i_{corr} - initial\ i_{corr}) \times T \times 14945.9 \tag{3.4}$$

The time required for different degrees of corrosion is tabulated in the Table 3.12 and Table 3.13 along with actual number of days observed for corrosion.

Table 3.12 Time calculation for different degree of corrosion in OPC Beams

Percentage of corrosion	Current (amps)	Expected duration of corrosion (days)	Actual duration of corrosion (days)
2.5	10	6	8
5	10	11	13
7.5	10	16	19
10	10	21	26

Table 3.13 Time calculation for different degree of corrosion in PPC Beams

Percentage of corrosion	Current (amps)	Expected duration of corrosion (days)	Actual duration of corrosion (days)
2.5	10	6	8
5	10	11	15
7.5	10	16	24
10	10	21	30

3.8 CORROSION RATE MEASUREMENTS USING GUARD RING

The surface of beam specimens were divided into a number of grids to locate suitable position of guard ring probe to polarize the definite area on concrete rebar as shown in Fig. 3.6. At each grid, corrosion current density was measured by Linear Polarization Resistance (LPR) technique. The guard ring device is 150mm in diameter and consists of two probes, an outer probe and an inner probe which has a diameter of 75mm.When power is passed through the guard ring it will measure the resistivity of

the bar. The outer probe will block the current from dispersing to outside of probe and the current is measured by inner probe. Since corrosion is not uniform everywhere, grid to grid values vary. Exposure condition, especially temperature and humidity, can alter icorr in chloride contaminated concrete (Elsener 2005). The values of polarization resistance (Rp) were measured and icorr was estimated using stern-grey equation: icorr = B/Rp, (B value was assumed to be 26 mV (Bhaskar et al. 2010)).

In this process, the reinforcing steel is polarized by an internal auxiliary electrode potentiostat and the instantaneous course of the response current is displayed on a portable computer that controls the guard ring device. Steel area polarized by a current applied from an outer guard ring electrode which is controlled by two sensor electrodes positioned between the inner auxiliary and outer guard ring electrode (Law et al. 2000). Corrosion rate is considered negligible when i_{corr} rate is less than 1mA/m^2 (Manera et al. 2008).

To study the level of the existing corrosion in the beam specimen, the initial current density was measured using the measurement system of corrosion "Gill AC". Beam specimens were divided into number of grids to locate the probe guard ring for polarize the definite area in the concrete reinforcing bars as shown in Fig. 3.7. At each grid, the corrosion current density was measured by the LPR technique.

Fig. 3.6 Beam specimen marked in to number of grid to measure corrosion current density

(a)   (b)

(c)
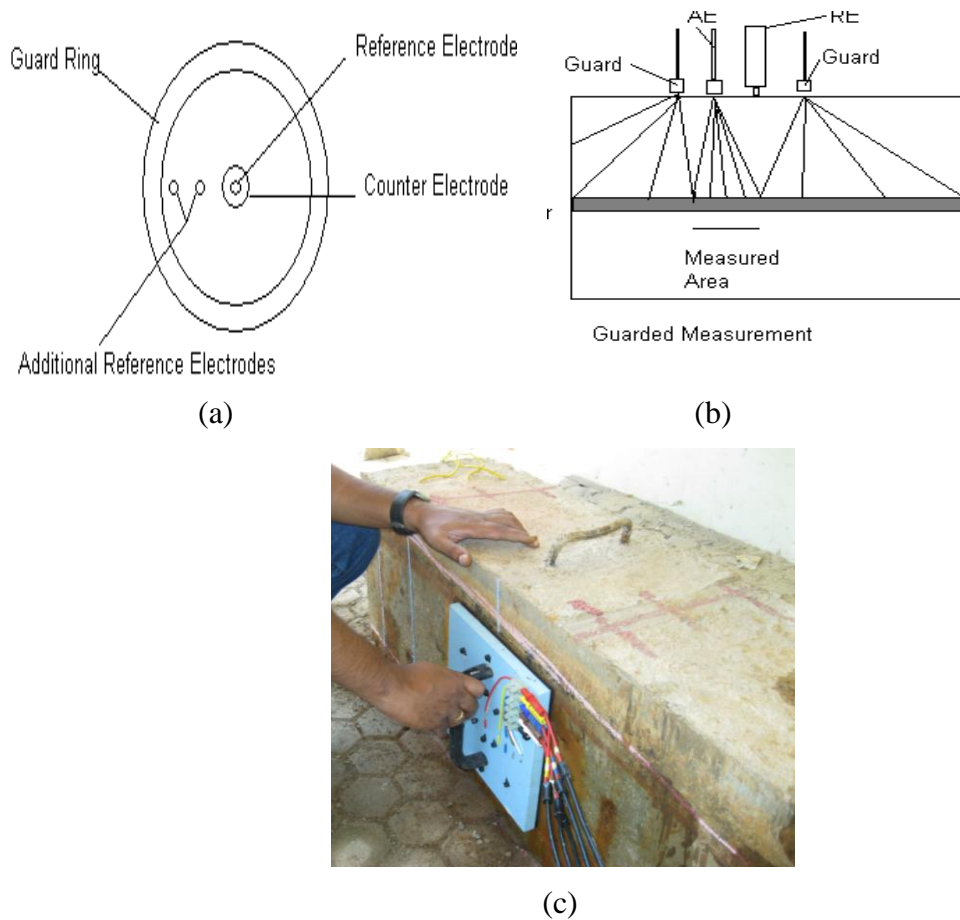
Fig. 3.7 (a), (b) and (c) Different views of guard ring

The current density for control specimen and corroded specimen is shown in the Table 3.14 and Table 3.15.

Table 3.14 Corrosion current density of OPC specimens

Grid Number		Corrosion current density, i_{corr} (mA/cm^2)					
		1	2	3	4	5	Avg
Beams	Control Beam	0.0036	0.0039	0.0044	0.0037	0.0045	0.0040
	2.5% Corroded Beam	0.0220	0.0231	0.0238	0.0241	0.0246	0.0236
	5% Corroded Beam	0.0268	0.0274	0.0282	0.0285	0.0276	0.0277
	7.5% Corroded Beam	0.0306	0.0298	0.0308	0.0295	0.0302	0.0302
	10% Corroded Beam	0.0302	0.0296	0.0288	0.0282	0.0294	0.0292

Table 3.15 Corrosion current density of PPC specimens

Grid Number		Corrosion current density, i_{corr} (mA/cm^2)					
		1	2	3	4	5	Avg
Beams	Control Beam	0.0037	0.0038	0.0040	0.0038	0.0042	0.0039
	2.5% Corroded Beam	0.0236	0.0242	0.0234	0.0226	0.0246	0.0237
	5% Corroded Beam	0.0248	0.0260	0.0265	0.0262	0.0247	0.0256
	7.5% Corroded Beam	0.0246	0.0244	0.0249	0.0252	0.0245	0.0247
	10% Corroded Beam	0.0268	0.0272	0.0256	0.0264	0.025	0.0262

3.9 EXPERIMENTAL SETUP TO MEASURE STRENGTH AND DEFLECTION OF BEAM SPECIMENS

Flexural tests of cantilever beam were conducted using a specially prepared loading frame. Loading set up was built on the existing bed in the laboratory to test the vertical cantilever beam and point load applied at the free end of the beam in the transverse direction. To achieve the fixation at the fixed end of the beam, high-strength hydraulic jack was used against the section of the steel column at the other side of the beam. Full fixity was achieved at the lower end of the beam by adjusting the movement of the of a hydraulic jack arm.

The load frame was designed as a steel frame, built section formed by two ISMC-100 sections with face to face alignment, Hilty bolts of 16 mm diameter, capacity 40kN were filled in the reaction bed to fix the loading frame to the reaction bed. The load frame was designed to withstand a concentrated load of 100kN, which was the expected reaction of the beam element. The frame design calculations are given in Appendix III.

All beams were tested as cantilever beams in a 150kN capacity steel testing frame made up of rolled steel joists, the beam having a span of 1750mm was fixed at one end for a bearing length of 400mm. The span and load points were kept constant for

all the beams. The concentrated load was applied on the free end of a beam as shown schematically in Fig. 3.8(a). The load spreader arm, wherever used was a rolled steel joist which was supported on the rollers kept on the loading points. Over the load spreader arm the proving ring of 200kN capacity was placed to measure the applied load, over which the hydraulic jack of 20kN was fixed to the rolled steel joist of the loading frame. The pump of hydraulic jacks was operated by a hand lever. Fig. 3.8(b) shows the test set up.
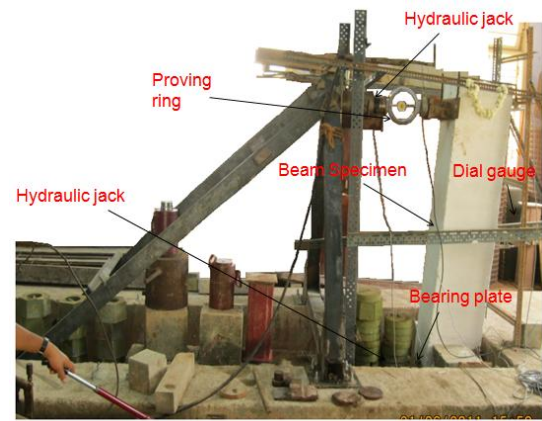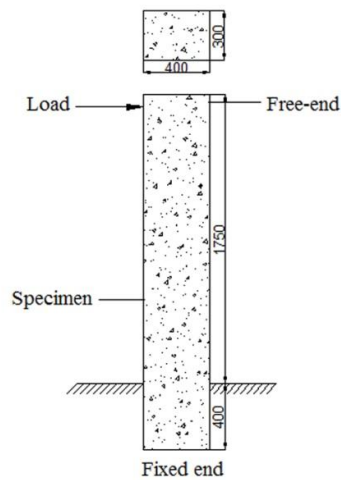
Fig. 3.8 (a) Schematic diagram of specimen **Fig. 3.8 (b) Test setup**

3.10 CALCULATION OF ULTIMATE MOMENT CAPACITY OF BEAM

This section deals with the calculation of ultimate moment of controlled beams of size 300mm × 400mm, with 30mm clear cover. Beam was reinforced with 2 of 20mm Φ bars and 1 of 16mm Φ bars at both tension and compression sides. Actual strength of concrete obtained from cube tests and steel was used for the design. Ultimate moment of resistance was calculated according to code IS 456: 2000 without partial safety factors (Pillai and Menon 2009). Calculations are explained in Appendix IV.

3.11 CALCULATION OF CHLORIDE CONCENTRATION IN A TANK

3.11.1 Test program

Following apparatus were used to calculate concentration of chloride in tank: 50-ml burette, 5-ml volumetric pipette, $AgNO_3$ (0.141N), potassium chromate (pale yellow) indicator, burette stand, two 250-ml Erlenmeyer flasks, wash bottle filled with distilled water, and funnel. Samples were collected from different tanks as shown in Fig. 3.9.

One ml of sample collected from the tank, was added to distilled water in a conical flask and 10 drops of potassium chromate (indicator) were added. This solution was titrated against the silver nitrate solution till colour changed from pale yellow to brick red. Same step was repeated 3 times. A schematic representation of the test set-up is shown in Fig. 3.10.
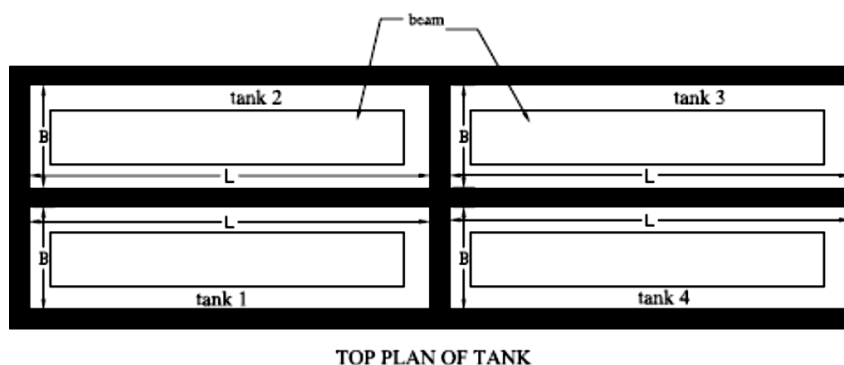
TOP PLAN OF TANK

Fig. 3.9 Plan of tank

3.11.2 Calculation of chloride concentration

Typical burette reading for a solution taken from a tank is shown in Table 3.16

Table 3.16 Burette readings for test samples

Initial reading	Final reading	Volume of $AgNO_3$
0ml	5ml	5ml
5ml	9.8ml	4.8ml

One ml of 0.141N AgNO$_3$ contains 5mg of chloride (Cl) which is used as titrand. The sample taken from the tank is titrated against AgNO$_3$ to determine the chloride ion concentration in the sample. After titration the reading in the burette was 4.9 ml. This value was then used to calculate the amount of chloride which was about 24.5 ml in the sample.

Molecular weight of sodium chloride is the summation of molecular weight of sodium and molecular weight of chloride.

Therefore molecular weight of NaCl = 23 + 35.46 =58.46 molecular weight

Now the amount of salt required for one litre of water is calculated as,

$$= \frac{Amount\ of\ Cl\ in\ solution \times Molecular\ wt\ of\ NaCl}{Equivalent\ wt\ of\ Cl}$$

$$= \frac{24.5 \times 58.46}{35.46}$$

$$= 40.39\ g/ltr$$
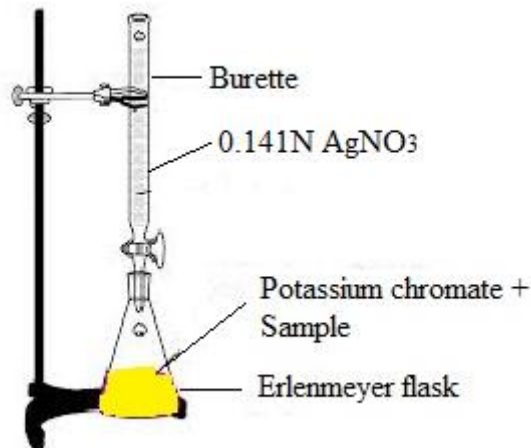
Fig. 3.10 Schematic representation of NaCl test of sample
(Source http://csip.cornell.edu/)

Volume of water excluding beam and cubes,
    = (volume of tank 1) – (volume of beam in tank 1) – (volume of cubes in tank 1)

= (2.96×0.52×0.5) – (2.15×0.3×0.4) – (10×0.1×0.1×0.1)

= 0.5016m^3

= 501.6ltr

Therefore salt required for 501.6ltr of water $= \dfrac{501.6 \times 40.39}{1}$

$= 20259.62$g or 20.25kg

3.12 STRAIN MEASUREMENT USING MECHANICAL STRAIN GAUGE

Strain is defined as the amount of deformation per unit length of an object when load is applied. Strain may be compressive or tensile and is normally measured by strain gauges.

The strain gauge consists of a main beam demec invar two conical positioning points, one fixed and the other mounted on a special knife edge. The points are pre-perforated plates of stainless steel that is attached to the structure by means of an adhesive. Displacement of the centre of rotation is measured by the strain gauge which is fixed on a base plate of the invar beam. The design is such that the thermal motion within the instrument is negligible. Fig. 3.11 shows the mechanical gauges.

In the present study, lateral strains were measured using a 100mm demountable mechanical (demec) strain gauge with a range of ±10 to ±5000 micro strains. Lateral deformation of the RC beams due to steel corrosion was assessed by monitoring lateral strains on concrete at various potential cracking regions. For longitudinal strains on the tensile face of beams, six stainless steel targets for the demec gauge were glued to the concrete surface at a spacing of 100mm c/c. Similarly both tensile strain and compression strain were measured on sides of the beam at the fixed end of the specimen and a total 16 demec buttons were used at a distance 100mm c/c, as shown in Fig. 3.12.

Fig. 3.11 Mechanical strain gauges (100mm) used to measure strain
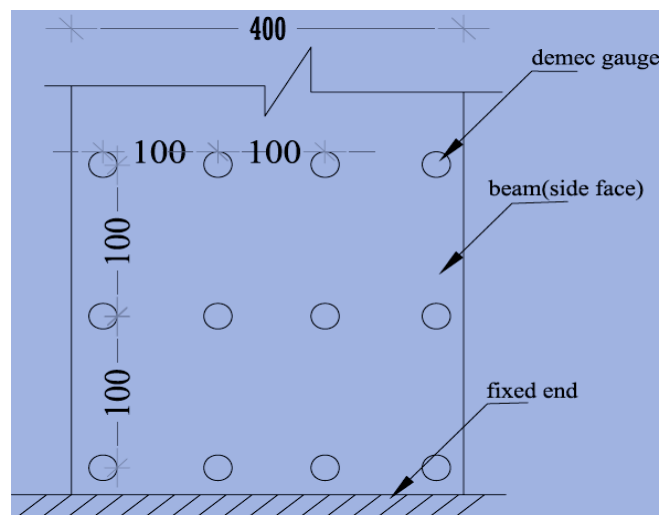
Fig. 3.12 Location of targets for strain measurements on beams.

3.13 STRAIN MEASUREMENTS USING LABVIEW (DAQ SYSTEM)

3.13.1 General

Before fixing the strain gauges, the surface of the rebar was ground smoothly to make surface of the rebar plain. Surface of the rebars were cleaned by acetone. Strain gauges were fixed on the reinforcement, one on the top of the rebar and another on the bottom of the rebar as shown in Fig. 3.13(a) and (b). On the top of the strain gauge cotton cloth was rolled to protect the strain gauge from the concrete, Araldite solution was used on the surface of the cotton cloth. This was kept for one day and when

52

surface became hard, concreting was carried out (Cabrera 1996).Third strain gauge which was fixed on the surface of concrete and connected to DAQ device as shown in Fig. 3.14(a) and (b).

| (a) | (b) |

Fig.3.13 Fixing of strain gauges on the rebar

| (a) | (b) |
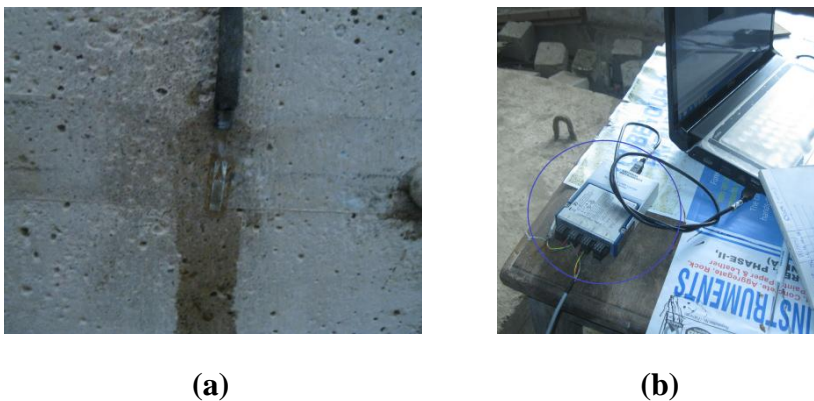
Fig. 3.14 Fixing of strain gauge on the surface of the concrete and connecting to DAQ device

3.13.2 Strain gauge

The most common method to measuring the strain with the aid of a strain gauge. The electrical resistance of the strain gauge proportional to the strain acting on it. Bonded metallic straingauge is very widespread. The metallic strain gauge consists of metal foil shipped in grid fashion. This pattern maximizes the impact of strain experienced. The total lengths of the metal wire or foil are called the active length of the bonded metallic grid strain gauge, as shown in Fig. 3.15. The effect of the shearing strain and Poisson strain is reduced by reducing the cross-sectional area of the grid. To ensure the accuracy of the strain, the strain gauge be properly mounted on the test specimen.

The sensitivity of the strain gauges is extensively represented using Gauge Factor (GF). Gauge factor is defined as the ratio of fractional changes in electrical resistance to the length. The gauge factor for metallic strain gauges is typically around two. The strain gauge used for experiments was YFLA-5 for 4-core shielded 3m cable for stainless steel, gauge resistance $120\pm0.3\Omega$.
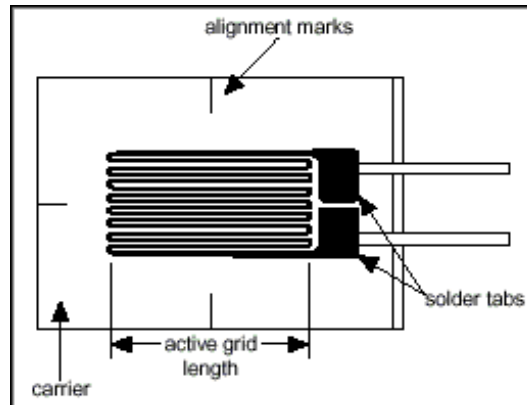
Fig.3.15 Bonded metallic strain gauge

3.13.3 Strain measurement

Practical values of strains are in milli order. Thus, accurate measurement of the resistance is required. There are different ways to identify the accuracy of the resistance strain gauge. The most common method is the Wheatstone bridge shown in the Fig. 3.16. General Wheatstone bridge consists of four resistive voltage source V_{EX} for excitation of the circuit (Parnas and Bilir 1996).
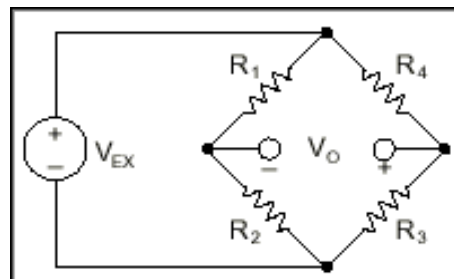
Fig. 3.16 Wheastone bridge

The output voltage V_O can be expressed as

$$V_0 = \left[\frac{R_3}{R_3 + R_4} - \frac{R_2}{R_1 + R_2} \right] \bullet V_{EX} \tag{3.5}$$

The equation shows that the output voltage V_O is zero only if $R_1/R_2 = R_4/R_3$. At this condition the bridge is in balanced condition. The output voltage gives a non-zero value towards any change in the resistances of the arms.

If one of the arms of the bridge is replaced with a strain gauge, the strain corresponding to the resistance change in the results of any changes in a non-zero voltage. Let the nominal value of the strain gauge resistance is expressed as R_G, then the change in resistance corresponding to the change in strain, D_R can be represented as $D_R = R_G \cdot GFe$.

Assuming the balanced condition with strain gauge, i.e.; the arm resistances $R_1 = R_2$ and $R_3 = R_G$, then the bridge equation V_O/V_{EX} can be expressed as a function of strain as

$$\frac{V_0}{V_{EX}} = \frac{GF \bullet \varepsilon}{4} \left(\frac{1}{1 + GF \bullet \dfrac{\varepsilon}{2}} \right) \tag{3.6}$$

The term $1/(1+GF \cdot \varepsilon/2)$ makes the equation nonlinear with respect to strain as shown in Fig. 3.17.
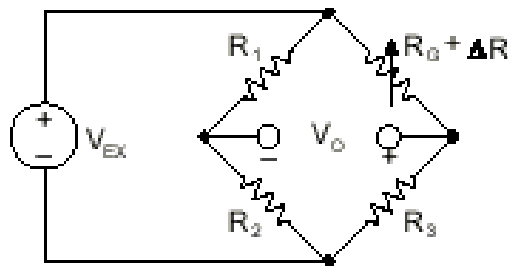
Fig. 3.17 Quarter bridge

3.13.4 Signal conditioning for strain gauges

Since strain is measured in terms of very small changes in resistance, the reliability of the measurement depends on so many factors, such as proper selection and use of the bridge, signal conditioning, wiring, and data acquisition components. The accuracy of the strain measurement is ensured by considering the following:

1. Bridge completion
2. Excitation
3. Remote sensing
4. Amplification
5. Filtering
6. Offset nulling
7. Shunt calibration

1. Bridge completion – Precision resistors will be used to complete the bridge, if it is not a full-bridge configuration. Half-bridge (change of season) to complete the circuit with the strain gauge resistors R_1 and R_2 are shown in Fig. 3.18.
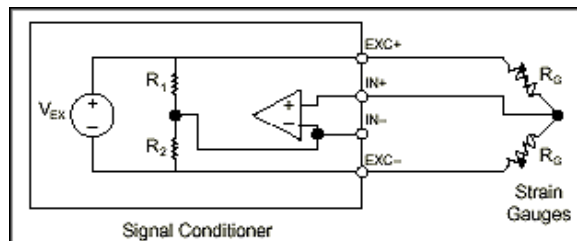
Fig. 3.18 Connection of half bridge strain gauge circuit

2. Excitation – Constant voltage source as the excitation for bridge. There is no standard for the value of the voltage level. Usually the voltage of 3 to 10V is used. Use higher voltage may result in errors due to self-heating.

3. Remote sensing – If the strain gauges are placed away from the excitation source, there is an error, because the cross is used to connect the strain gauge the likelihood of the voltage drop across the resistor wire. In some remote sensing signal conditioning function can compensate for this error.

4. Amplification − Most of the strain gauge bridge and each strain sensor based on excitation voltage output is relatively small and in practice it is less than 10mV/V. Thus, the signal to an amplifier having a regulator to increase the voltage and reduce the signal - noise ratio.

5. Filtering – Ambient noise strain gauge measurements will lead to erroneous results. It is low-pass filters which eliminate the high frequency noise.

6. Offset nulling – Even without any application of strain in many cases, a nonzero offset voltage is generated due to small variations in resistances of the arms and lead resistance. Offset nulling can be performed by either hardware or software.

7. Shunt Calibration – This is a procedure to verify that a strain measurement system with respect to the known strain output.

3.13.5 NI Compact DAQ with strain gauges

NI Compact DAQ hardware provides the plug-and-play simplicity of USB to sensor and electrical measurements. Here universal C Series module NI 9219 is used for strain measurement. The NI 9219 is a 4-channel module designed for multipurpose testing in any NI Compact DAQ or Compact RIO chassis. NI 9219 can be used for measurement of different signals such as strain gauges, load cells, thermocouples, RTDs, and other powered sensors. The channels are selectable individually, so it is possible to do different measurements on each of the four channels. Each channel of NI 9219 consists of six-spring terminal connectors. It is used for direct signal connectivity and contains built-in quarter-, half-, and full-bridge support.

Positive signals from the source is connected to the positive input signal (HI) and the signal source to the negative terminal of the input signal (LO) signal is negative. The excitation terminals for sensor excitation require a separate connection. The signal names are listed in Table 3.17 and Table 3.18 Terminal assignment.

Table 3.17 Signal names

Module	Terminal	Signal name	Signal description
CH0 CH1 CH2 CH3	1	T+	TEDS Data
	2	T-	TEDS COM
	3	EX+/HI	Positive excitation or input signal
	4	HI	Positive input signal
	5	EX-/LO	Negative excitation or input signal
	6	LO	Negative input signal

Table 3.18 Terminal assignments

Mode	Terminal					
	1	2	3	4	5	6
Voltage	T+	T–	—	HI	LO	—
Current	T+	T–	HI	—	LO	—
4-Wire Resistance	T+	T–	EX	HI	EX–	LO
2-Wire Resistance	T+	T–	HI	—	LO	—
Thermocouple	T+	T–	—	HI	LO	—
4-Wire RTD	T+	T–	EX	HI	EX–	LO
3-Wire RTD	T+	T–	EX	—	EX–	LO
Quarter-Bridge	T+	T–	HI	—	LO	—
Half-Bridge	T+	T–	EX	HI	EX–	—
Full-Bridge	T+	T–	EX	HI	EX–	LO
Digital In	T+	T–	—	HI	LO	—
Open Contact	T+	T–	HI	—	LO	—

3.13.6 Wire resistance and quarter-bridge modes

In the 2 and 4-wire resistance bridge mode, both ends of the resistor or the instrument are connected to the HI and LO terminals throughout the NI USB-9219. These patterns of the current source, the load current changes based on the resistance between the HI and LO terminals. The resulting value is calculated from the measured voltage. 2 and 4-wire resistance bridge mode does not compensate for lead resistance. Fig. 3.19 gives a schematic diagram of the connection.
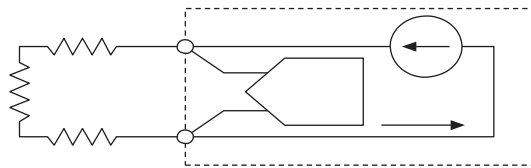
Fig. 3.19 Illustration of the connection

3.13.7 NI Lab view virtual program

The virtual graphical program is as shown in Fig. 3.20. The program continuously monitors the strain value until the stop button is pressed. The strain values with respect to time are plotted on a graph in the front panel as shown in Fig. 3.21.The strain values versus time are also stored as data file for future analysis.
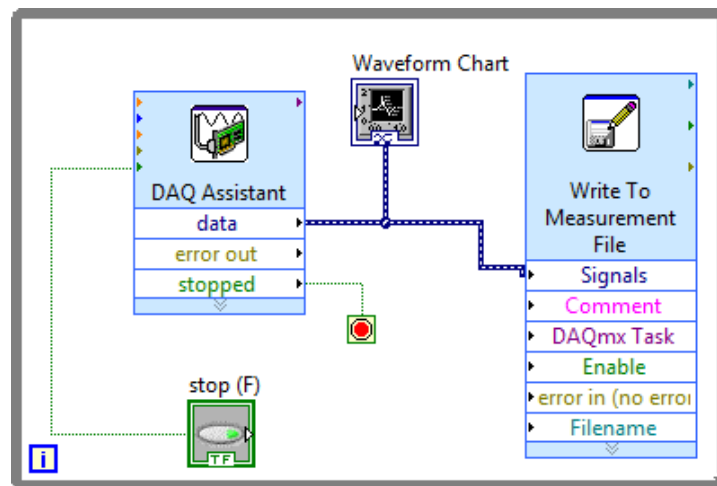
Fig. 3.20 DAQ flow chart
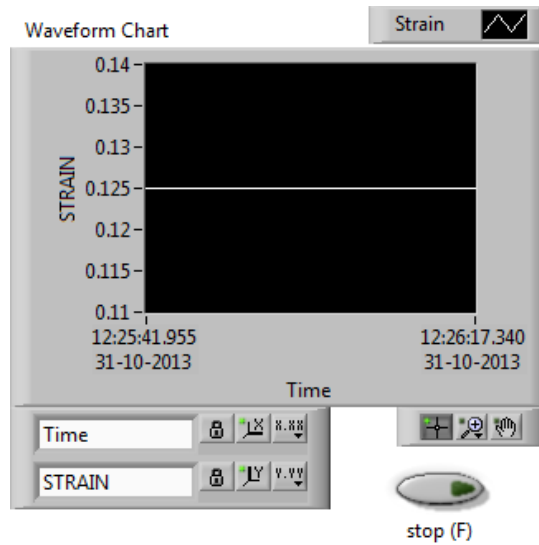
Fig. 3.21 DAQ wave form chart

In the graph on the front panel, strain is taken in y-axis and time is taken on x-axis. The strain values are in the order of micro strain.

3.14 CRACK MEASUREMENT

In this study the crack was measured using Concrete Crack Microscope (Elcometer 900) as shown in Fig. 3.22. Crack widths were recorded for all specimens after the accelerated corrosion stage. The cracks were observed on the tension side of the beam at the fixed end at every intervals of load. The least count of the Crack Microscope was 0.02 mm.

Fig. 3.22 Concrete crack microscope

3.15 EXPERIMENTAL PHOTOS OF BEAMS FOR VARIOUS LEVELS OF CORROSION

Figs. 3.23 (a), (b), (c), (d), (e), (f) and (g) show the experimental setup for various levels of corrosion. The pictures show the beam bottom fixity, fitted with dial gauges to measure deflections for each load interval. The cracks were measured using crack microscope for every load interval for various levels of corrosion.

(a) Beam fixity   **(b) Specimen fitted with dial gauge**

(c) , (d) and (e) Crack measurements

(f) Crack mesurement by   (g) Strain measurements

crack measuring microscope

Fig. 3.23 Experimental photos of beams for various levels of corrosion

These cracks were marked on the beam specimen. Markings on the beam were very difficult to visualize due to surface moisture on the beam as the rate of corrosion increased. For every load interval strains were measured using mechanical strain gauge.

CHAPTER 4

NUMERICAL MODELLING

4.1 GENERAL

Numerical modeling was performed using the ANSYS software. To create the finite element model in ANSYS 2013, there are several tasks to be completed for the model to run correctly. The models can be made with the quick command-line or Graphical User Interface system (GUI). For this model, the GUI has been used to build the model. This section describes the different tasks and inputs used to create the FE model.

4.2 MODELING METHODS

4.2.1 Concrete

A solid eight node element was used to model Solid65 concrete. The solid has eight nodes with three degrees of freedom at each node - the translations in node x, y and z directions. This element has the ability of plastic deformation, cracking and breaking in three orthogonal directions. Geometry and the position of the nodes, for this element type are shown in Fig. 4.1.
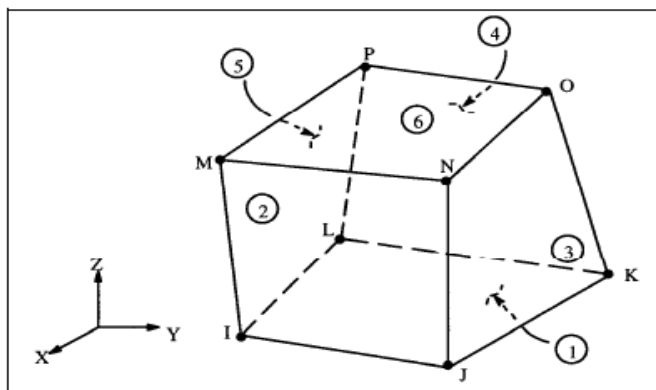
Fig. 4.1 Solid 65 3-D reinforced concrete solid (Wolanski 2004)

Improve the performance for concrete model was a difficult task. Concrete is a brittle material and a substantially have different properties in compression and tension. The tensile strength of concrete is normally 8 to 15% of the compressive strength. Fig. 4.2 shows a typical stress-strain curve for concrete.
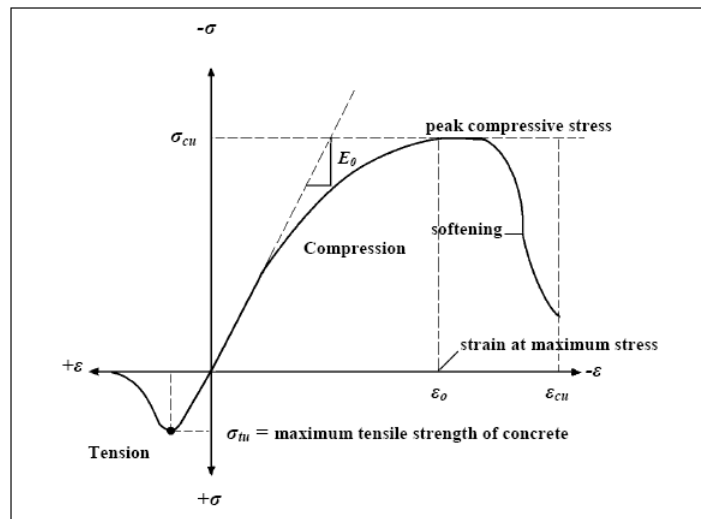
Fig. 4.2 Uniaxial compressive and tensile stress-strain curve for concrete (Wolanski 2004)

In compression, the concrete stress - strain curve is linearly elastic up to about 30% of the maximum compression strength. Above this point, the compressive stress increases to a maximum. After reaching the maximum compressive strength, σ_{cu}, the curve drops to a softening zone, and eventually crushing failure occurs at an ultimate strain ε_{cu}. In tension, the stress-strain curve is roughly linear elastic to maximum tensile strength. After this point, the concrete cracks, the intensity gradually reduced to zero.

For concrete, ANSYS requires input data for material properties as follows:

Elastic modulus (Ec).

Ultimate uniaxial compressive strength (f'c).

Ultimate uniaxial tensile strength (modulus of rupture, f_{cr}).

Poisson's ratio (ν).

Shear transfer coefficient (β*t*).

Compressive uniaxial stress-strain relationship for concrete.

Poisson's ratio for concrete was assumed to be 0.2. The shear transfer coefficient, βt, represents conditions of the crack face. The value of βt ranges from 0.0 to 1.0, with 0.0 representing a smooth crack (complete loss of shear transfer) and 1.0 representing a rough crack (no loss of shear transfer).

The ANSYS program requires the uniaxial stress-strain relationship for the concrete under pressure. Numeric expressions Eq. 4.1 and 4.2 were calculated using Eq. 4.3 to construct the stress-strain curve in uniaxial compression of the concrete in this study.

$$f = \frac{E_c \varepsilon}{1+(\frac{\varepsilon}{\varepsilon_0})^2} \tag{4.1}$$

$$\varepsilon_0 = \frac{2f'c}{Ec} \tag{4.2}$$

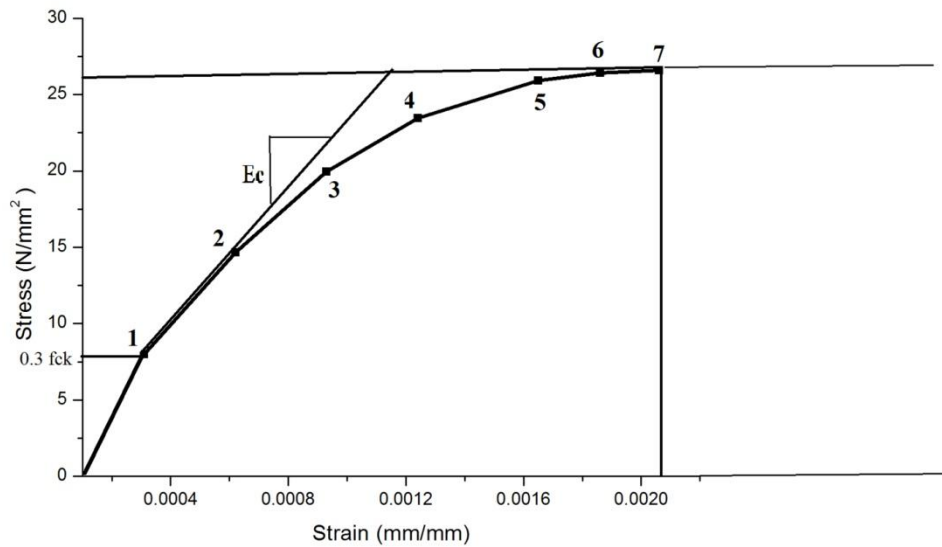$$E_c = \frac{f}{\varepsilon} \tag{4.3}$$

where:

f = stress at any strain

ε = strain at stress f

ε_0 = strain at the ultimate compressive strength $f'c$

Fig. 4.3 shows the simplified compressive uniaxial stress-strain relationship that was used in this study.

Fig. 4.3 Simplified compressive uniaxial stress-strain curve for concrete

The simplified stress-strain curve for each beam model is constructed from eight points connected by straight lines. The curve starts at zero stress and strain. Point No. 1, at $0.30f'c$, is calculated for the stress-strain relationship of the concrete in the linear range (Eq. 4.3). Point Nos. 2, 3, 4, 5 and 6 were obtained from Eq. 4.1, in which ε_0 was calculated from Eq. 4.2. Point No. 7 was at ε_0 and $f'c$. In this study, an assumption was made of perfectly plastic behaviour after Point No.7.

4.2.2 Steel reinforcements

A Link8 element was used to model the steel reinforcement. Two nodes are required for this element. Each node has three degrees of freedom, translations in the nodal x, y and z directions. The element is also capable of plastic deformation. The geometry and node locations for this element type are shown in Fig. 4.4.

Characteristics namely, elastic modulus and yield stress of the steel used in finite element analysis to follow the material properties used in the design of the experimental studies. The steel for the finite element models was assumed to be an elasto- plastic material and identical in tension and compression.

66

Poisson's ratio is assumed to be 0.3 for steel. Fig. 4.5 shows the stress - strain curve for steel reinforcement.
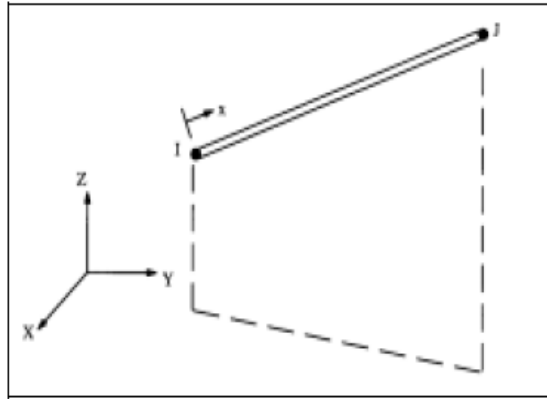
Fig. 4.4 Link8 – 3-D spar (Wolanski 2004)
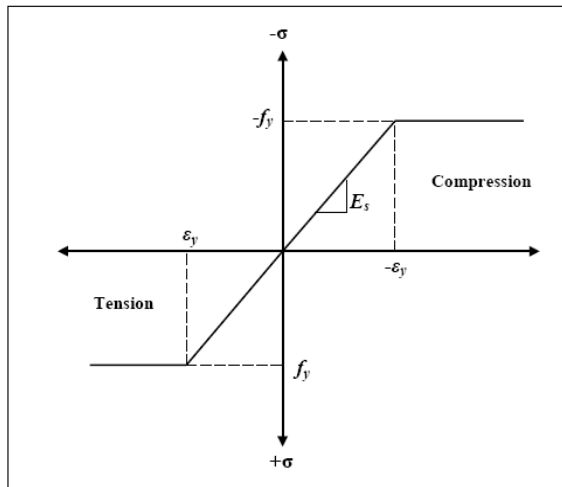
Fig. 4.5 Stress-strain curve for steel reinforcement (Wolanski 2004)

In this model reinforcement in the discrete model uses bar elements that are connected to concrete mesh nodes. Therefore, the concrete and the reinforcement mesh share the same nodes and concrete occupies the same regions occupied by the reinforcement. There are different models are available as shown in Fig. 4.6.
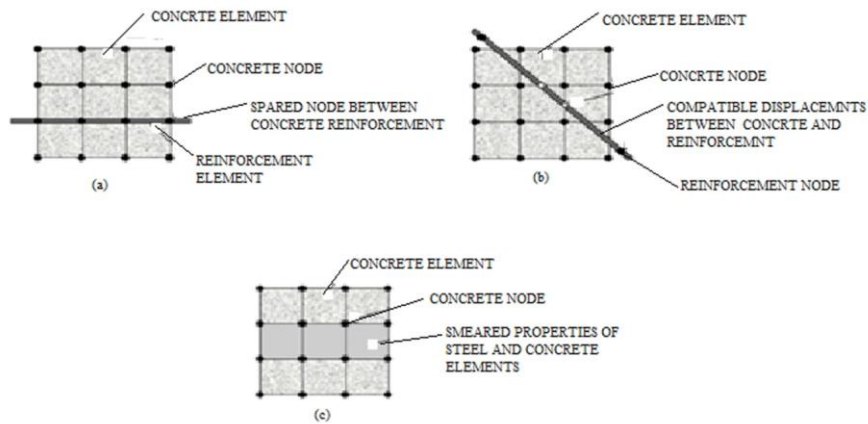
Fig. 4.6 Model for reinforcement in reinforced concrete (Tavarez 2001):
a) discrete: b) embedded: c) smeared

4.2.3 Real constants

For real constants of this model are listed in Table 4.1. Note that the single element comprising real constant. There is no real constant presence Solid65 unit.

Table 4.1 Real constants for ANSYS model

Real Constant Set	Element Type	Particulars	Constants		
			Real Constant for Rebar 1	Real Constant for Rebar 2	Real Constant for Rebar 3
1	Solid 65	Material No.	0	0	0
		Volume Ratio	0	0	0
		Orientation Angle THETA 1	0	0	0
		Orientation Angle PHI 1	0	0	0
2	Link 8	Cross-sectional Area (mm^2)	314		
		Initial Strain (mm./mm)	0		
3	Link 8	Cross-sectional Area (mm^2)	201		
		Initial Strain (mm./mm)	0		
4	Link 8	Cross-sectional Area (mm^2)	113		
		Initial Strain (mm./mm)	0		

Real constant set 1 is used for the Solid65 element. It requires real constants for rebar assuming a smeared model. Values can be entered for Material Number, Volume Ratio and Orientation Angles. The material number according to the type of material for the reinforcement. The orientation angles refer to the orientation of the reinforcement in the smeared model. ANSYS allows the user to enter three rebar materials in the concrete. Each material corresponds to x, y and z directions in the element. The reinforcement has uniaxial stiffness and the directional orientation was defined by the user. In the present study the beam was modelled using discrete reinforcement. Therefore, a value of zero was entered for all real constants which turned the smeared reinforcement capability of the Solid65 element off.

Real constant sets 2, 3 and 4 are defined for the Link8 element. Values for cross-sectional area and initial strain were entered. Cross-sectional areas in sets 2 refer to the reinforcement of 20mm bar, sets 3 refers to the reinforcement of 16mm bar, sets 4 refers to the reinforcement of 12mm bar. A value of zero was entered for the initial strain because there is no initial stress in the reinforcement.

4.2.4 Material properties

Parameters needed to define the material models can be found in Table 4.2.

Table 4.2 Material models for the ANSYS model

Material Model Number	Element Type	Material Properties			
1	Solid 65				
		Linear Isotropic			
		Modulus of Elasticity	25742		
		Poisson's Ratio	0.2		
		Multi Linear Isotropic			
		Reference Point	Strain	Stress	

		Point 1	0.00031	7.98	
		Point 2	0.00062	14.668	
		Point 3	0.00093	19.94	
		Point 4	0.00124	23.47	
		Point 5	0.00165	25.92	
		Point 6	0.00186	26.42	
		Point 7	0.00206	26.6	
		Concrete			
		Shear Transfer Coefficients for an open crack	0.2		
		Shear Transfer Coefficients for an closed crack	0.9		
		Uniaxial tensile cracking stress	3.61		
		Uniaxial crushing stress	-1		
		Linear Isotropic			
		Modulus of Elasticity	2.1×10^5		
3	link 8	Poisson's Ratio	0.3		
		Bilinear Isotropic			
		Yield Stress	480		
		Tangent Modulus	24		

4.2.5 Modelling

The beam was modelled as volumes. The model was 2150mm long, with a cross-section of 300mm×400mm. The mesh volume of the beam is shown in Fig. 4.7. The FE mesh for the reinforcement is shown in Fig. 4.8.
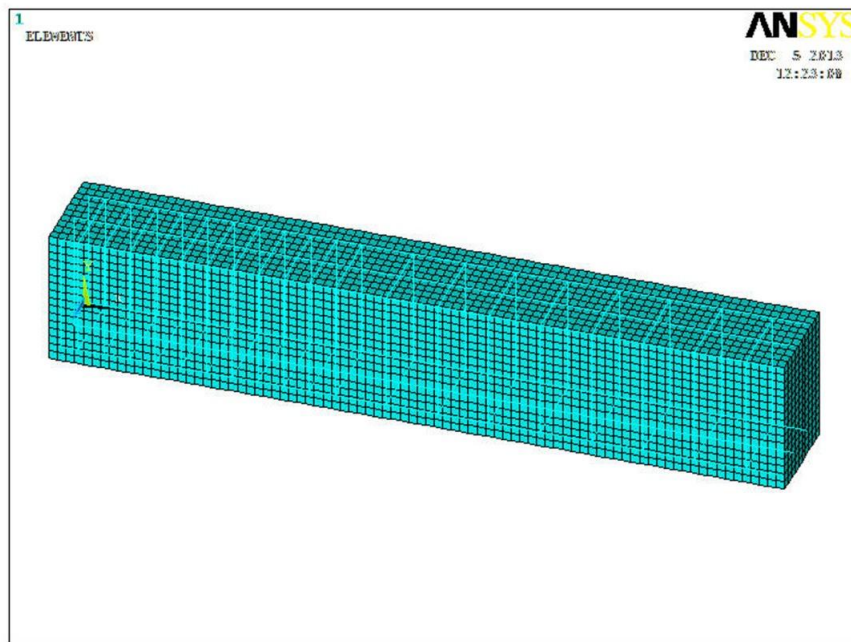
Fig. 4.7 Mesh of concrete elements in beam model
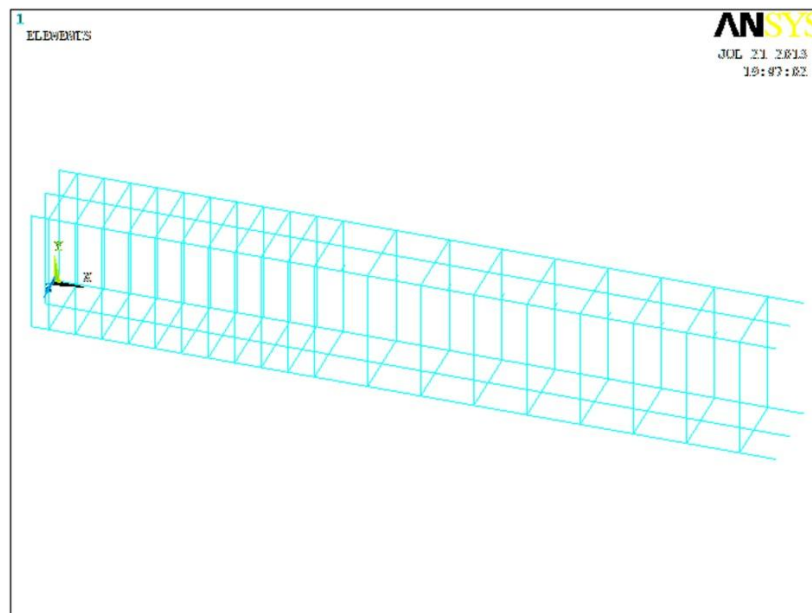
Fig. 4.8 Mesh of reinforcement in a beam model

Link8 elements were used to generate the flexural and shear reinforcement. Reinforcement exists at a plane of symmetry and in the beam. Fig. 4.9 shows that the rebar shares the same nodes at the points that it intersects the shear stirrups. The

element type number, material number, and real constant set number for the model were set for each mesh as shown in Table 4.3.
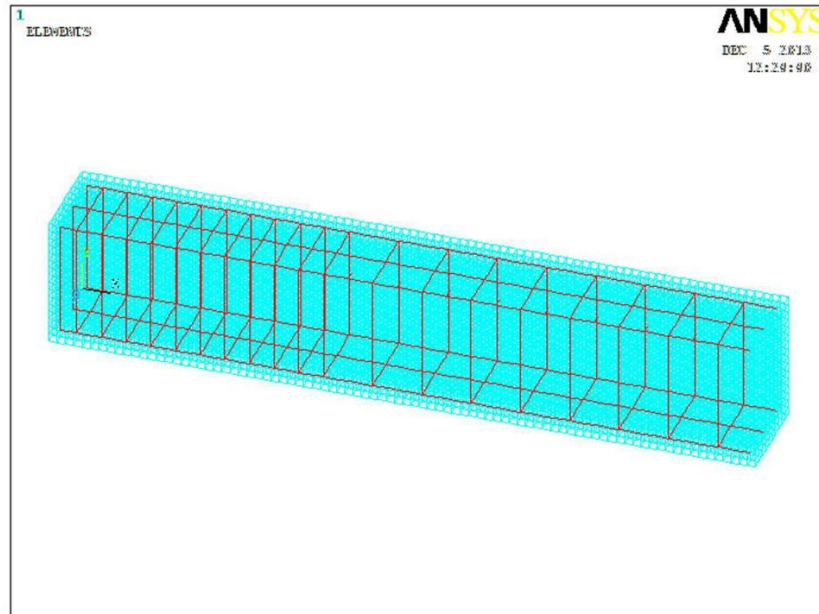
Fig. 4.9 Mesh of reinforcement and concrete

Table 4.3 Mesh attributes for the model

Model Parts	Element Type	Material Number	Real Constant Set
Concrete Beam	1	1	1
Rebar of 20mm	3	3	3
Rebar of 16mm	3	3	4
Stirrup of 12mm	3	3	5

4.2.6 Meshing

To achieve good results from the Solid65 element, the use of a rectangular mesh was suggested. Therefore, the mesh was set up such that square or rectangular elements were created (Fig. 4.7). This accurately sets the width and length of elements in the

plates to be consistent with the elements and nodes in the concrete portions of the model.

The overall mesh of the concrete is shown in Fig. 4.7. The necessary element divisions were noted. No mesh for the reinforcement was needed because individual elements were created in the modelling through the nodes created by the mesh of the concrete. However, the necessary mesh attributes as described above need to be set before each section of the reinforcement was created.

4.2.7 Numbering controls

The command merge items merge separate entities that have the same location. These items will then be merged into single entities. Caution has to be taken when merging entities in a model that has already been meshed because the order in which merging occurs is significant. Merging nodes can result in some of the nodes becoming "orphaned" that is, the nodes lose their connection with the solid model. The orphaned nodes can cause certain operations (such as boundary condition transfers, surface load transfers, and so on) to fail. Care should be taken to always merge in the order that the entities appear. All precautions were taken to ensure that everything was merged in the proper order.

4.2.8 Loads and boundary conditions

Displacement boundary conditions are necessary to constrain the model to obtain a unique solution. To ensure that the model acts the same way as the experimental beam boundary conditions need to be applied at points of symmetry, where the supports and loadings exist.

The symmetry boundary conditions initially set first. The model is symmetric about two planes. The boundary conditions for two planes of symmetry are shown in Fig. 4.10. A model distance of 0 to 400mm was restrained in all three directions in X, Y and Z.
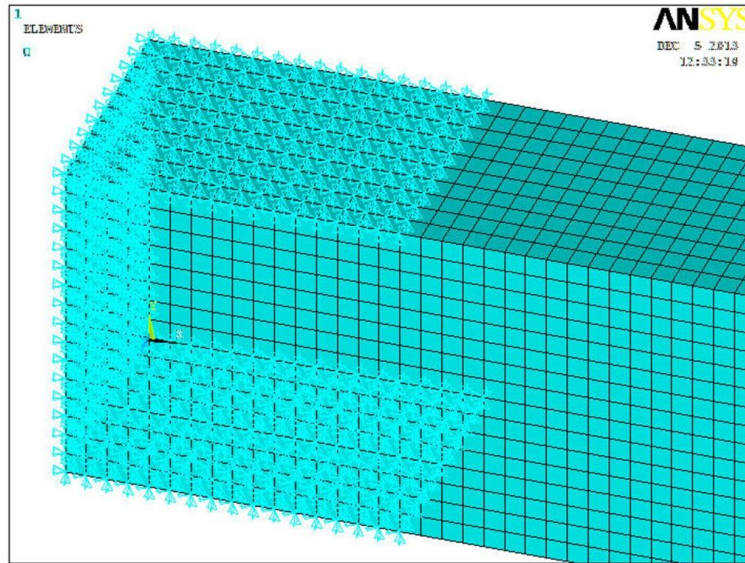
Fig. 4.10 Boundary condition for Support

The force, P, was applied across the entire centre line of the plate. The force applied at each node on the element was one eleventh of the actual force applied. Fig. 4.11 illustrates the applied loading.
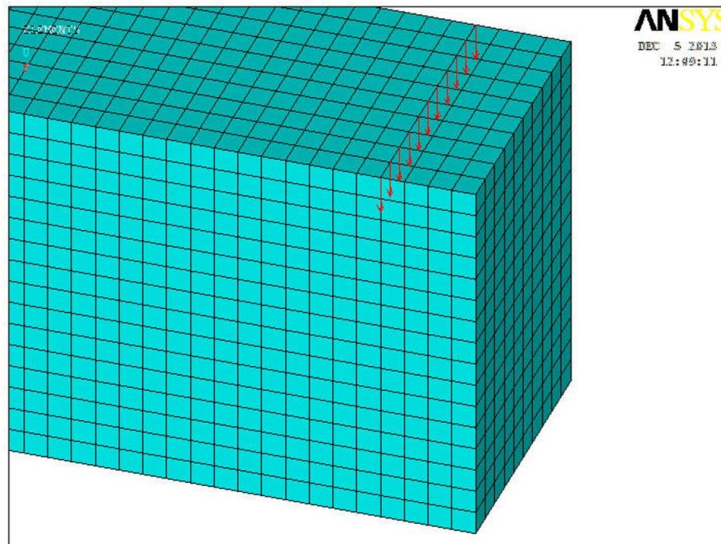
Fig. 4.11 Loading Conditions

74

4.2.9 Analysis type

The finite element model for this analysis is a simple beam under transverse loading. For the purposes of this model, the Static analysis has been employed.

The Restart command was utilized to restart an analysis after the initial run or load step has been completed. The solution controls command dictates the use of a linear or non-linear solution for the finite element model. Typical commands utilized in a nonlinear static analysis are shown in Table 4.4.

Table 4.4 Commands used to control nonlinear analysis

Analysis Options	Small Displacement
Calculate Prestress Effect	No
Time at End of Load Step	5000
Automatic Time Stepping	On
Number of Substeps	20
Max. Number of Substeps	20
Min. Number of Substeps	20
Write Items to Result File	All Solution Items
Frequency	Write Every Substep

In the particular case in this analysis as a model was small and static displacement. The time at the end of the loading step relates to the processing load for the loading step. Table 4.4 shows the first step of load (until the first cracking). The sub steps are set to indicate load increments used for this analysis. The commands used to control the solver and outputs were shown in Table 4.5.

Table 4.5 Commands used to control output

Equation Solvers	Sparse Direct
Number of Restart Files	1
Frequency	Write Every Substep

All of these values were set to default values in ANSYS. Commands for nonlinear algorithm and convergence criteria are listed in Table 4.6. All nonlinear algorithm value is set to the default value.

Table 4.6 Nonlinear algorithm and convergence criteria parameters

Line Search	off	
DOF Solution Predictor	Program Chosen	
Maximum No. of iterations	10000	
Set Convergence Criteria		
Label	F	U
Tolerance	0.1	0.1
Norm	L2	L2
Min. Ref.	-1	-1

In this study, the beam convergence behaviour using various tolerance values have been analysed. In this study tolerance value used for force and displacement was 0.1.

4.2.10 Analysis process for the Finite Element Model

The model for finite element analysis was established to consider three different behaviours: initial cracking of the beam, yielding of the steel reinforcement and the strength limit state of the beam. The Newton-Raphson method of analysis was used to calculate the nonlinear response. The application of the loads up to failure was done incrementally as required by the Newton-Raphson procedure. After the execution of each load increment restart option was used to go to the next step after convergence. Wolanski used default convergence criteria up to the formation of initial crack. Thereafter, the force convergence criteria were dropped and a tolerance limit of 0.25 was used for displacement convergence criteria. A listing of the load steps, sub steps, and loads applied per restart file as analysed. The load steps used in the present study is shown in Table 4.7.

Table 4.7 Load increment for analysis of Finite Element Model

Beginning Time	Time at End of Load Step	Load Step	Sub Step
0	5000	1	20
5000	10000	2	20
10000	15000	3	20
15000	20000	4	20
20000	25000	5	20
25000	30000	6	20
30000	35000	7	20
35000	40000	8	20
45000	50000	9	20
55000	60000	10	20
60000	65000	11	20
65000	70000	12	20
70000	75000	13	20
75000	80000	14	20
80000	85000	15	20
90000	95000	16	20
95000	96000	17	25
96000	97000	18	25
97000	98000	19	25
98000	99000	20	25
99000	100000	21	25
100000	101000	22	25

.

CHAPTER 5

RESULTS AND DISCUSSIONS

5.1 GENERAL

The main reason for premature failure of reinforced concrete structures which are steel corrosion. The oxides generated during active corrosion of reinforcement induce a pressure on the surrounding concrete that leads the formation of crack. As an important feature of corrosion, longitudinal cracks provide a visual indication of the reinforcement corrosion with in concrete. The following sections focus on the development of crack in beams made of OPC and PPC.

The RC beam specimens were cast as specified in Section 3.4. In the present study 5 control specimens and 16 corroded specimens (2.5%, 5%, 7.5% and 10% of corrosion) prepared with OPC and PPC mix were tested as cantilever beams, in a specially prepared loading set up to determine the flexural capacity. Two hydraulic jacks were used: one to fix the beam bottom to the reaction bed and other at the top of the set up to apply the loads. By this set up, beams deflection, strain, crack width were measured using dial gauge, mechanical strain gauge and crack microscope (Elcometer 900) respectively.

The beam is monitored using dial gauge, crack width and strain measurements were done for every 5kN increase in load. The deflections of all concrete beams, in general, linearly increases and the first set of flexural cracks were observed at the fixity (bottom) of the concrete beams. The load deflection curve for all specimens beam show a linear elastic behaviour at first, but after the first crack of the load deflection curve becomes non-linear many cracks develop bending and deflection of the beam increases considerably.

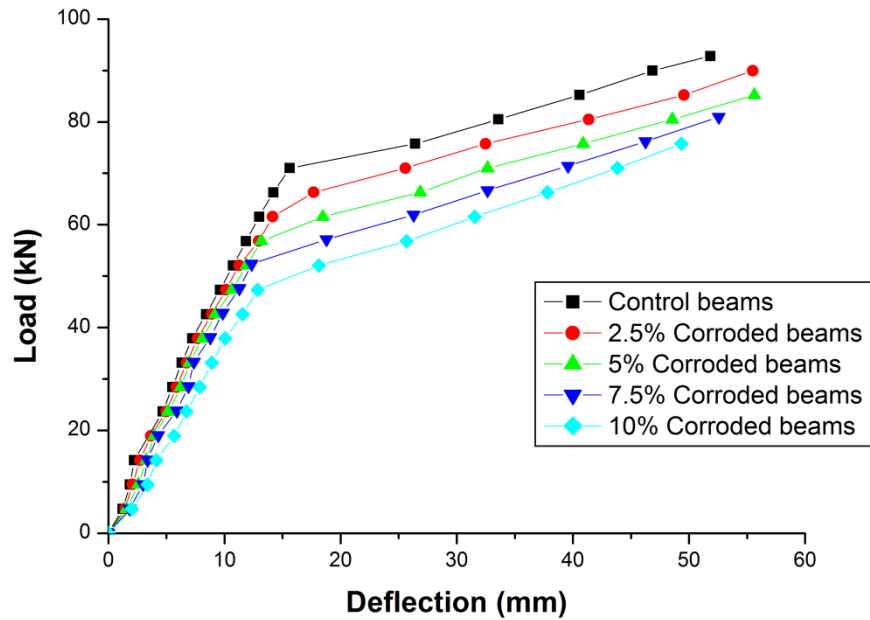## 5.2 EFFECT OF CORROSION ON LOAD-DEFLECTION BEHAVIOUR FOR OPC AND PPC BEAMS

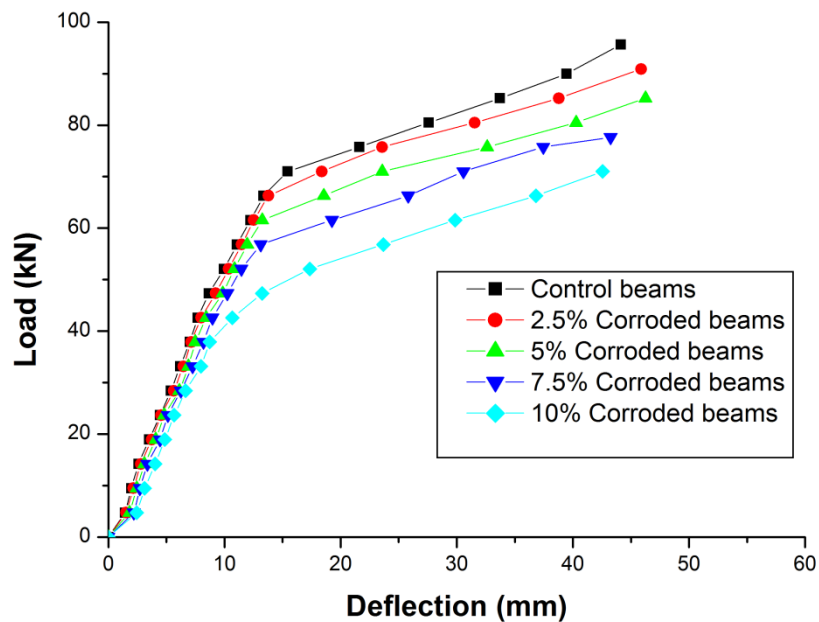
Fig. 5.1 Load v/s Deflection for OPC beams

Fig. 5.2 Load v/s Deflection for PPC beams

Fig. 5.1 and Fig. 5.2 show the deflection values against applied load for OPC and PPC beams respectively for different rates of corrosion. The Control Beams (CB) failed at an average load of 92kN. It was observed that as the rate of corrosion increased, the deflections of the beams also increased for a given load. Considering 75.8kN as a reference load, for an increase in corrosion percentage by 2.5% to 10%, the deflection increased from 18.7% to 46.5% compared to CB of OPC beams. For PPC beams, deflection increased from 16% to 63.7% when corrosion rate was increased from 2.5% to 10%. As the rate of corrosion increases, cross section area of the bar reduces, higher deflection is observed but beams fail at lesser loads, as expected. This composite structure, where the rim of the tempered martensite acts as the load-bearing element and the comparatively soft ferrite-pearlite core, provides the rebars with ductility.

From the above discussion, it is clear that the stiffness of the beams reduces with the increase in corrosion rate. With increase in corrosion, the beams exhibit large deflection compared to control beam specimens. The reason for such behavior is mainly the change in the values of modulus of elasticity of steel and concrete as the corrosion rate increases. The beams failed at lesser load and with more deflection, compared to control beams.

5.3 ACTUAL NUMBER OF DAYS REQUIRED FOR VARIOUS LEVEL OF CORROSION IN OPC AND PPC BEAMS
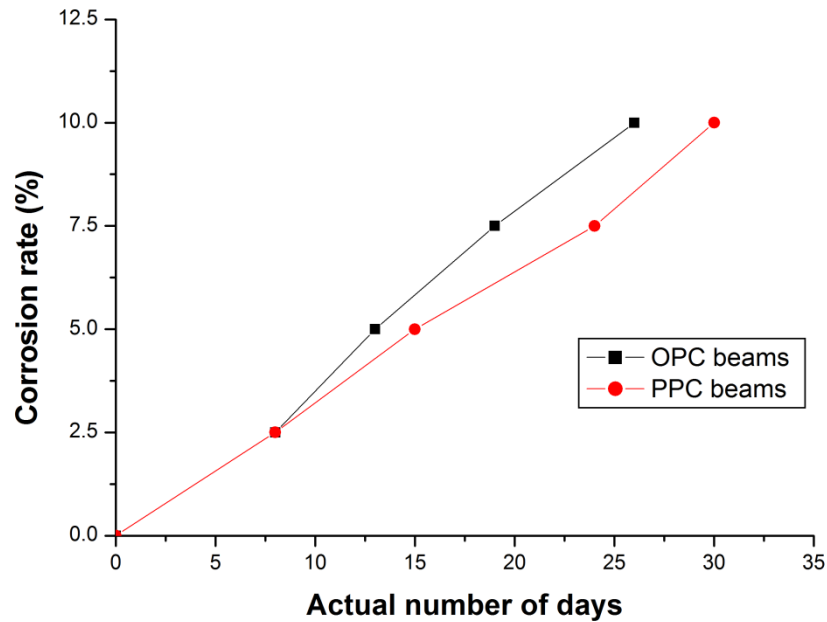
Fig. 5.3 Corrosion rate v/s Actual number of days

Fig. 5.3 shows the actual number of days required for OPC and PPC beams for various level of corrosion. Up to 2.5% corrosion the number of days required for OPC and PPC beams are same, as the required rate of corrosion increased OPC beams required less number of days to achieve target corrosion rate compared to PPC beams. Since both beams are subjected to same target corrosion rate load bearing capacity of both beams get affected. For normalizing it to 20days OPC beams are corroded to 7.5% while PPC beams are corroded to 6.25%. The reason for decrease in number of days in OPC beams is due to the higher porosity of OPC beams.

5.4 NORMALIZED VALUES FOR OPC AND PPC CORRODED BEAMS

Table 5.1 Normalized values for OPC beams

Specimen	Load(P) (kN)	Deflection (δ) (mm)	P/δ	Normalized P/δ
Control beam	92.80	51.85	1.79	1
2.5% corroded beam	89.96	55.49	1.62	0.90
5% corroded beam	85.23	55.62	1.53	0.85
7.5% corroded beam	80.95	52.56	1.54	0.86
10% corroded beam	75.75	49.35	1.54	0.86

Table 5.2 Normalized values for PPC beams

| Specimen	Load(P) (kN)	Deflection (δ) (mm)	P/δ	Normalized P/δ
Control beam	95.64	44.12	2.17	1
2.5% corroded beam	90.91	45.89	1.98	0.91
5% corroded beam	85.23	46.25	1.84	0.85
7.5% corroded beam	77.65	43.25	1.80	0.83
10% corroded beam	71.02	42.57	1.67	0.77

Table 5.1 and Table 5.2 show that as the rate of corrosion increases the load carrying capacity of beams decreases, but an increase in deflection rate was observed for both OPC and PPC beams. P/δ values decrease as the rate of corrosion increases compared with CB. As the rate of corrosion increases from 2.5% to 10%, normalized (P/δ) values decrease from 10% to 14% for OPC beams. Normalized (P/δ) values decreases from 9% to 23% in PPC beams for similar rates of corrosion.

From the above observations it is clear that as the rate of corrosion increases, the load carrying capacity of OPC beams is more than PPC beams. Also, in the deflection criteria PPC beams are stiffer than OPC beams.

5.5 EFFECT OF CORROSION ON I_{CORR} VALUES

5.5.1 Measured i_{corr} values from ACM for different rate of corrosion
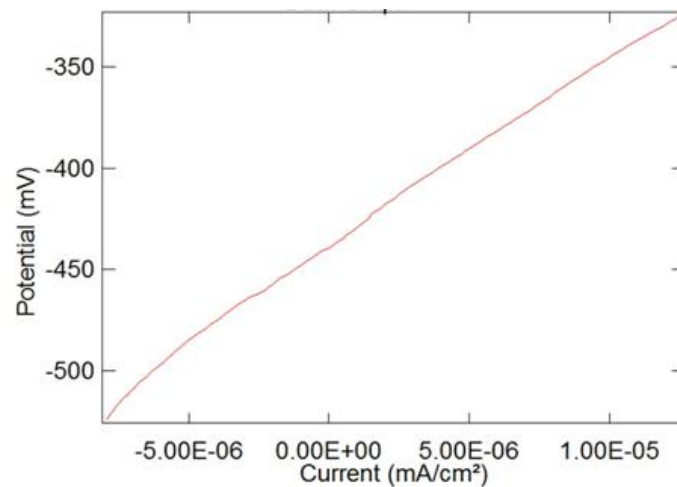
(a) OPC Beams
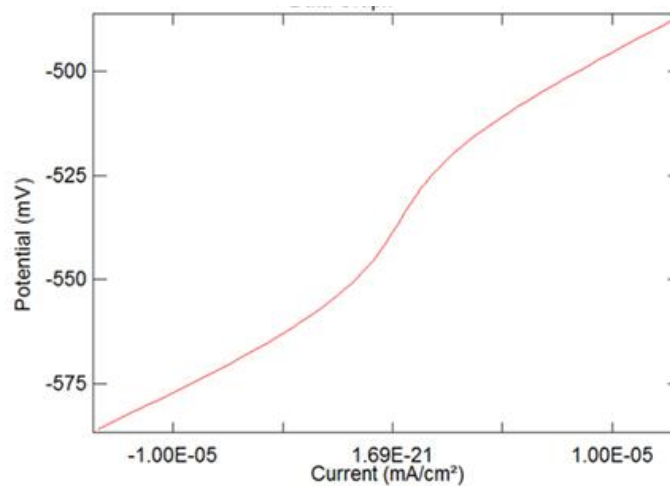
(b) PPC Beams

Fig. 5.4 (a) and (b) ACM instrument results of I_{corr} values for 2.5% corroded beams

The corrosion results obtained from ACM instrument are shown in Fig. 5.4 (a) and (b) for 2.5% Corrosion current density of OPC and PPC beams. The results of i_{corr} values are tabulated in Table 3.14 and Table 3.15. It is assumed that $i_{corr} = i_{applied}$ for calculating the corrosion percentage. The actual corrosion percentage was determined experimentally using the ratio of the change in mass to the original mass. The above two results are compared and a good agreement is observed.

5.5.2 Effect of corrosion on time (days) for OPC and PPC beams
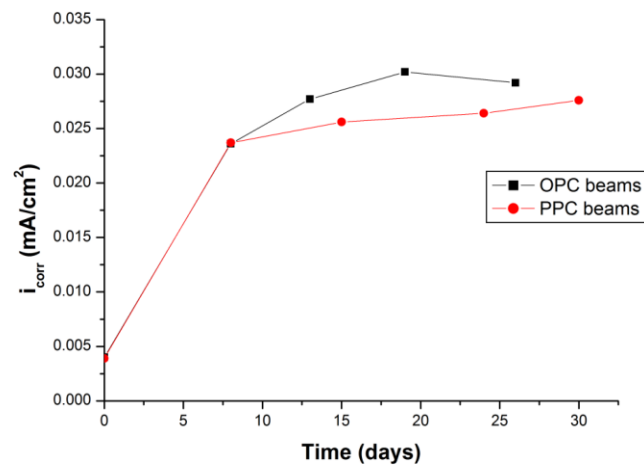
Fig.5.5 Variation of i_{corr} values with duration in days

From Fig. 5.5 it can be observed that an OPC beam take more current density (i_{corr}) and requires less number of days to achieve the expected corrosion, whereas PPC beams take less i_{corr} and hence, require more number of days to achieve the expected corrosion. This reduced rate of corrosion in PPC beams is due to the presence of pozzolanic material in cement which makes obstruction for chloride ion migration to the concrete and it is less porous than OPC. PPC beams are 15% corrosion resistance than OPC.

5.5.3 Effect of corrosion on i_{corr} values of OPC and PPC beams
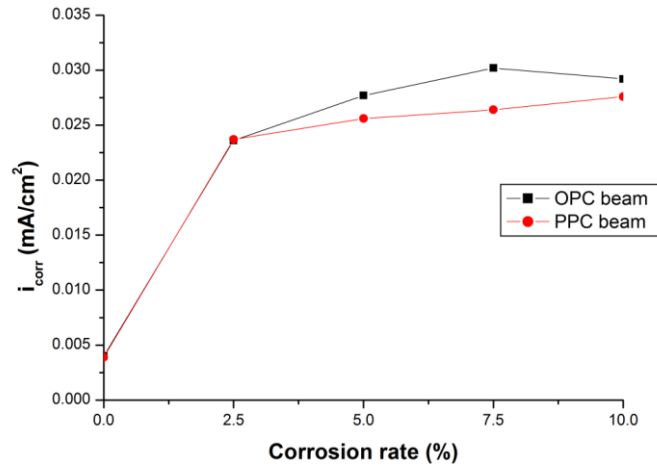
Fig. 5.6 Variation of i_{corr} values with corrosion rate

Fig.5.6 shows the variation of i_{corr} value with change in rate of corrosion. As the rate of corrosion increases from 2.5% to 10%, the i_{corr} rate also increases. Up to 2.5% rate of corrosion for both OPC and PPC beams have same i_{corr} values. For OPC beams after 2.5% corrosion i_{corr} value increases from 14.8% to 19.2%. For PPC beams it increases from 7.4% to 9.6% for similar rates of corrosion.

From the above observations it is concluded that i_{corr} values, required to corrode the OPC beams, are more compared to PPC beams.

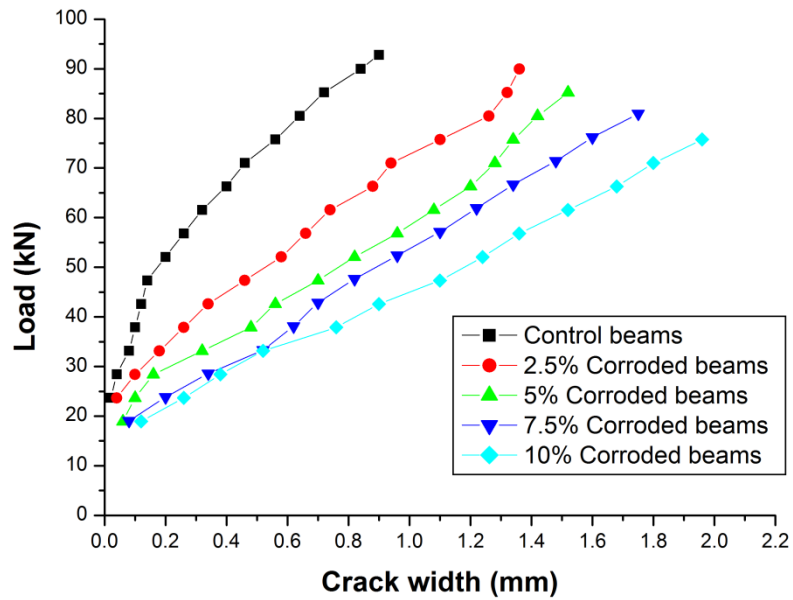## 5.6 EFFECT OF CORROSION ON CRACK WIDTH FOR OPC AND PPC BEAMS

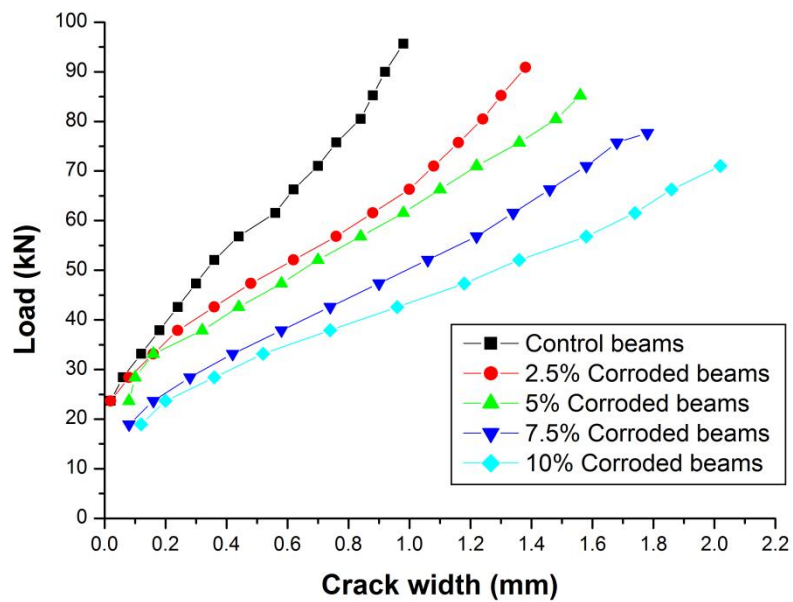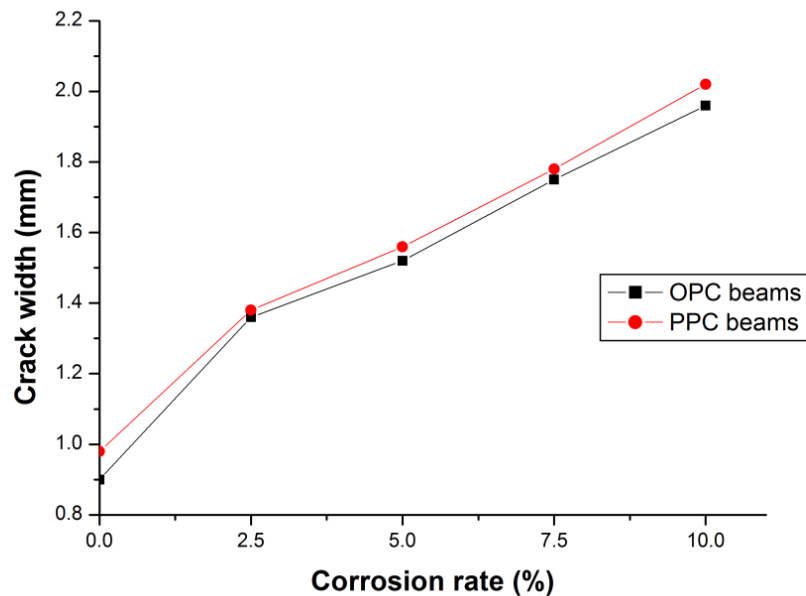**Fig. 5.7 Load v/s Crack width for OPC beams**

Fig. 5.8 Load v/s Crack width for PPC beams

Fig. 5.9 Crack width v/s corrosion rate

The increase in crack width with the increase in corrosion rate and load can be observed in Fig. 5.7 and Fig. 5.8 for OPC and PPC beams respectively. It is clear from the Figs. that with increase in corrosion rate load carrying capacity of beams reduce. There were many cracks formed for each load increment and only maximum crack width for each load increment is presented here. The crack width is measured for each load increment. First crack started to appear at a load of 20kN. The maximum crack width observed was 0.9mm for OPC control beam. As corrosion level is increased from 2.5% to 10%, the crack width increases from 1.36mm to 1.96mm for OPC beams. The maximum crack width observed was 0.98mm for PPC in case of control beam. As corrosion level is increased from 2.5% to 10%, the crack width increases from 1.38mm to 2.02mm for PPC beams. The development of crack width can be attributed to factors like curing method and concrete ingredient variation. There are two types cracks, the crack that penetrates in to the concrete cover (external cracks) and the cracks which develop between two steel bars (internal cracks). In the present study external cracks were observed.

Fig. 5.9 shows that as the rate of corrosion increases crack width also increases in both OPC and PPC beams. The crack widths of the both specimens are almost same but

change in load condition. The above results indicate that rate of corrosion achieved by accelerated corrosion technique is reasonably good.

5.7 EFFECT OF CORROSION ON LOAD BEARING CAPACITY OF OPC AND PPC BEAMS

Table 5.3 and Table 5.4 represent the moment capacity of OPC and PPC beams for different corrosion rate. As the rate of corrosion increases steel cross-section reduces in the beams. It is observed from the tables that as the rate of corrosion increases there is a reduction in moment carrying capacity in both OPC and PPC beams. In accelerated corrosion test, the PPC beams behaved more corrosion resistant than OPC and PPC beams took more number days for same chloride concentration to achieve target corrosion level. This is due to the presence of pozzolana in PPC.

Table 5.3 Moment capacity of OPC beams

% Corrosion	Ultimate load (kN)	Ultimate Moment (kNm)	% Reduction in moment
0	92.8	162.40	--
2.5	89.96	157.43	3.06
5	85.23	149.15	8.16
7.5	80.95	141.66	12.78
10	75.02	131.29	19.16

Table 5.4 Moment capacity of PPC beams

% Corrosion	Ultimate load (kN)	Moment (kN-m)	% Reduction in moment
0	94.7	165.73	--
2.5	90.91	159.10	4.00
5	85.23	149.15	10.00
7.5	77.65	135.88	18.00
10	71.02	124.29	25.01

From the tables, it is seen that as the rate of corrosion increases PPC beams are having large reduction of moments compared to OPC beams. As the rate of corrosion increases, bar diameter reduces. Formation of rust in between concrete and

reinforcement leads to the formation of cracking. Consequently load carrying capacity of the beams also decreases.

5.8 MOMENT CURVATURE RELATION FOR OPC AND PPC BEAMS

5.8.1 General

A major concern in the design of reinforced concrete beams is how they deform under applied loads (i.e. flexural behaviour). Beams resist bending and deflections by developing internal moments and shears. The deformation of a beam resulting from a bending moment is measured by curvature. Moment curvature relationships are important since they are fundamental to the understanding of member ductility and the redistribution of elastic moments before collapse. Curvature is the rotation per unit length along the axis of a member subjected to bending.

Curvature ($\emptyset$) can be conveniently measured from the linear strain distribution as,

$$\emptyset = \frac{\epsilon_{st} + \epsilon_c}{d} \tag{5.1}$$

Where ϵ_{st} is the tensile strain, ϵ_c is the compressive strain and d is the effective depth in mm (Pillai and Menon, 2009).

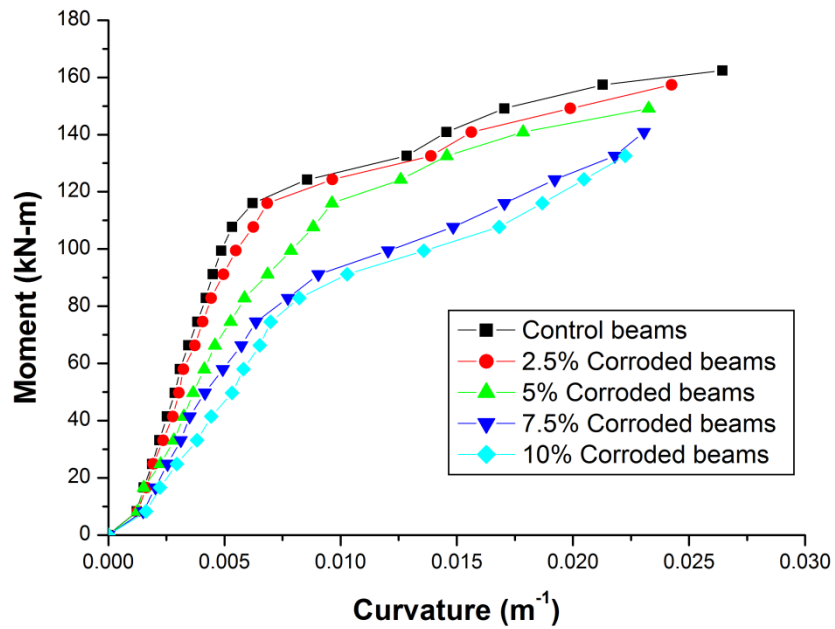**5.8.2 Effect of corrosion on moment-curvature relation for OPC and PPC beams**

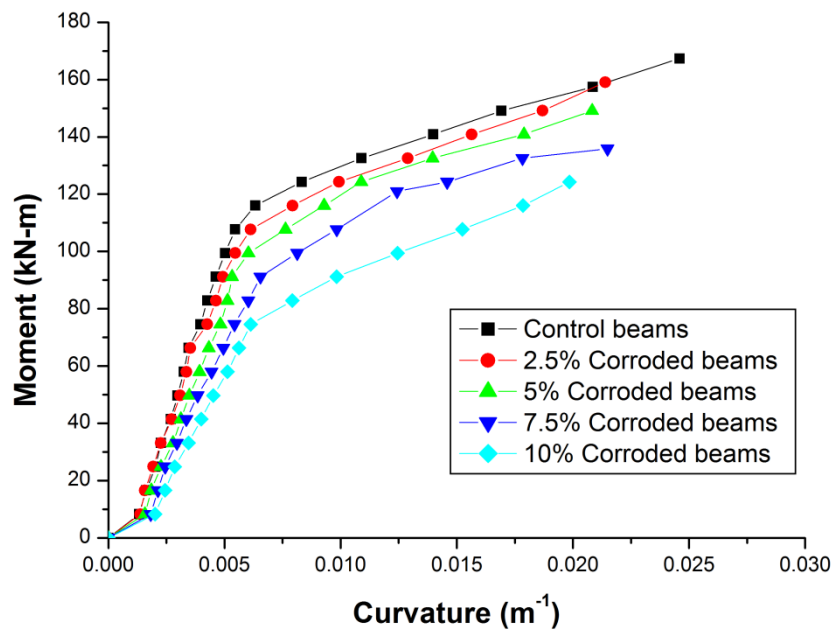**Fig. 5.10 Moment curvature relation for OPC beam**

**Fig. 5.11 Moment curvature relation for PPC beam**

Fig. 5.10 and Fig. 5.11 show the variation of moment with curvature for OPC and PPC beams respectively with different levels of corrosion. It is clear that with increase in corrosion moment carrying capacity decreases and curvature increases. As the rate of corrosion increases, surface area of bar decreases, resulting in increase of curvature of the beams. It is observed that as corrosion level is increased for OPC beams compared to CB from 2.5% to 10%, curvature values increase from 7.5% to 42.3% and for PPC beams compared to CB curvature values increase from 16.1% to 58% for similar increase of corrosion rate.

5.9 STRAIN VALUES FOR DIFFERENT RATE OF CORROSION

Strain values were measured mechanically using demec gauge in the beams for different load intervals. Both tensile and compression strain values were recorded for different levels of corrosion. Along with this, strains were also measured using lab view which is a virtual instrumentation. Both readings were compared for different levels of corrosion using graphical representation. NI DAQ was used for assessing the data for two strain gauges which were embedded inside the concrete and for one strain gauge which was placed on the surface of the concrete.
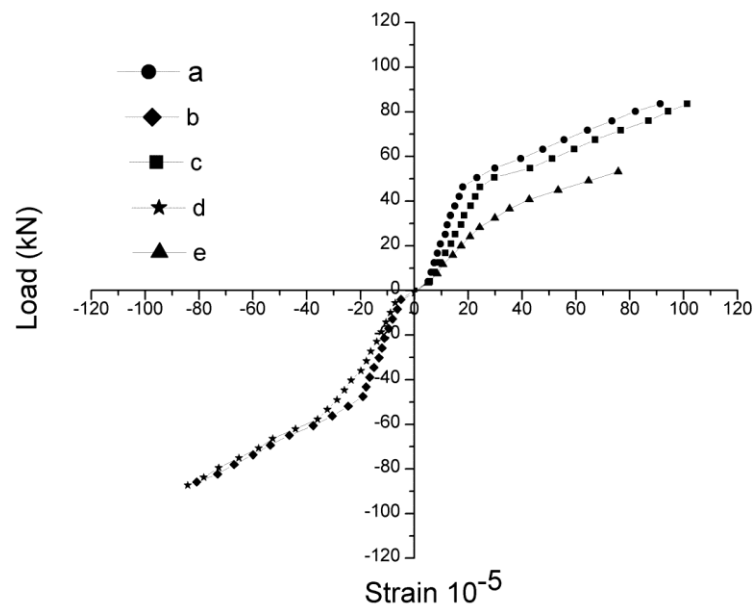
Fig. 5.12 Load v/s Strain for control beam
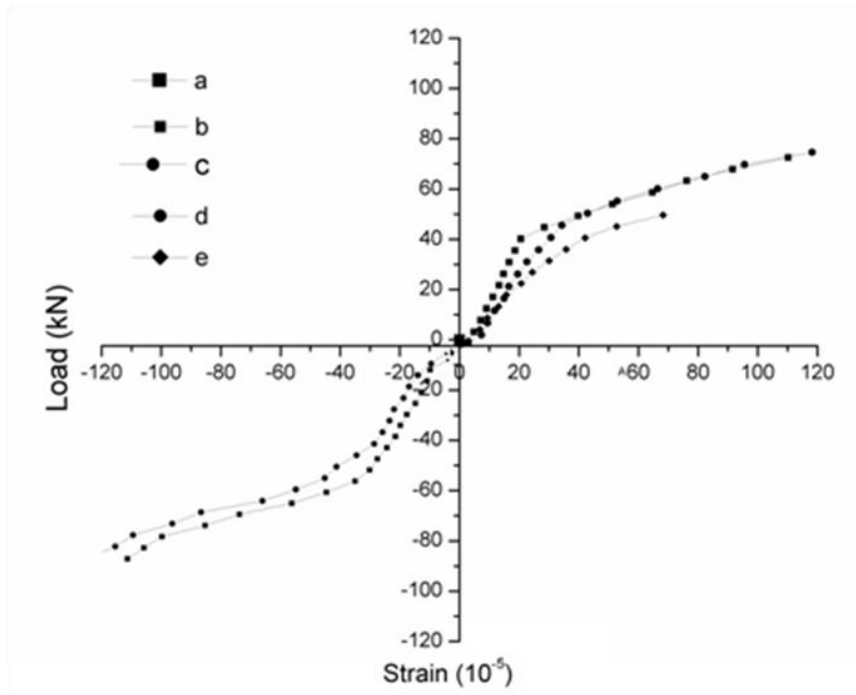
Fig. 5.13 Load v/s Strain for 2.5% corroded beam
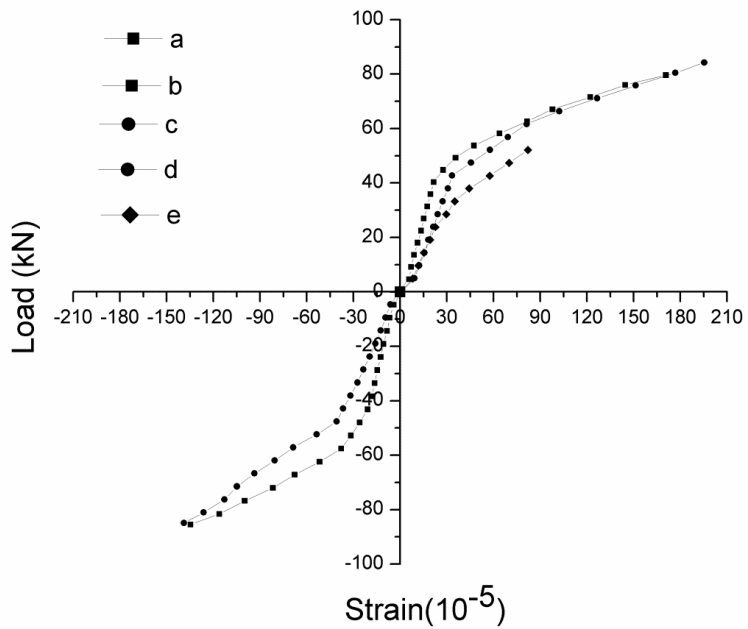
Fig. 5.14 Load v/s Strain for 5% corroded beam

Fig. 5.15 Load v/s Strain for7.5% corroded beam

Fig. 5.16 Load v/s Strain for 10% corroded beam

94

In the above graphs the legends a, b, c, d, e represent different types of strain measured. 'a' represents average tensile strains obtained mechanically. 'b' represents average compression strain obtained mechanically. 'c' represents tensile strain values obtained from lab view. 'd' represents compression strain values obtained from lab view. 'e' represents strain values measured on the surface of the concrete obtained from lab view.
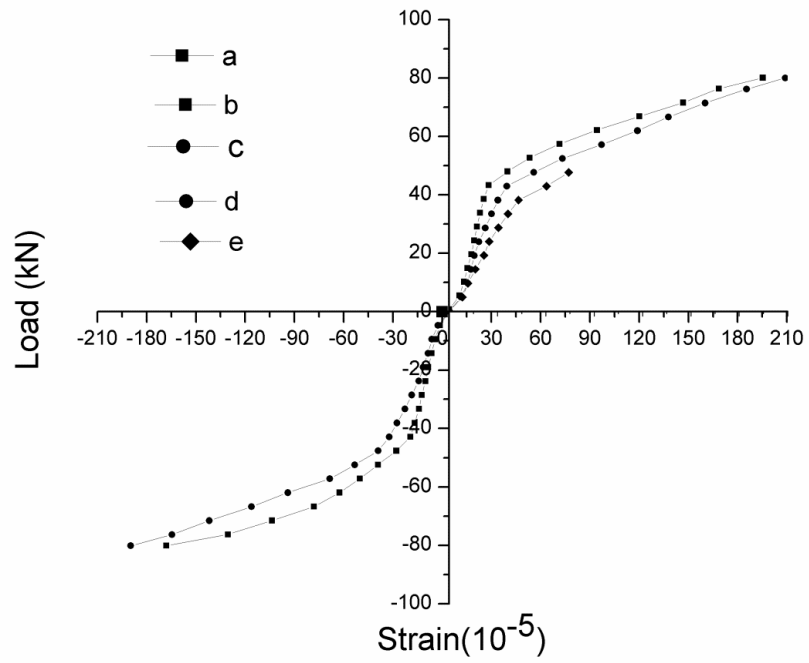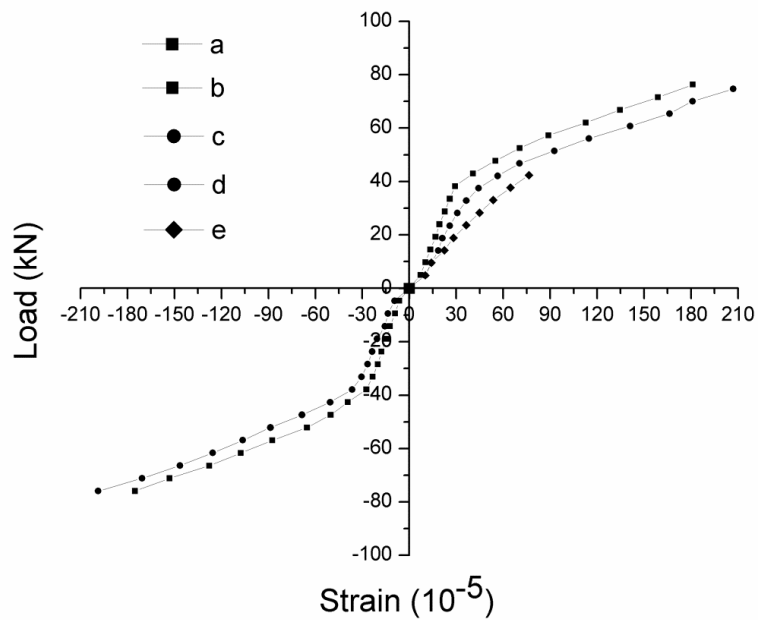
Fig. 5.12 shows the load v/s strain values for control beams (i.e., non corroded or 0% corrosion). As the rate of loading increases, strain values gradually increase till yielding of steel. When steel starts yielding, strain values drastically increase. The tensile strain values obtained from lab view were 10% more than average tensile strain obtained mechanically using demec buttons. The compression strain values obtained from lab view were 4% more than average compression strain obtained mechanically. Surface strain gauge stopped at a load of 61.6kN indicating failure of specimen.

Figs. 5.13 to 5.16 show the load v/s strain values for corroded beams of different level of corrosion. As the rate of loading increases strain values gradually increase. As the rate of corrosion increases the strain values increase but specimens fail at lesser loads compared to control beam. The tensile strain values obtained from lab view for 2.5%, 5%, 7.5% and 10% corroded beams were respectively 5.6%, 12.5%, 6.2% and 12.5% more than average strain values. The compression strain values obtained from lab view for 2.5%, 5%, 7.5% and 10% corroded beams were respectively 13.6%, 4.6%, 10.6% and 11.8% more than average compression values.

As the rate of corrosion increases mechanical properties of the steel will decrease. As cross section area reduces, beams fail at a lesser load compared to control beam. As rate of corrosion increases the tensile strain and compression strain values are more compared to control beams. The stiffness of the beams are reduced when rate of corrosion increased.

5.10 FINITE ELEMENT ANALYSIS FOR CANTILEVER OPC BEAM

5.10.1 General

This section draws comparison between behavioural characteristics of the experimental results and FEM model. The beam behaviour at initial cracking, steel yielding and at the failure, load deflection characteristics and the crack development are included in the following discussion. This is to ensure that the elements, material properties, real constants and convergence criteria are adequate to model the response of the member.

5.10.2 Crack development of the beam model

Crack development was observed in the beam model when load was increased. The deflection of the control beam when first crack is initiated is shown in Fig. 5.17. The propagation of cracks are shown in the Fig. 5.18. Fig. 5.18 (a) shows the first crack at 15.5kN, Fig. 5.18(b) shows development of crack for 30kN, Fig. 5.18(c) shows development of crack for 50kN, Fig. 5.18(d) shows development of crack for 70kN, Fig. 5.18(e) shows development of crack for 80kN, Fig. 5.18(f) shows development of crack for 90kN, Fig. 5.18(g) shows development of crack for failure load 100.52kN. Fig. 5.19 shows the deflection of the beam at the time of failure.
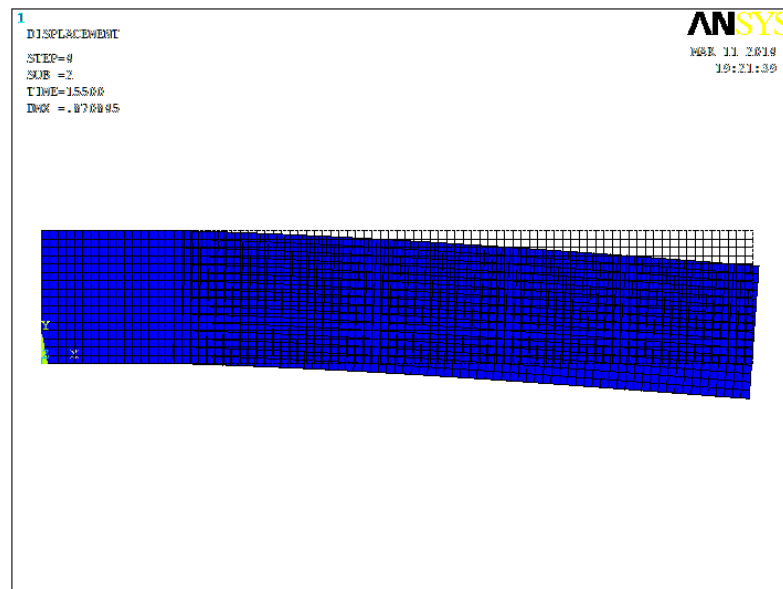
Fig. 5.17 Deflection at first crack of control beam
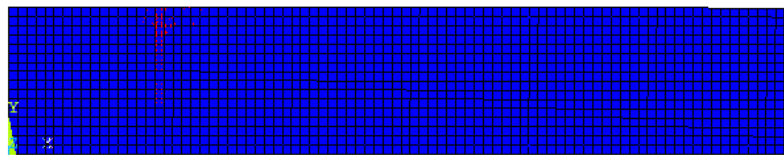
Fig. 5.18(a)
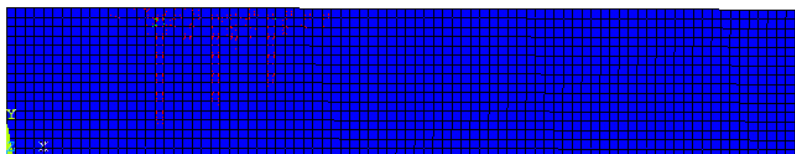
Fig. 5.18(b)
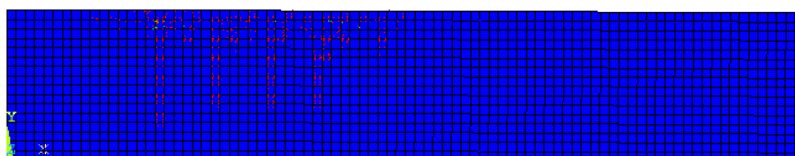
Fig. 5.18(c)
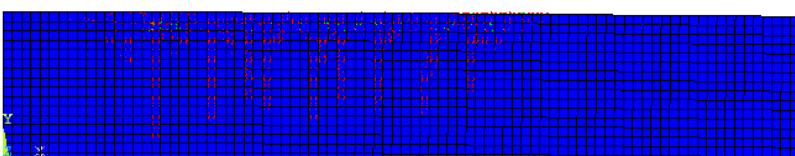
Fig. 5.18(d)
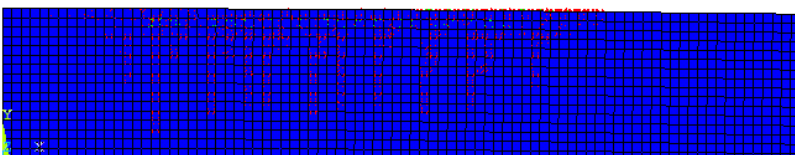
Fig. 5.18(e)
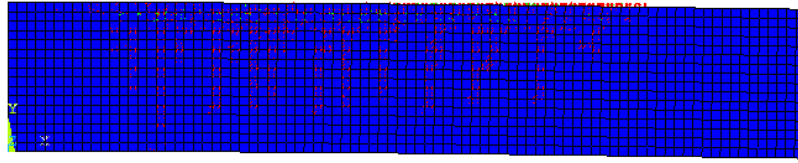
Fig. 5.18(f)
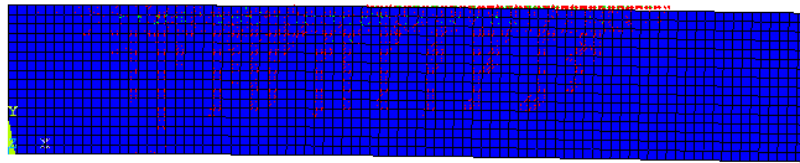
Fig. 5.18(g)

Fig.5.18 Crack development of the beam model for different loading
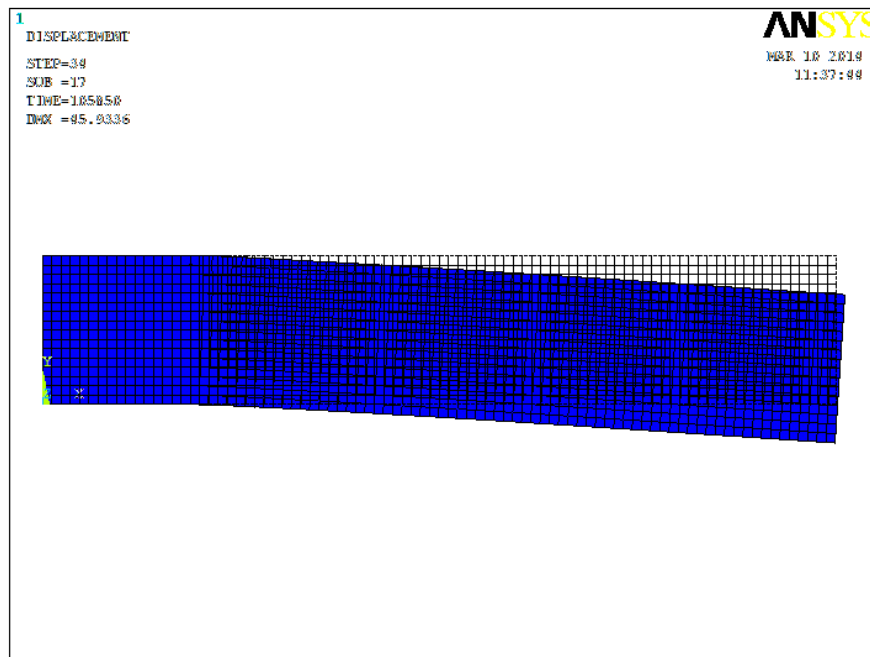
Fig. 5.19 Deflection of the beam at the time of failure

5.10.3 Comparison of experimental results and numerical modelling for different levels of corrosion

The FE analysis of the model was considered to examine different behaviours: initial cracking of the beam, yielding of the steel reinforcement, deflection and the strength limit state of the beam. The Newton-Raphson method was used to compute the nonlinear response. The application of the loads up to failure was done incrementally. After each load increment, the restart option was used to go to the next step after convergence. As the rate of corrosion increases the surface area of the bar reduces as in Eq. 5.2 (Shetty et al. 2014). Table 5.5 shows reduction of bar diameter after corrosion using Eq. 5.2.

$$\Phi_1 = \Phi \times \sqrt{1 - \frac{p}{100}} \qquad (5.2)$$

where,

Φ is the initial diameter of the bar in mm

p is the corrosion percentage

Φ_1 is the reduced diameter of the bar in mm

Table 5.5 Reduction of the bar diameter after corrosion

Diameter (mm)	2.5%	5%	7.5%	10%
20	19.75	19.49	19.24	18.97
16	15.80	15.60	15.39	15.18
12	11.85	11.69	11.54	11.38
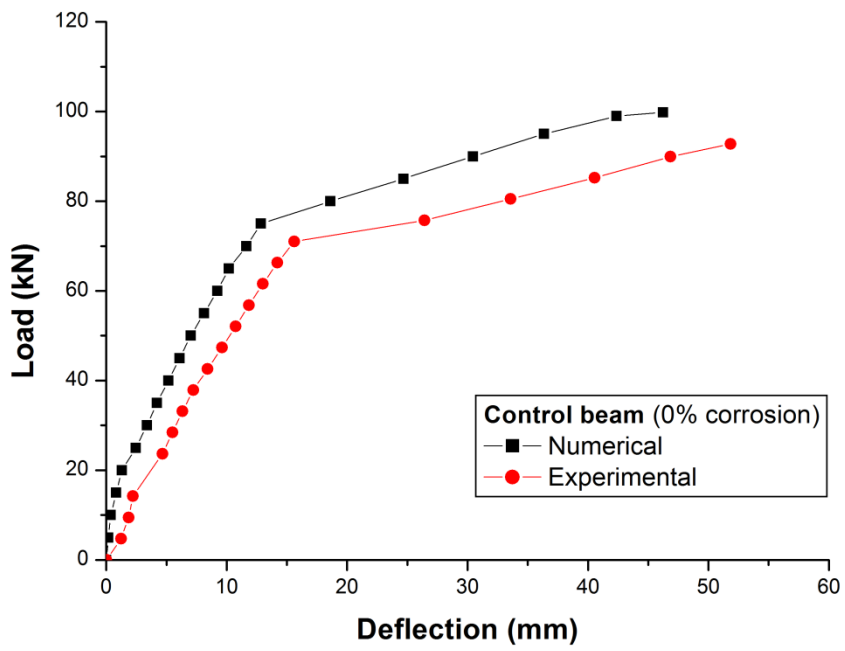
Fig. 5.20 Load v/s Deflection for control beams
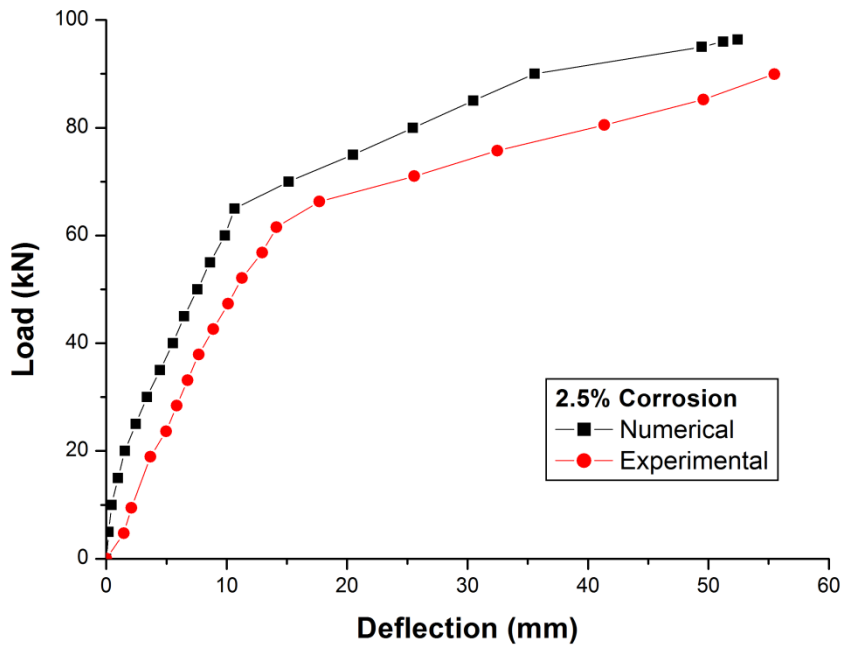
Fig. 5.21 Load v/s Deflection for 2.5% corroded beams

100
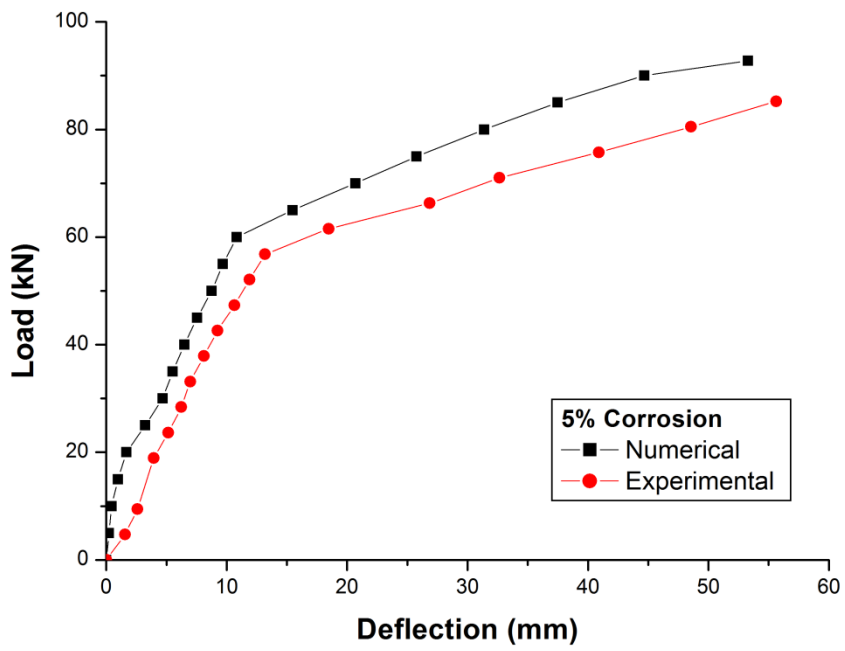
Fig. 5.22 Load v/s Deflection for 5% corroded beams
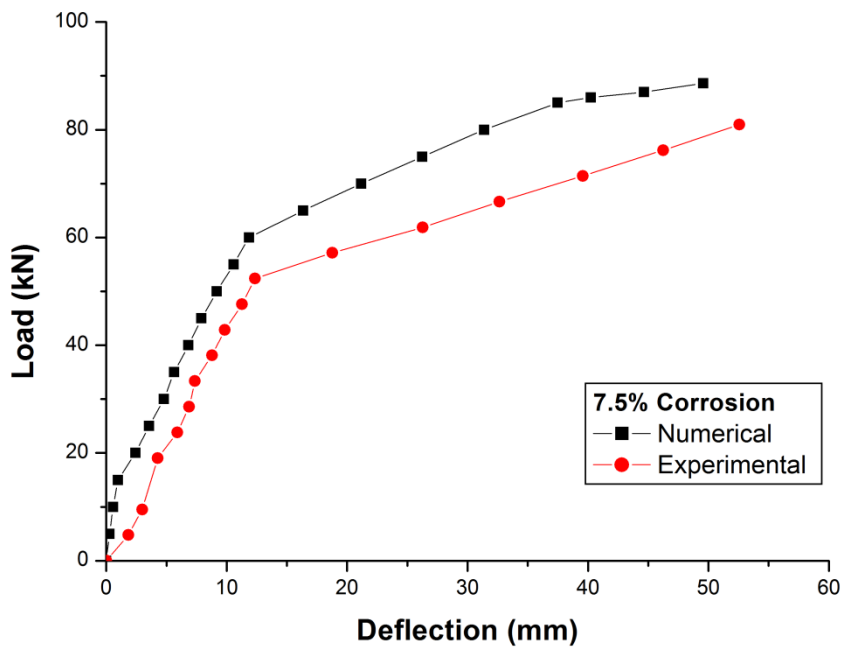
Fig. 5.23 Load v/s Deflection for 7.5% corroded beams
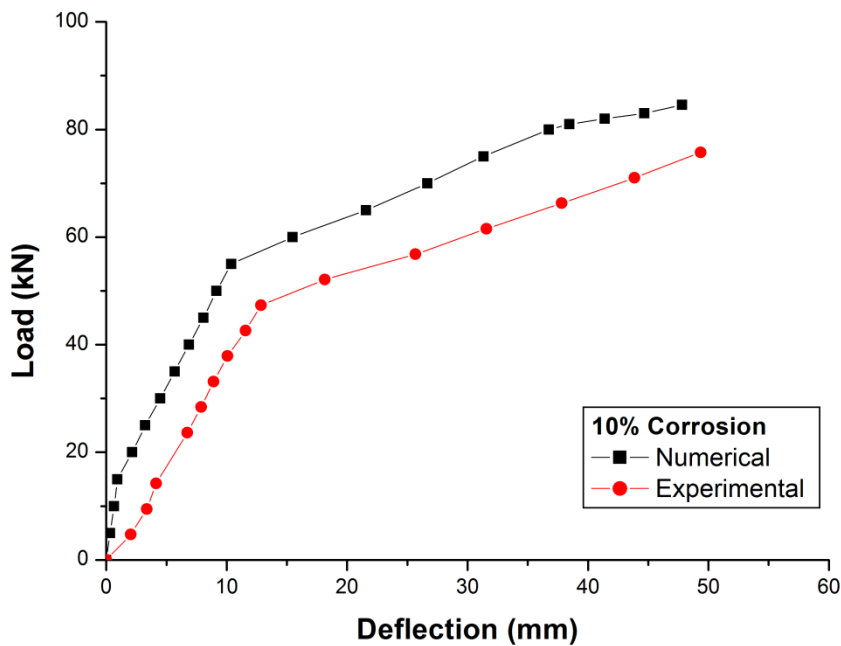
Fig. 5.24 Load v/s Deflection for 10% corroded beams

Fig. 5.20 shows the comparison between experimental and numerical model of OPC control beam. The maximum deflection observed at the time of failure in experiment was 51.9mm and in numerical modelling was 46mm. A large deviation in curve was observed at yielding of steel. Table 5.6 shows the yielding of steel and failure load for various levels of corrosion in experimental and numerical model of beams.

In the numerical modelling, the cantilever beam model is restrained in all the three directions X, Y and Z and hence the model is rigidly fixed at the bottom. But in experiments fixity is provided at the bottom by using hydraulic jack and it is very difficult to achieve complete fixity. This factor in experiments caused more deflection in beams compared to numerical model. The deflections during experiments were about 12% more compared to numerical model. This difference may also be due to variation in the actual values of material properties and actual fixity conditions.

Table 5.6 Comparison of yield load and ultimate load for different levels of corrosion

Corrosion	Experimental Results		Numerical Results	
	Yield load (kN)	Ultimate load (kN)	Yield load (kN)	Ultimate load (kN)
0% (Control beam)	75.8	92.8	79.4	100.5
2.5%	66.3	89.9	68.6	96.4
5%	61.5	85.2	64.2	92.7
7.5%	57.2	80.9	59.3	88.6
10%	52.1	75.8	54.7	84.6

Figs. 5.21 to 5.24 show the load-deflection relationship for various levels of corroded beams. As the rate of corrosion increases for experiments from 2.5% to 10%, the load during the yielding of steel decrease from 12.5% to 31.3% and also the corresponding failure loads decrease from 3.1% to 18.3%. Further, it was observed that with increase in corrosion levels from 2.5% to 10%, deflection values increased by 18.7% to 46.5%. From the results of numerical model it is observed that as the rate of corrosion increases for numerical models from 2.5% to 10%, the load during yielding of steel decreases from 12.5% to 30% and the failure loads decreases from 4% to 15.8%. Further it is observed that with increase in corrosion levels from 2.5% to 10% deflection values increase from 15.3% to 39%. In the above, all the results are compared with those for control beams. It is observed that numerical models are slightly stiffer than experiments for various levels of corrosion.

.

CHAPTER 6

CONCLUSIONS

6.1 CONCLUSIONS

- It was observed that the control beams attained the higher load carrying capacity of about 23% more compared to theoretical ultimate load.
- It was observed that PPC beams behaved stiffer than OPC beams.
- Time required in days for different levels of corrosion can be calculated using the proposed equation

$$T = \frac{\rho}{I} \times \pi DL \times 1.1835 \times 10^{-3}$$

- From the experimental investigations carried out in this research, it is concluded that ACM instrument can be a good alternative to measure corrosion rate which in turn can be used for calculating the amount of reinforcement corrosion.
- The studies show that NI DAQ system can be a good alternative to measure the strain values for different rate of corrosion.
- As the rate of corrosion increases form 2.5% to 10%, stiffness and load carrying capacity decrease rapidly while deflection, crack width and curvature increase in beam specimens.
- Considering safety issue designers usually provide more reinforcement in beams and in columns. This should be optimised because in the coastal regions reinforcement is more prone to corrosion. If reinforcements are more, the rate of corrosion will also be more which will lead to cracks in the structure and eventually reduce the load bearing capacity of the structure.
- PPC beams were more corrosion resistant than OPC beams but when comes to load bearing capacity, the OPC performed better compared to PPC beams (Chemistry of the detailed interface between reinforcement and concrete has to be studied).

- PPC beams are 15% more corrosion resistant than OPC beams as chloride migration in PPC beams is less compared to OPC beams.
- In RC beams as the rate of corrosion reaches to 10% the spalling of concrete took place in Accelerated corrosion technique.
- In the accelerated corrosion the power was supplied to the reinforcement which acted as anode. The main reason for corrosion was potential drop between the anode and the cathode because of that corrosion takes place. If this potential drop was controlled by passing small power to the affected area and voltage maintained constant then rate of corrosion can be controlled in the structure.
- The numerical results match fairly well with the results of experimental investigations for the range of models and levels of corrosion considered in the study.
- This study indicates that Finite Element analysis can be applied satisfactorily to predict ultimate load, deflection and crack pattern of RC beams subjected to corrosion.

6.2 SCOPE OF FUTURE STUDIES

- ❖ Non destructive testing of specimens and analyzing corrosion rate by chemical analysis.
- ❖ Testing the specimens subjected to actual marine conditions and comparing the behaviour and mechanical performance of such specimens with specimens subjected to accelerated corrosion.
- ❖ Finite element analysis for different sizes of reinforcements, cover depth and for various levels of corrosion with different grades of concrete.
- ❖ Comparing accelerated and naturally corroded specimens and develop mathematical model to predict corrosion.

REFERENCES

- Ahmad, S. (2003). "Reinforcement corrosion in concrete structures, its monitoring and service life prediction–a review." *Journal of Cement & Concrete Composites*, 25(4-5), 459–471.

- Ahmad, S. (2009). "Techniques for inducing accelerated corrosion of steel in concrete." *Arabian Journal for Science and Engineering*, 34(2), 95–104.

- Almusallam, A. (2001). "Effect of degree of corrosion on the properties of reinforcing steel bars." *Construction and Building Materials*, 15, 361-368.

- Alonso, C., Andrade, C., Rodriguez, J., and Diez, J. M. (1998). "Factors controlling cracking of concrete affected by reinforcement corrosion." *Materials and Structures*, 31, 435-441.

- Andrade, C., and Alonso, C. (1996). "Corrosion rate monitoring in the laboratory and on site." *Construction Building Materials*, 10, 315-28.

- Andrade, C., Alonso, C., and Sarria, J. (2002). "Corrosion rate evolution in concrete structures exposed to the atmosphere." *Cement & Concrete Composites*, 24, 55–64.

- Andres, A., Gitierrez, S., and Guilen, J. (2007). "Residual flexure capacity of corroded reinforced concrete beams." *Journal of Engineering Structures*, 29, 1145-1152.

- ANSYS Commands Reference, (2011). ANSYS Inc., http:/www.ansys.com.

- Apostolopoulos, C. A., and Papadakis, V. G. (2008). "Consequences of steel corrosion on the ductility properties of reinforcement bar." *Construction and Building Materials*, 22, 2316–2324.

- Balafas, I., and Burgoyne, C. J. (2010). "Environmental effects on cover cracking due to corrosion." *Cement and Concrete Research*, 40, 1429-1440.

- Ballim, Y., and Reid, J. C. (2003). "Reinforcement corrosion and the deflection of RC beams–an experimental critique of current test methods." *Journal of Cement & Concrete Composites*, 25, 625–632.

- Bhaskar, S., Bharatkumar, B. H., Ravindra, G., and Neelamegam. M. (2010). "Effect of corrosion on the bond behavior of OPC and PPC concrete." *Journal of Structural Engineering*, 37 (1), 37-42.

- Boutz, M. M. R., Wegen, G. V., Haverkort, R., and Roelfstra, P. E. (2008). "Service Life Design of Concrete Structures by Numerical Modelling of Chloride Ingress." Tailor Made Concrete Structures, Walraven and Stoelhorst, eds., *Taylor & Francis Group*, London, 59-64.

- Cabrera, J. G. (1996). "Deterioration of concrete due to reinforcement steel corrosion." *Journal of Cement & Concrete Composites*,18, 47-59.

- Care, S., and Raharinaivo, A. (2007). "Influence of impressed current on the initiation of damage in reinforced mortar due to corrosion of embedded steel." *Cement and Concrete Research*, 37, 1598–1612.

- Castro, P., Weva, and Balancim, M. (1997). "Corrosion of reinforced concrete in a tropical marine environment and in accelerated tests." *Construction and Building Materials*, 11(2), 75-81.

- Chansawat, K., Potisuk, T., Miller, T., Yim, S., and Damian, K. (2009). "FE Models of GFRP and CFRP Strengthening of Reinforced Concrete Beams." *Advances in Civil Engineering*, Article ID 152196.

- Coronelli, D., Hanjari, K. Z., and Lundgren, K. (2013)." Severely Corroded RC with Cover Cracking." *Journal of Structural Engineering*, 139(2), 221-232.

- Damian, K. Thomas, M., and Solomon, Y. (2001). "Finite Element Modeling of Reinforced Concrete Structures Strengthened with FRP Laminates." Report for Oregon Department of Transportation, Salem.

- Elsener, B. (2005). "Corrosion rate of steel in concrete-Measurements beyond the Tafel law." *Corrosion Science*, 47, 3019-3033.

- Fontana, M. G. (2005). "Corrosion Engineering." Tata McGraw-Hill Education Private Limited, New Delhi.

- Glass, G. K. (2003). "Reinforcement corrosion." Advanced concrete technology set, J. Newman and B. S. Choo, eds., Butterworth-Heinemann, Oxford, 1–27.

- Ibrahim, A., and Salman, W. (2009). "Finite Element Analysis of Reinforced Concrete Beams Strengthened With CFRP in Flexural." *Diyala Journal of Engineering Sciences*, 2, 88-104.

- IS 10262: (2009). Recommended guidelines for concrete mix design, Bureau of Indian Standards, New Delhi.

- IS 1489 (Part-I):1991. Portland Pozzolana cement-Specifications, Bureau of Indian Standards, New Delhi.

- IS 2386 (Part III):1963. Methods of test for aggregates for concrete: Specific gravity, density, voids, absorption and bulking, Bureau of Indian Standards, New Delhi.

- IS 4031:1988. Methods of physical tests for hydraulic cement, Bureau of Indian Standards, New Delhi.

- IS 456:2000. Plane and reinforced concrete-code of practice, Bureau of Indian Standards, New Delhi.

- Ismail, M., Muhammad, B., and Mohemmed, E. I. (2010). "Compressive strength loss and reinforcement degradations of reinforced concrete structure due to long-term exposure." *Construction and Building Materials*, 24, 898-902.

- Kostogloudis, G. C., Kalogridis, D., Ftikos, C., Malami, C., Georgali, B., and Kaloidas, V. (1998). "Comparative investigation of corrosion resistance of steel reinforcement in alinite and portland cement mortars." *Cement and Concrete Research*, 28(7), 995–1010.

- Law, D. W., Millard, S. G., and Bungey, J. H. (2000). "Linear polarisation resistance measurements using a potentiostatically controlled guard ring." *NDT and E International,* 33, 15–21.

- Li, C. Q., Lawanwisut, W., Zheng, J. J., and Kijawatworawet, W. (2005)."Crack width due to corroded bar in reinforced concrete structures." *International Journal of Materials and Structural Reliability*, 3, 87-94.

- Li, C. Q. (2003). "Life cycle modeling of corrosion affected concrete structures initiation." *Journal of Materials in Civil Engineering*, 15(6), 594–601.

- Li, C. Q., Zheng, J. J., Lawanwisut, W., and Melchers, R. E. (2007). "Concrete Delamination Caused by Steel." *Journal of Materials in Civil Engineering*, 19(7), 591–600.

- Liang, M. T., Wang, K. L., and Liang, C. H. (1999). "Service life prediction of reinforced concrete structures."*Cement and Concrete Research*, 29(9), 1411–1418.

- Malumbela, G., Alexander, M., Moyo, P. (2010)." Variation of steel loss and its effect on the ultimate flexural capacity of RC beams corroded and repaired under load." *Construction and Building Materials*, 24, 1051–1059.

- Malumbela, G., Alexander, M., Moyo, P. (2010). "Interaction between corrosion crack width and steel loss in RC beams corroded under load." *Cement and Concrete Research*, 40(9), 1419-1428.

- Manera, M., Venesland, Q., and Bertolini, L. (2008). "Chloride threshold for rebar corrosion in concrete with addition of silica fume." *Corrosion Science*, 50 554-560.

- Manoharan, R., Jabalan, P., Palanisamy, N. (2008). "Experimental Study on Corrosion Resistance of TMT Bar in Concrete." Proceedings of International conference on construction and building Technology. 22, 239-250.

- Maruya, T., Takeda, H., Horiguchi, K., Koyama, S., and Hsu, K. (2007). "Simulation of Steel Corrosion in Concrete Based on the Model of Macro-cell Corrosion Circuit." *Journal of Advanced Concrete Technology*, 5(3), 343-363.

- Melchers, R.E., and Li, C. Q. (2009). "Reinforcement corrosion initiation and activation times in concrete structures exposed to severe marine environments." *Cement and Concrete Research*, 39, 1068–1076.

- Ortega, N. F., and Aveldano, R. R. (2008). "Analysis of concrete beams during the corrosion process on reinforcement under tensile stress." *The Open Construction Building Technology Journal*, 2(1), 243–250.

- Pan, T., and Wang, L. (2011). "Finite-element analysis of chemical transport and reinforcement corrosion-induced cracking in variably saturated heterogeneous concrete." *Journal of Engineering Mechanics*, 137(5), 334-345.

- Parande, A., Dhayalan, P., Karthikeyan, M. S., Kumar, K., and Palaniswamy, N. (2008). "Assessment of structural behavior of non-corroded and corroded RCC beams using finite element method." Sensors & Transducers Journal, 96(9), 121-136.

- Park, R., and Paulay, T. (2013). Reinforced Concrete Structures, John Wiley & Sons, Inc. New York.

- Parnas, L. and Bilir, O. (1996) "Staingauge methods for measurements of opening mode stress intensity factor." *Engineering Fracture Mechanics*, 55(3), 485-492.

- Phuvoravan, K. (2010). "Effect of steel corrosion level on flexural behaviour of reinforced concrete beam." Report from Kasestart University, Bangkok, Thailand.

- Pillai, S. U., and Menon, D. (2009). "Reinforced Concrete design." Tata McGraw-Hill Education Private Limited, New Delhi.

- Poupard, O., L'Hostis, V., Catinaud, S., and Petre-Lazar, I. (2006). "Corrosion damage diagnosis of a reinforced concrete beam after 40 years natural exposure in marine environment." *Cement and Concrete Research*, 36(3), 504–520.

- Qiao, G., Xiao, H., and Sun, G. (2011). "Identification of the reinforcing steel's corrosion state in RC beams based on electrochemical sensor." *Sensor Review*, 31(3), 218-227.

- Ray, A., Mukerjee, D., Sen, S. K., and Battacharya, A. (1997). "Microstructure and Properties of Thermo-mechanically Strengthened Reinforcement Bars: A Comparative Assessment of Plain Carbon and Low-Alloy Steel Grades." *Journal of materials Engineering and performance*, 6, 335-343.

- Revathy, J., Suguna, K., and Raghunath, P. N. (2009). "Effect of corrosion damage on the ductility performance of concrete columns." *India American Journal of Engineering and Applied Science,* 2, 324-327.

- Rodriguez, J., Ortega, L. M., and Casal, J. (1997). "Load carrying capacity of concrete structures with corroded reinforcement." *Construction and Building Material*, 11(4), 239-248.

- Saether, I., and Sand, B. (2009). "FEM simulations of reinforced concrete beams attacked by corrosion." Northern Research Institute Narvik (Norut Narvik), Norway.

- Saifullah, I., Hossain, M. A., Uddin, S. M. K., Khan, M. R. A., and Amin, M. A. (2011). "Nonlinear analysis of RC beam for different shear reinforcement patterns by Finite Element Analysis." *International Journal of Civil & Environmental Engineering*, 11(1), 86-98.

- Shetty, A., Venkataramana, K., and Babunarayan, K. S. (2014). "Flexural bond strength behaviour in OPC concrete of NBS beam for various corrosion levels." *Structural Engineering and Mechanics*, Techno Press, 49(1), 81-93.

- Shetty, M. S. (2010). "Concrete Technology." S. Chand and Company Limited, New Delhi.

- Soleymani, H. R, and Ismail, M. E. (2004). "Comparing corrosion measurement methods to assess the corrosion activity of laboratory OPC and HPC concrete specimens." *Cement and Concrete Research*, 34, 2037-2044.

- SP 23: (1982). Handbook on concrete mixes, Bureau of Indian Standards, New Delhi.

- Tavarez, F. A. (2001). "Simulation of behaviour of composite grid reinforced concrete beams using explicite Finite Element Methods." Master Thesis, University of Wisconsin, Madison.

- Val, D. V. (2007). "Deterioration of strength of RC beams due to corrosion and its influence on beam reliability."*Journal of Structural Engineering*, 133(9), 1297–1306.

- Val, D. V., Chernin, L., and Stewart, M. (2009). "Experimental and Numerical investigation of corrosion induced cover cracking in reinforced concrete structures." *Journal of Structural Engineering*, 135(4), 376-385.

- Vasudevan, G., and Kothandaraman, S. (2011). "Parametric study on Nonlinear Finite Element Analysis on flexural behaviour of RC beams using ANSYS." *International Journal of Civil and Structural Engineering*, 02, 98-111.

- Vidal, T., Castel, A., and Francois, R. (2003)."Analyzing crack width to predict corrosion in reinforced concrete."*Cement and Concrete Research*, 34, 165-174.

- Vidal, T., Castel, A., and Francois, R. (2007). "Corrosion process and structural performance of a 17 year old reinforced concrete beam stored in chloride environment." *Cement and Concrete Research*, 37, 1551-1561.

- Vu, K., and Stewart, M. G. (2002). "Service Life Prediction of Reinforced Concrete Structures Exposed To Aggressive Environments." 9th International Conference on the Durability of Building Materials and Components, Brisbane, Australia.

- Wei-liang, J., and Yu-xi, Z. (2001). "Effect of corrosion on bond behaviour and bending strength of reinforced concrete beams." Journal of Zhejiang University.

- Wolanski, A. B. S. (2004). "Flexural Behaviour of Reinforced and Prestressed Concrete Beams Using Finite Element Analysis." Master's Thesis, Marquette University, Milwaukee, Wisconsin.

- Xiaoming, Y., and Hongqiang, Z. (2012). "Finite element investigation on load carrying capacity of corroded RC beam based on bond slip." *Jordan Journal of Civil Engineering*, 6, 134-146.

- Yoon, S., Wang, K., Weiss, W. J., and Shah, S. P. (2001). "Interaction between loading, corrosion, serviceability Reinforced concrete." *ACI Materials Journal*, 97(6), 99-181.

- Zhang, W., and Ba, H. (2011). "Accelerated life test of concrete in chloride environment." *Journal of Materials in Civil Engineering*, 23(3), 330-334.

APPENDIX I

AI-1 MIX DESIGN OF M20 GRADE CONCRETE USING 43 GRADE OPC

AI-1.1 Design considerations:

a) Characteristic compressive strength   20 MPa
of concrete required @ 28 days

b) Maximum size of aggregate   20 mm (Angular)

c) Degree of workability   0.9 (Compacting factor)

d) Degree of quality control   Good

e) Type of exposure   Severe

f) Target mean strength of concrete

$$F_{ck} = f_{ck} + \text{t.s}$$

where,

F_{ck} = Target average compressive strength of concrete at 28 days

f_{ck} = Characteristic compressive strength of concrete at 28 days

s = Standard deviation

t = A statistical constant, depending upon the accepted proportion of low results and the number of test

Assuming, t = 1.65, i.e., characteristic strength is defined as that value below which not more than 5% (1 in 20) results are expected to fall, using Table 1 of IS 10262:1982

Assuming s = 4.0 as per IS 456:2000

Target mean strength of concrete

$$F_{ck} = f_{ck} + \text{t.s}$$

$$= 20 + 1.65 \times 4$$

$$= 26.60 \text{ MPa}$$

g) Selection of water and sand content.

By considering,

      Water cement ratio = 0.5

      Cement content = 320kg/m^3

Sand content as percentage of total aggregate by absolute volume is equal to 40 %.

Therefore water content = $0.5 \times 320 = 160$ kg/m^3

For change in the value of W/C ratio, compacting factor and sand belonging to zone II, the following adjustment is required.

Change in condition	Water content percentage	Percentage sand in total aggregate
For sand conforming to zone III	0	0
For increase in value of compacting factor by (0.85-0.80) i.e., 0.05	+3.0	0
For decrease in water-cement ratio by (0.60-0.50) i.e., 0.10	0	-2.0
Total	+3.0	-2.0

Required sand content as percentage of total aggregate by absolute volume

= 40 - 2.0 = 38 %

Required water content = 160 + (0.03 x 160) = 164.80 kg/m^3

h) Determination of coarse and fine aggregate content.

From Table 3 of IS 10262:1982, for the specified maximum size of aggregate of 20mm, the amount of entrapped air in the wet concrete is 2%. With the known quantities of water and cement per unit volume of concrete and the ratio of fine to total aggregate was determined, the total aggregate content per unit volume of concrete was calculated from the following equations.

$$V = \left[W + \left(\frac{C}{Sc} \right) + \left(\frac{1}{P} \frac{f_a}{S_{fa}} \right) \right] \left(\frac{1}{1000} \right) \tag{1}$$

$$V = \left[W + \left(\frac{C}{Sc} \right) + \left(\frac{1}{(1-P)} \frac{c_a}{S_{ca}} \right) \right] \left(\frac{1}{1000} \right) \tag{2}$$

Where,

V = Absolute volume of fresh concrete, which is equal to gross volume (m^3) minus the volume of entrapped air (m^3)

W = Mass of water (kg/m^3) of concrete

C = Mass of cement (kg/m^3) of concrete

S_c = Specific gravity of cement = 3.14 (From Table 3.1)

P = Ratio of fine aggregate to total aggregate by absolute volume

f_a, c_a = Total masses of fine aggregate and coarse aggregate (kg/m^3) of concrete respectively

S_{fa}, S_{ca} = Specific gravities of saturated surface dry fine aggregate and coarse aggregate respectively, S_{fa} = 2.56 and S_{ca} = 2.66 (From Table 3.3 and Table 3.5)

$$(1-0.02) = \left[164.80 + \frac{320}{3.14} + \frac{1}{0.38} \times \frac{f_a}{2.60}\right]\frac{1}{1000} \qquad \text{(From Eq. 1)}$$

$$f_a = 704.72 \text{ kg/ m}^3$$

$$(1-0.02) = \left[164.80 + \frac{320}{3.14} + \frac{1}{0.62} \times \frac{c_a}{2.66}\right]\frac{1}{1000} \qquad \text{(From Eq. 2)}$$

$$C_a = 1176.35 \text{ kg/ m}^3$$

APPENDIX II

AII-1 MIX DESIGN OF M20 GRADE CONCRETE USING PPC CONFIRMING TO IS 1489:1991

AII-1.1 Design considerations:

a) Characteristic compressive strength of concrete required @ 28 days — 20 MPa

b) Maximum size of aggregate — 20 mm (Angular)

c) Degree of workability — 0.9 (Compacting factor)

d) Degree of quality control — Good

e) Type of exposure — Severe

f) Target mean strength of concrete

$$F_{ck} = f_{ck} + \text{t.s}$$

Target mean strength of concrete

$$F_{ck} = f_{ck} + \text{t.s}$$

$$= 20 + 1.65 \times 4$$

$$= 26.60 \text{ MPa}$$

g) Selection of water and sand content.

By considering,

Water cement ratio = 0.5

Cement content = 330 kg/m^3

Sand content as percentage of total aggregate by absolute volume is equal to 47%.

Therefore water content = $0.5 \times 330 = 165$ kg/m^3

For change in the value of W/C ratio, compacting factor and sand belonging to zone II, the following adjustment is required.

Change in condition	Water content percent	Percentage sand total in aggregate
For sand conforming to zone III	0	0
For increase in value of compacting factor by (0.85-0.80) i.e., 0.05	+3.0	0
For decrease in water-cement ratio by (0.60-0.50) i.e. 0.10	0	-2.0
Total	+3.0	-2.0

Required sand content as percentage of total aggregate by absolute volume

$= 47 - 2.0 = 45$ %

Required water content $= 165 + (0.03 \times 165) = 169.95$ kg/m^3

h) Determination of fine and coarse aggregate content.

$$(1 - 0.02) = \left[169.95 + \frac{330}{2.92} + \frac{1}{0.45} \times \frac{f_a}{2.60} \right] \frac{1}{1000} \qquad \text{(From Eq.1)}$$

$$f_a = 817.01 \text{ kg/ m}^3$$

$$(1 - 0.02) = \left[169.95 + \frac{330}{2.92} + \frac{1}{0.55} \times \frac{c_a}{2.66} \right] \frac{1}{1000} \qquad \text{(From Eq.2)}$$

$$C_a = 976.03 \text{ kg/ m}^3$$

119

APPENDIX III

AIII-1 DESIGN CALCULATION OF LOADING FRAME ELEMENTS

AIII-1.1 Member- 1 and 2

Type: Compression member

Design axial force: 62.720kN

Effective length: 3680 mm

Select two ISMC-100 @ 90.3N/m, front to front with zero clear spacing.

Sectional properties of ISMC-100

Sectional area = 1170 mm^2

Moment of inertia about x axis, $I_{xx} = 1864 \times 10^3$ mm^4

Moment of inertia about y axis, $I_{yy} = 259 \times 10^3$ mm^4

Width of flange, b = 50 mm

Thickness of flange t_f = 7.5 mm

Thickness of web t_w = 4.7 mm

Sectional properties for built up section;

Total cross sectional area = 2340 mm^2

$I_{xx} = 2 \times 1864 \times 10^3 = 3728 \times 10^3$ mm^4

$I_{yy} = 2[\, 259 \times 10^3 + 1170 \times 29^2] = 2485 \times 10^3$ mm^4

Minimum radius of gyration, $r_{min} = \surd\, (2485 \times 10^3/2340) = 32.59$ mm

Minimum slenderness ratio, $\lambda_{min} = (3680/\, 32.59) = 112.92 < 180$

Therefore design is ok

For $\lambda_{min} = 103.516$ and $f_y = 250$, $\sigma_{ac} = 64$ MPa

Therefore total load carrying capacity = $64 \times 2340 = 149.76$ kN > 62.720kN

Therefore provide ISMC-100 front to front with zero spacing

AIII-1.2 Member- 3 and 4

Type: Tension member

Design axial force: 41.36 kN

Effective length: 1750 mm

Select two ISMC-100 @ 90.3N/m, front to front with zero clear spacing.

Therefore total area provided = 2340 mm^2

Allowable tensile stress = $0.6 \times \sigma_{at}$ = 0.6×250 = 150 N/mm^2

Therefore net area required = 41360 / 150 = 275 mm^2 < 2340 mm^2
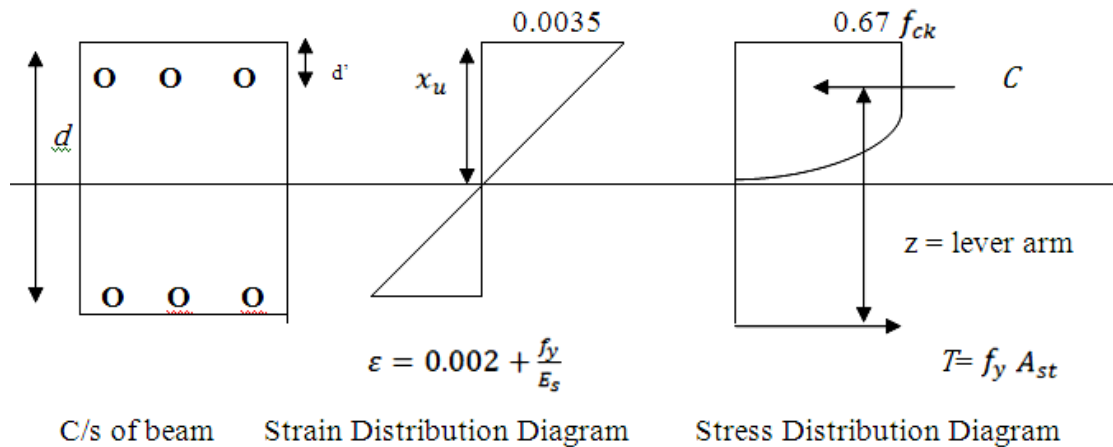
Therefore section provided is sufficient

Minimum radius of gyration r_{min} = 32.59 mm

Minimum slenderness ratio, λ_{min} = (1750/ 32.59) = 53.69 < 180

Therefore section is safe, provide ISMC-100 front to front with zero spacing

APPENDIX IV

AIV-1 ULTIMATE MOMENT CALCULATIONS FOR BEAMS

C/s of beam   Strain Distribution Diagram   Stress Distribution Diagram

AIV-1 Stress-Strain diagram of rectangular beam without partial safety of factor

Le*t* C be the compression force in concrete and T be the Tension force in the steel

C = Area of stress block × width of cross sction

$$C = 0.543 \times f_{ck} \times x_u \times b$$

$T = f_y \times$ Area of steel tension steel

$$T = f_y \times A_{st}$$

$f_{ck} = 26.6$ N/mm^2

fy = 480 N/mm^2

d = 360 mm

d' = 40 mm

To obtain depth of neutral axis (x_u) equating equation

$$\frac{x_u \text{max}}{0.0035} = \frac{0.0035\,(360 - x_u \text{max})}{0.002 + \frac{fy}{Es}}$$

$$x_u \text{max} = 0.7955\,(360 - x_u \text{max})$$

$$x_u\text{max} = 159.5 \text{ mm}$$

$$C_{uc}+C_{us}=T_u \text{.................}(a)$$

$C_{uc}=0.543 \times f_{ck} \times x_u \times b$

$C_{uc}=4320.54 \times x_u$

$C_{us} = f_y - 0.67 \times f_{ck}$

$C_{us} =462.131\text{N}$

$T_u = f_y \times A_{st}$

$T_u = 398\times10^3 \text{ N}$

Put all the values in equation (a)

$x_u=92.01$ mm

$$x_u < x_u max$$

Therefore section is under reinforced

To determine ultimate moment capacity

$$M_u = C_{uc}(d-0.416x_u)+C_{us}(d-d')$$

$M_u = 0.543\, f_{ck}x_u b\, (d - 0.416x_u) + 462.131\times 320$

$M_u = 0.543 \times 26.67 \times 92.01 \times 300\, (360 - 0.416 \times 92.01) + 462.131\times 320$

$$M_u = 128.416 \times 10^6 \text{ N} - \text{mm}$$

Therefore Ultimate load $Wu = \dfrac{M_u}{l} = \dfrac{128.416\times10^6}{1750} = 73.38 \times 10^3 \text{ N}$

Where,

M_u = Ultimate moment in N- mm

C_{uc} = Compressive force in Concrete

C_{us} = Compressive force in Steel

d = Effective depth in mm

$X_{u =}$ Depth of Neutrals axis in mm

d' = Effective cover in mm

l = Effective length in mm

AIV-1.1 I_{eff} calculations for OPC beams (as per IS 456 2000)

$$\frac{bn^2}{2} + (1.5m-1) \times Asc \times (n-d_c) = m \times Ast \times (d-n)$$

$$\frac{300n^2}{2} + (1.5 \times 10.53 - 1) \times 829.4 \times (n-40) = 10.53 \times 829.4 \times (360-n)$$

n = 100.675 mm

$$I_{cr} = \frac{bn^3}{3} + m \times Ast \times (d-n)^2 + (1.5m-1) \times Asc \times (n-d_c)^2$$

$$= \frac{300 \times 100.675^3}{3} + 10.53 \times 829.4 \times (360-100.675)^2 +$$

$$(1.5 \times 10.53 - 1) \times 829.4 \times (100.675 - 40 \ )^2$$

$$I_{cr} = 0.7345 \times 10^9 \, mm^4$$

Now, (as per IS 456 2000 Annex C)

$$I_{eff} = \frac{I_{cr}}{1.2 - \dfrac{M_r}{M} \times \dfrac{Z}{d} \times (1 - \dfrac{x}{d}) \times \dfrac{bw}{b}}$$

$$= \frac{0.7345 \times 10^9}{1.2 - \dfrac{28.8821}{75.102} \times \dfrac{326.44}{360} \times (1 - \dfrac{100.675}{360}) \times 1}$$

$$I_{effOPC} = 0.774 \times 10^9 \, mm^4$$

Similarly for PPC beams

$$I_{effPPC} = 0.82624 \times 10^9 mm^4$$

where

b = Breadth of the beam in mm

n or x = Neutral axis depth in mm

m = Modular ratio

Ast = Area of tension steel in mm^2

Asc = Area of compression steel in mm^2

d = Effective depth of the beam in mm

d_c = Depth of cover in mm

I_{cr} = Moment of inertia of the cracked section in mm^4

I_{eff} = Effective moment of inertia in mm^4

Mr = Cracking moment in N-mm

M = Ultimate moment under service loads in N-mm

Z= Lever arm in mm

b = Breadth of compression face in mm

b_w = Breadth of web in mm

AIV-1.2 Deflection calculation for beam specimen

$$\partial = \frac{PL^3}{3EI_{eff}}$$

Where,

P = Load in N

L = Effective length in mm

E = Modulus of elasticity of concrete in N/mm^2

I_{eff} = Moment of inertia (calculated as per IS 456- 2000 Annex C) in mm^4

$$\partial_{\max OPC} = P \times 8.950 \times 10^{-4} = 65.54 mm$$

$$\partial_{\max PPC} = P \times 8.7885 \times 10^{-4} \quad = 64.35mm$$

PUBLICATIONS BASED ON PRESENT RESEARCH WORK

INTERNATIONAL JOURNALS

Poornachand Pandit, Akshatha Shetty, Katta Venkataramana, K. S. Babunarayan, Indrani Gogoi, Praveen B. B, Mahesha, Shivaprasad Naik and Arun Sedamkar, (2012), "Experimental investigations on the flexural strength of reinforced concrete beams," *International Journal of Earth sciences and Engineering,* Vol.5, No.4, August,2012, 1042-1045.

Poornachandra Pandit, Ansal.V, K. Venkataramana and Parthiban P (2013), "Experimental investigation on corroded reinforced concrete beam in coastal environment using strain gauges," *International Journal of Engineering and Innovative Technology*,Vol.3,No.5, November,2013, 416-422.

Poornachandra Pandit, Katta Venkataramana, K. S. Babunarayan, Bhagyashri Parla and Yokinobu Kimura, (2014), "Experimental studies on the effect of corrosion on the flexural strength of RC beams," *International Journal of Earth sciences and Engineering*, Vol.7, No.1 February, 2014, 320-324.

Poornachandra Pandit, Katta Venkataramana and K. S. Babunarayan, (2014), "Experimental and numerical investigation of flexural behaviour of accelerated corroded beams," *Jounrnal of Civil Engineering Technology and Research,* Vol.2, No.1, June, 2014, 429-440.

CONFERENCES

Poornachand Pandit, Indrani Gogoi and K. S. Babunarayan, (2011), "Effect of corrosion on performance of reinforced concrete structure using pushover analysis."*International Conference on Advances in Civil Engineering (ACE- 2011)* held at K L University, Vaddeswaram, Andhra Pradesh during 21-23 October 2011.

Poornachand Pandit, Mahesha, Shivaprasad Naik, Akshatha Shetty, Katta Venkataramana, K.S. Babunarayan and Indrani Gogoi, (2012), "Load carrying capacity of OPC and PPC concrete beams." *International Conference on Emerging*

Trends in Engineering (ICETE 2012) held at NMAM Institute of Technology, Nitte, Karnataka during 15-16 May 2012.

Poornachand Pandit, Mahesha, Shivaprasad Naik, Akshatha Shetty, Katta Venkataramana, K.S. Babunarayan, Indrani Gogoi and Chinnagiri Gowda, (2012), "Accelerated test of concrete beams in coastal environment." *International Conference on Advances in Architecture and Civil Engineering (AARCV-2012)* held at M.S. Ramaiah Institute of Technology, Bengaluru, Karnataka during 21-23 June 2012.

Poornachandra Pandit, Katta Venkataramana, K.S.Babunarayan and Bhagyashri Parla, (2013) "Experimental studies on the effects of corrosion on the flexural strength of RC beams." *3rd International Engineering Symposium – IES 2013*, Kumamoto University, Japan during 4-6 March 2013.

Poornachandra Pandit, Katta Venkataramana and K.S.Babunarayan, (2014) "Experimental and numerical investigation of flexural behaviour of accelerated corroded beams." *International Conference on Recent Advances in Engineering Sciences-(ICRAES-2014)* held at M.S. Ramaiah Institute of Technology, Bengaluru, Karnataka during 4-5 September 2014.

CURRICULUM VITAE

Name   : POORNACHANDRA PANDIT

Contact No.   : +91-9481228498

E-Mail   : poornachandra16@gmail.com

                           poornachandrapandit@ gmail.com

Date of Birth   : 11-12-1983

Permanent address : Mahanilaya, H.No. 7-5-203,

                           Jawaharnagar

                           Raichur- 584103, Karnataka.

Educational Qualifications

Degree	University	Year of Passing	Percentage
B.E (Civil Engineering)	V.T.U	2002-2006	63.6
M.Tech (Structural Engineering)	NITK	2008-2010	7.83 (CGPA)

Industrial Experience

Employer	Post held	Date of joining	Date of leaving
Sobha Developers PVT. Ltd., Bangalore	Site Engineer	05/06/2006	14/08/2007

Research Publications

	Published	Under review/communicated
Journal Papers	4	**2**
Conference Publications	5	